Boundary-Integral Formulations for Three-Dimensional Fluid-Structure Interaction

by

Van Chi Luu

B.S. Aerospace Engineering, Iowa State University (1988)

Submitted to the
Department of Aeronautics and Astronautics
in Partial Fulfillment of the Requirements for the Degree of

Master of Science

at the

MASSACHUSETTS INSTITUTE OF TECHNOLOGY

September 1991

Signature of Author_____
Department of Aeronautics and Astronautics
August 1, 1991

Certified by_____
Dr. David S. Kang
Thesis Advisor
Charles Stark Draper Laboratory

Certified by_____
Professor John Dugundji
Thesis Supervisor
Department of Aeronautics and Astronautics

Accepted by_____
Professor Harold Y. Wachman
Chairman, Department Graduate Committee

Boundary-Integral Formulations for Three-Dimensional Fluid-Structure Interaction

by

Van Chi Luu

Submitted to the Department of Aeronautics and Astronautics on August 1, 1991 in Partial Fulfillment of the Requirements for the Degree of

Master of Science

at the

MASSACHUSETTS INSTITUTE OF TECHNOLOGY

ABSTRACT

Numerical techniques are presented for the determination of the added mass matrix and the excess pressure induced in a fluid of infinite extent by a totally submerged vibrating elastic structure. For relatively low vibrational frequencies, the effect of the surrounding fluid can be incorporated into an added mass matrix merely superimposed upon the structural mass matrix for the solution of the structural response. For higher vibrational frequencies, the simultaneous solution of the elastic and fluid field relationships is required in order to solve the general interaction problem. For this coupled fluid-structure interaction problem, the elastic response of the structure is modeled using finite element method. The acoustic field equations relating the structure's surface pressure and its surface normal velocities are used to form an acoustic impedance matrix, which gives an expression for the fluid-structure interaction forces. These forces are then coupled with the external applied forces, the structural mass matrix, and the stiffness matrix to form the dynamic equilibrium equations for the coupled system.

Thesis Advisor: Dr. David S. Kang
Thesis Supervisor: Professor John Dugundji

Acknowledgements

I would like to express my sincere gratitude to my thesis advisor, Dr. David S. Kang, for his countless guidance and encouragement. Unlike many professors/researchers in many universities, Dr. Kang cares not only about the education of his students, he also pays great attention to their welfare. Being a master student at M.I.T. for the last two years was exciting and challenging. However, the inevitable stress and frustration that come with being a graduate student would have driven me to insanity without the continuous moral support and helps of Dr. Kang. I owed my education to Dr. Kang, and I appreciate very much for everything he has done for me.

I would like to thank all my colleagues at the Draper Laboratory for their friendship and support: Naz Bedrossian, Howard Clark, Joe Nadeau, Ashok Patel, and Dave Roberts.

Special thanks go to Naz Bedrossian and his wife for all their helps in the last two years.

Last, but not least, I would like to thank my family and all my friends in Iowa and St. Louis, especially my friends at McDonnell Douglas Missile Systems Company.

This research was done at The Charles Stark Draper Laboratory, Inc.

Table of Contents

List of Figures

0. Introduction

Structural vibrations in a fluid are usually coupled to motion of the surrounding fluid. The natural vibrational frequencies, the mode shapes of the structure, and the far-field acoustic pressure induced by the vibrating structure must be found, in general, from a coupled fluid-structure analysis. If the structure is immersed in a fluid of which the density is much less than the average density of the structure (say, for example, air), the effect of the surrounding fluid on the natural frequencies and mode shapes of the structure can be neglected. On the other hand, if the density of the fluid is of the same order of magnitude as the average density of the structure (such as water), the surrounding fluid can alter the natural frequencies and mode shapes of the structure significantly; thus, the presence of the fluid cannot be neglected and a coupled fluid-structure problem must be solved in order to obtain the correct natural frequencies and mode shapes.

At low vibrational frequencies, however, it is known that the fluid pressure on the wetted surface of the structure is in phase with the structural acceleration, and the surrounding fluid appears to the structure like an added mass. Thus, for relatively low frequencies[1] the effect of the fluid on the structure are embodied in an added mass matrix that is merely superimposed upon the structural mass matrix. At higher frequencies, the fluid impedance (the ratio of fluid pressure to velocity) is mathematically complex, since both mass-like and damping-like effects are involved. In this case, the fluid can no longer be treated simply as an added mass to the structure and the external fluid equations must be coupled to the structural equations in order to obtain solutions to the interaction problem.

---

[1] Low frequency implies that $\lambda_{st}^2 << \lambda_{ac}^2$, where λ_{st} is a characteristic structure wave length for the motion of the structure's surface, and $\lambda_{ac} = c/f$ is a characteristic acoustic wave length for the motion where f is a characteristic frequency and c is the speed of sound in that fluid. Therefore, if the applied excitation frequencies are less than roughly one-third of the structure's lowest natural frequency of vibration, the effect of the fluid can be incorporated into an added mass matrix superimposing on the structural mass matrix.

The main goal of this thesis is to address the steady state fluid-structure interaction problem described by a totally submerged vibrating elastic body in an acoustic medium of infinite extent. Both low and high vibrational frequencies of the structure will be studied using boundary integral equation (BIE) method. Boundary integral equation formulations are chosen because they appear to be more attractive for this problem as compared to other popular numerical techniques such as finite element or finite difference,[2] since they 1) reduce the dimensionality of the problem by one, 2) obviate the need to model the infinite far-field boundary condition of the acoustic medium, 3) are flexible in handling arbitrary boundary conditions, and 4) can easily handle arbitrary geometries.

The main structure of this thesis can be divided into two parts: 1) to calculate the added mass matrix for low frequency vibrations of a totally submerged structure, and 2) to calculate the surface and the far-field pressures of a totally submerged vibrating body using the integral Helmholtz equations.

---

[2] Currently, this is the general feeling among researchers in the acoustic field. However, advances in other field in recent years may change this in the future. See the discussions in Section 3.

1. Low Frequency Fluid-Structure Interaction

For fluid-structure interaction situations where the fluid viscosity effects are negligible and the vibrational frequencies are low, the fluid can be treated as inviscid and incompressible (Refs. 16, 17). The added mass calculation then requires solving Laplace's equation in the fluid domain exterior to the structure. This calculation can be performed using either boundary integral method or finite element method, among others. Sections 1.1 and 1.2 describe in details the theoretical basis and numerical procedure for calculating the added mass matrix using the boundary integral method.

1.1 Added Mass Calculation Using Boundary Integral Method

Consider a three-dimensional elastic body immersed and at rest in an infinite, inviscid, incompressible fluid which is also at rest. If the surface of the body is made to oscillate about its equilibrium position, the resulting motion of the fluid will be irrotational and acyclic (Ref. 17); hence, the velocity can be expressed as the negative gradient of a scalar potential function φ, that is, $\underline{V} = -\nabla\varphi$. Also, in such a motion the pressure exerted by the fluid on the surface of the body is finite, and to generate the motion the body requires only a finite amount of energy, which is shared between the fluid and the body. The kinetic energy of the fluid is therefore finite, and so the velocity of the fluid at infinity must be zero. Thus, the governing equation for the fluid motion is Laplace's equation

$$\nabla^2\varphi = 0\,, \tag{1.1a}$$

and the boundary conditions are

$$\nabla\varphi \cdot \underline{n} \equiv \varphi' = -|\underline{u}| \tag{1.1b}$$

on the surface and

$$|\nabla\varphi| = 0 \tag{1.1c}$$

at infinity. The vector $\underline{n}$ in Eq. (1.1b) is the outward unit normal at the surface, $\underline{u}$ is the surface velocity in the normal direction [both $\underline{n}$ and $\underline{u}$ are defined as positive pointing into the fluid (Fig. 1.1)], and ∇ is the gradient operator. The problem defined by Eqs. (1.1a-c) is known as the *external Neumann problem*. According to Sobolev (Ref. 21), the solution of an external Neumann problem which has continuous first-order derivatives right up to the boundary is unique, and the solution of the problem can be determined to within an arbitrary additive constant. Many methods, both analytic and numerical, have been developed for solving this problem. One of the classical methods is to reduce the problem to an integral equation over the boundary surface.

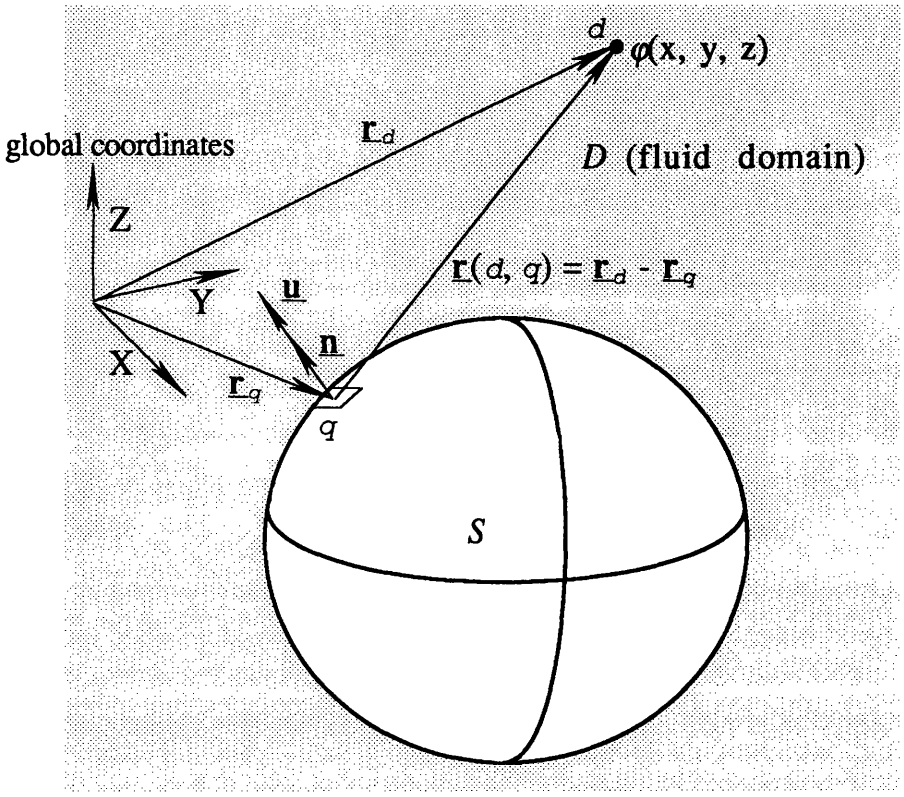

Figure 1.1 An elastic body immersed in an infinite, inviscid, incompressible fluid.

Consider a unit point source located at a point q on the surface of the body whose Cartesian coordinates are x_q, y_q, z_q. At another point d in the fluid domain (with coordinates x, y, z) the potential induced at this point by the point source at q is[3]

$$\varphi(d) = \frac{1}{|\underline{r}(d, q)|}, \tag{1.2}$$

where $|\underline{r}(d, q)|$ is the distance between the points d and q (Fig. 1.1), namely,

---

[3] Except for a factor of $1/4\pi$, this is known as free-space Green's function for Laplace's equation. $\underline{r}(d, q)$ means the distance between points d and q where d represents a point ranging throughout the fluid domain D and q represents a point ranging only over the boundary S .

$$|\underline{r}(d, q)| = \sqrt{[(x - x_q)^2 + (y - y_q)^2 + (z - z_q)^2]} . \qquad (1.3)$$

In this equation q is usually referred to as the "source point" and d the "receiver point." The potential in Eq. (1.2) is a singular solution to Laplace's equation. It satisfies Eq. (1.1a) and Eq. (1.1c) at all points except the source point q. Because of the linearity of Laplace's equation, the potential due to any ensemble or continuous distribution of such sources that lies entirely on the boundary surface S (or interior to S) will also satisfy Eq. (1.1a) and Eq. (1.1c) in D exterior to the boundary. Therefore, a solution based on a continuous source distribution on the surface S can be formulated. If the source density (source per unit area) at a given point on the surface is denoted by $\sigma(q)$, then the potential at the receiver point d due to the continuous distribution of source at the surface is[4]

$$\varphi(d) = \int_S \left[\frac{\sigma(q)}{|\underline{r}(d, q)|}\right] dS. \qquad (1.4)$$

Eq. (1.4) expresses the velocity potential φ at an arbitrary point d in terms of an integral over the boundary of the fluid domain D. Regardless of the nature of the source density function $\sigma(q)$, the potential given by Eq. (1.4) satisfies two of the three equations of the external Neumann problem. The surface source density function is determined from the requirement that the potential must also satisfy the Neumann boundary condition, namely, Eq. (1.1b). Applying the boundary condition (1.1b) requires the evaluation of the limits of the spatial derivatives of Eq. (1.4) as d approaches a point s on the surface S (Fig. 1.2). Care is required in taking the derivatives of Eq. (1.4) because the derivatives of the integrand $1/|\underline{r}(d, q)|$ become singular as the surface is approached. When Eq. (1.4) is differentiated and the Neumann boundary condition is applied to it by allowing point d to approach point s, the result is the following expression for the surface source density distribution function $\sigma(q)$:

---

[4] $dS = dS(q)$ indicating that it is a surface element at point q: when q shifts, $dS(q)$ shifts.

$$\nabla\varphi \cdot \underline{\mathbf{n}} = \frac{\partial\varphi}{\partial \mathbf{n}_+} = -2\,\pi\,\sigma(s) + \int_S \left[\frac{\sigma(q)\cos\,[\theta(s,\,q)]}{|\underline{\mathbf{r}}(s,\,q)|^2}\right] dS \qquad (1.5)$$

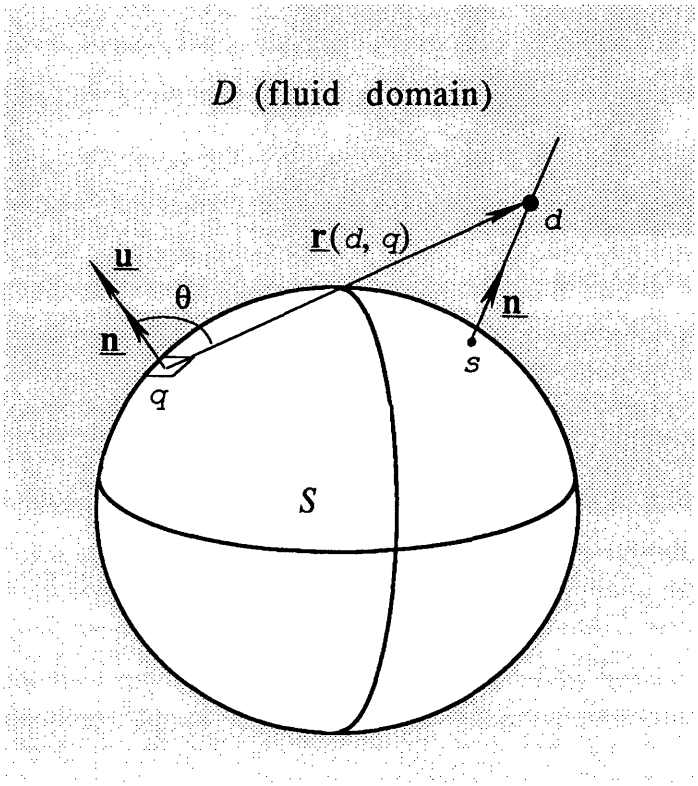

Figure 1.2 The receiver point approaches the surface S along the unit normal from the positive side of the surface.

where $\theta(s, q)$ is the angle between the unit normal at the source point and the vector $\underline{\mathbf{r}}(s, q)$, and $\partial\varphi / \partial \mathbf{n}_+$ is the normal derivative of φ on the boundary S approaching from the positive side of the surface. Eq. (1.5) is known as a *Fredholm integral equation of the second kind.* The term $2\,\pi\,\sigma(s)$ arises from the delta function that is brought in by the limiting process of approaching the boundary. It represents the contribution to the outward normal velocity at point s from the source density in the immediate neighborhood of s. The surface integral represents the contribution to the normal

velocity at s from the source density of the remainder of the boundary surface (Ref. 15).

Closed-form analytic solutions to Eqs. (1.4) and (1.5) are rare except for simple geometries. For arbitrary three-dimensional bodies, these integrals must be solved numerically. This can be accomplished in the following manner. The surface of the body is approximated by quadrilateral elements whose characteristic dimensions are small compared to those of the body. Over each element the value of the surface source density is assumed constant. This approximation reduces the problem of determining a continuous source density function $\sigma(q)$ to that of determining a discrete number of value of σ_i, one for each surface element. After the above procedure is completed, the unknown source distributions are eliminated from the equations. The fluid mass matrix is determined from a variational principle based on the fluid kinetic energy expression

$$KE_f = -\frac{1}{2}\rho_f \int_S \left(\varphi'(m)\ \varphi(m)\right) dS\ , \qquad (1.6)$$

where KE_f and ρ_f are the kinetic energy and the density of the fluid, respectively. The details of the above procedure are as follows. First, the surface of the body is divided into N quadrilateral elements to identify N distinct boundary integral relations (Fig. 1.3). Eq. (1.6) can be written in matrix form as

$$KE_{f_{disc}} = -\frac{1}{2}\rho_f \int_S \underline{\varphi}'^{T}\, \underline{\underline{dS}}\, \underline{\varphi} \qquad (1.7a)$$

or

$$KE_{f_{disc}} = -\frac{1}{2}\rho_f \int_S \underline{\varphi}^{T}\, \underline{\underline{dS}}\, \underline{\varphi}' \qquad (1.7b)$$

where the dimension of the column vectors $\underline{\varphi}$ and $\underline{\varphi}'$ is (N x 1), the dimension of the diagonal area matrix $\underline{\underline{dS}}$ is (N x N), and the superscript T denotes transpose of a vector or matrix. Next assume that the surface density function can be suitably represented, piecewise over N discrete patches of S_n, by constant σ_n (n = 1, 2, . . ., N). Based on the above assumptions Eqs. (1.4, 1.5) can be rewritten as

$$\underline{\varphi} = \underset{\sim}{B}\,\underline{\sigma} \tag{1.8a}$$

$$\underline{\varphi}' = -\underset{\sim}{C}\,\underline{\sigma} \tag{1.8b}$$

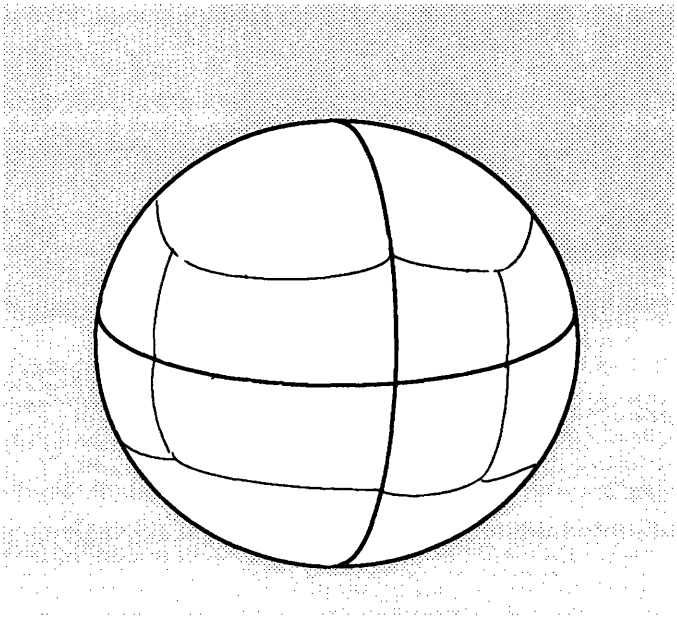

Figure 1.3 Discretization of the surface.

and the dimension of the matrices $\underset{\sim}{B}$ and $\underset{\sim}{C}$ is (N x N). Since the i^{th} component of the source density vector $\underline{\sigma}$ is independent of the control point within the i^{th} element (because constant source density within each element was assumed), Eqs. (1.8 a, b) may be expressed in terms of any desired set of control points $\underline{P}$ (= $[P_1, P_2, \ldots, P_N]^T$). Therefore, the potential and the source density vectors may be solved in terms of the surface normal velocity vector

$$\underline{\varphi}(P) = \underset{\sim}{B}(P)\,\underline{\sigma}(P) \tag{1.9a}$$

$$\underline{\sigma}(P) = -[\underset{\sim}{C}(P)]^{-1}\,\underline{\varphi}'(P) = [\underset{\sim}{C}(P)]^{-1}\,\underline{u}(P). \tag{1.9b}$$

In the above equations $\underline{\varphi}(\mathbf{P})$ (= $[\varphi_{P_1}, \varphi_{P_2}, \ldots, \varphi_{P_N}]^T$) denotes a set of discrete value of potentials evaluated at the control points $\underline{\mathbf{P}}$, $\underline{\sigma}(\mathbf{P})$ is the control point source density vector, $[\underline{\underline{C}}(\mathbf{P})]^{-1}$ is the inverse of the matrix $\underline{\underline{C}}$, and $\underline{\mathbf{u}}(\mathbf{P})$ is the normal velocity vector at $\underline{\mathbf{P}}$. Substituting Eqs. (1.8a, b) [with $\underline{\sigma} = \underline{\sigma}(\mathbf{P})$] and Eqs. (1.9a, b) into Eq. (1.7a):

$$\frac{-1}{2}\rho_f \int_S \underline{\varphi}'^T \underline{d\mathbf{S}}\, \underline{\varphi} = \frac{-1}{2}\rho_f \int_S \{-\underline{\underline{C}}\,\underline{\sigma}(\mathbf{P})\}^T\, \underline{d\mathbf{S}}\, \{\underline{\underline{B}}\,\underline{\sigma}(\mathbf{P})\}$$

$$= \frac{1}{2}\rho_f \int_S \{\underline{\underline{C}}\,[\underline{\underline{C}}(\mathbf{P})]^{-1}\,\underline{\mathbf{u}}(\mathbf{P})\}^T\, \underline{d\mathbf{S}}\, \{\underline{\underline{B}}\,[\underline{\underline{C}}(\mathbf{P})]^{-1}\,\underline{\mathbf{u}}(\mathbf{P})\}$$

$$= \frac{1}{2}\rho_f \int_S \{[\underline{\mathbf{u}}(\mathbf{P})]^T\,[\underline{\underline{C}}(\mathbf{P})^{-1}]^T\,\underline{\underline{C}}^T\}\, \underline{d\mathbf{S}}\, \{\underline{\underline{B}}\,[\underline{\underline{C}}(\mathbf{P})]^{-1}\,\underline{\mathbf{u}}(\mathbf{P})\}$$

$$= \frac{1}{2}\rho_f\, [\underline{\mathbf{u}}(\mathbf{P})]^T\,[\underline{\underline{C}}(\mathbf{P})^{-1}]^T \left[\int_S \underline{\underline{C}}^T\, \underline{d\mathbf{S}}\, \underline{\underline{B}}\right] [\underline{\underline{C}}(\mathbf{P})]^{-1}\,\underline{\mathbf{u}}(\mathbf{P})$$

$$= \frac{1}{2}\rho_f\, [\underline{\mathbf{u}}(\mathbf{P})]^T\, \underline{\underline{E}}\, [\underline{\mathbf{u}}(\mathbf{P})] \qquad (1.10)$$

where

$$\underline{\underline{E}} = [\underline{\underline{C}}(\mathbf{P})^{-1}]^T \left[\int_S [\underline{\underline{C}}^T]\, \underline{d\mathbf{S}}\, \underline{\underline{B}}\right] [\underline{\underline{C}}(\mathbf{P})]^{-1}. \qquad (1.11)$$

Similarly, substituting the same set of equations into (1.7b) yields

$$\frac{-1}{2}\rho_f \int_S \underline{\phi}^T \underline{d\mathbf{S}}\, \underline{\phi}' = \frac{-1}{2}\rho_f \int_S \{\underline{\underline{B}}\,\underline{\sigma}(\mathbf{P})\}^T\, \underline{d\mathbf{S}}\, \{-\underline{\underline{C}}\,\underline{\sigma}(\mathbf{P})\}$$

$$= \frac{1}{2}\rho_f \int_S \{\underline{\underline{B}}\,[\underline{\underline{C}}(\mathbf{P})]^{-1}\,\underline{\mathbf{u}}(\mathbf{P})\}^T\, \underline{d\mathbf{S}}\, \{\underline{\underline{C}}\,[\underline{\underline{C}}(\mathbf{P})]^{-1}\,\underline{\mathbf{u}}(\mathbf{P})\}$$

$$= \frac{1}{2}\rho_f \int_S \{[\underline{\mathbf{u}}(\mathbf{P})]^T\,[\underline{\underline{C}}(\mathbf{P})^{-1}]^T\,\underline{\underline{B}}^T\}\, \underline{d\mathbf{S}}\, \{\underline{\underline{C}}\,[\underline{\underline{C}}(\mathbf{P})]^{-1}\,\underline{\mathbf{u}}(\mathbf{P})\}$$

$$= \frac{1}{2}\rho_f [\underline{u}(P)]^T [\underline{\underline{C}}(P)^{-1}]^T \left[\int_S \underline{\underline{B}}^T \underline{\underline{dS}}\, \underline{\underline{C}}\right] [\underline{\underline{C}}(P)]^{-1}\, \underline{u}(P). \quad (1.12)$$

Since

$$[\underline{\underline{C}}(P)^{-1}]^T \left[\int_S \underline{\underline{B}}^T \underline{\underline{dS}}^T \underline{\underline{C}}\right] [\underline{\underline{C}}(P)]^{-1} =$$

$$[\underline{\underline{C}}(P)^{-1}]^T \left[\int_S \{[\underline{\underline{C}}^T]\, \underline{\underline{dS}}\, \underline{\underline{B}}\}^T\right] [\underline{\underline{C}}(P)]^{-1} = \underline{\underline{E}}^T$$

(note that $\underline{\underline{dS}}^T = \underline{\underline{dS}}$ since it is a diagonal matrix), therefore, Eq. (1.12) can be rewritten as

$$\frac{1}{2}\rho_f [\underline{u}(P)]^T \underline{\underline{E}}^T [\underline{u}(P)]. \quad (1.13)$$

Averaging Eq. (1.10) and Eq. (1.13) the discretized version of the fluid kinetic energy can be expressed as

$$KE_{f_{disc.}} = \frac{1}{2} \underline{u}^T \underline{\underline{M}}_f \underline{u} \quad (1.14)$$

where $\underline{\underline{M}}_f$ is the fluid mass matrix,

$$\underline{\underline{M}}_f = \frac{1}{2}\rho_f [\underline{\underline{E}} + \underline{\underline{E}}^T], \quad (1.15)$$

and $\underline{\underline{E}}$ is given by the expression in Eq. (1.11). Since constant source density on each element was assumed, the entries of the matrices $\underline{\underline{C}}^T$ and $\underline{\underline{B}}$ in the integral of Eq. (1.11) are constants. Therefore, the integral can be approximated by

$$\int_S [\underline{\underline{C}}^T]\, \underline{\underline{dS}}\, \underline{\underline{B}} \approx [\underline{\underline{C}}(P)]^T \underline{\underline{A}}\, [\underline{\underline{B}}(P)] \quad (1.16)$$

where $\underset{\sim}{A}$ is the (N x N) diagonal matrix (a_{ii} is the area of the i^{th} surface element). Substituting Eq. (1.16) for the integral in Eq. (1.11) yields

$$\underset{\sim}{E} = [\underset{\sim}{C}(P)^{-1}]^T \left[\int_S [\underset{\sim}{C}^T] \, \underset{\sim}{dS} \, \underset{\sim}{B} \right] [\underset{\sim}{C}(P)]^{-1}$$

$$= [\underset{\sim}{C}(P)^{-1}]^T [\underset{\sim}{C}(P)]^T \, \underset{\sim}{A} \, [\underset{\sim}{B}(P)] \, [\underset{\sim}{C}(P)]^{-1}$$

or

$$\underset{\sim}{E} = \underset{\sim}{A} \, [\underset{\sim}{B}(P)] \, [\underset{\sim}{C}(P)]^{-1}. \qquad (1.17)$$

From Eqs. (1.15) and (1.17), it is seen that the calculations of the matrices $\underset{\sim}{B}(P)$ and $\underset{\sim}{C}(P)$ form the basis of the present method for the added mass calculation. The entries of the matrices $\underset{\sim}{B}(P)$ and $\underset{\sim}{C}(P)$ are the potentials and velocities, respectively, that are induced at the control point of the i^{th} element by a unit point source density on the j^{th} element. They are obtained by integrating over the element in question the formulas for the potential and velocity, namely, Eqs. (1.4) and (1.5). With unit source density Eqs. (1.4) and (1.5) depend only on the location of the point at which the potential and velocity are being evaluated and the geometries of the source elements; therefore, for simple quadrilateral elements the integration of Eqs. (1.4) and (1.5) over the source elements can be performed analytically.

1.2 Calculation of the Potential and Velocity Induced by a Quadrilateral Element at a Point in Space

From the discussion in the last section, it is clear that the added mass matrix can be assembled once the potential and velocity matrices are obtained. The purpose of this section is to derive the formulas necessary for calculating the entries of matrices $\underset{\sim}{\mathbf{B}}(\mathbf{P})$ and $\underset{\sim}{\mathbf{C}}(\mathbf{P})$. Following the procedure outlined in Ref. 12, the formulas are obtained by performing the integration of the basic point-source equations over a surface element. For quadrilateral elements used to approximate the surfaces of three-dimensional bodies, the integration of Eq. (1.4) is most conveniently done in local element coordinate system. Consider a typical surface element as shown in Fig. 1.4. A local coordinate system (ξ, η, ζ) is chosen such that the origin of the coordinates is located at the centroid of the element. The element is taken to lie in the $\xi\eta$-plane, and the ζ-axis points in the direction of the unit outward normal of the element. Assuming that four-noded quadrilateral elements are used to approximate the surface of the body. The four corner points of the element are denoted by subscripts 1-4, where the numbering denotes the order in which the corner points of the element are encountered as one traverses along the perimeter in a clockwise sense (as view from the positive ζ-axis). In the $\xi\eta$-plane the coordinates of the corner points are $\xi_n, \eta_n, 0$ where n = 1-4. The maximum dimension of the element is denoted by d_{max} (Fig. 1.5). In order to facilitate the calculations of certain equations to be derived later, the ξ-axis is taken to be parallel to the vector from corner point 1 to corner point 3. Consider a point g in space with **local** coordinates x, y, z (Fig. 1.5). The distance between this point and a point $(\xi_e, \eta_e, 0)$ on the element in question is

$$\mathbf{r} = \sqrt{(x - \xi_e)^2 + (y - \eta_e)^2 + z^2} \,. \qquad (1.18)$$

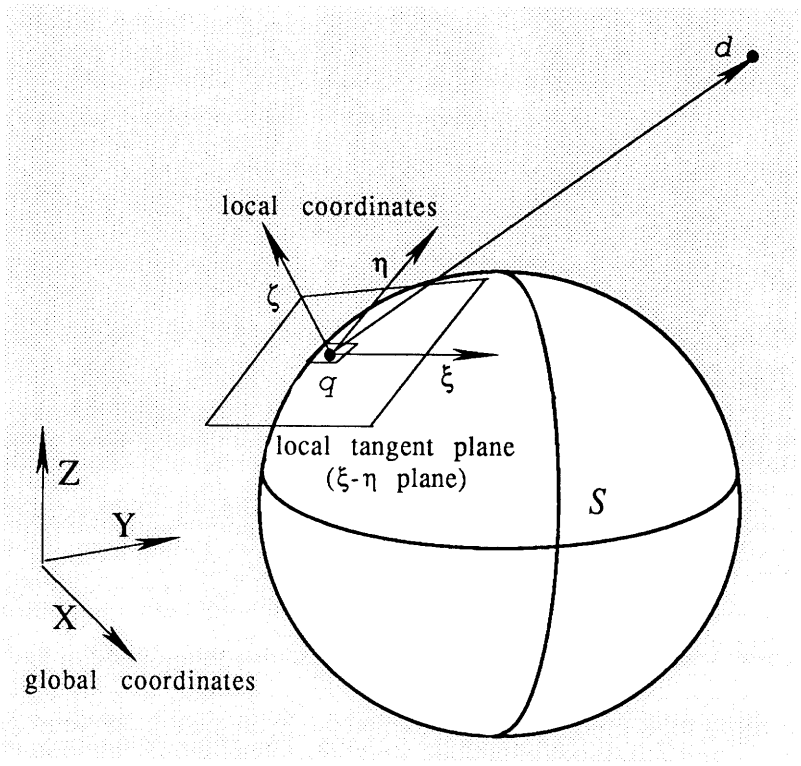

Figure 1.4 Local element coordinate system.

For a unit point source density, the potential at the point (x, y, z) induced by an infinitesimal element $d\xi\, d\eta$ is

$$d\varphi = \frac{1}{\mathbf{r}}\, d\xi\, d\eta = \frac{1}{\mathbf{r}}\, dA\ . \qquad (1.19)$$

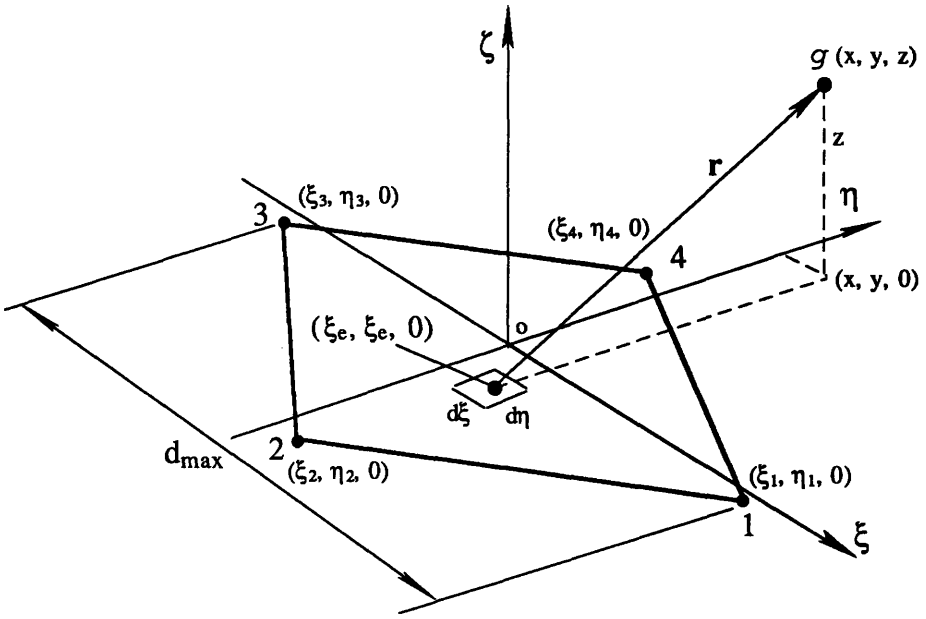

Figure 1.5 A typical four-noded quadrilateral element and its local coordinates.

The total potential at (x, y, z) induced by the quadrilateral element is then

$$\varphi(x, y, z) = \int_S d\varphi = \int_S \left[\frac{1}{r}\right] dA , \qquad (1.20)$$

where the domain of the area integral is the surface element. In order to facilitate the integration of Eq. (1.20), a cylindrical coordinate system, ($\mathcal{R}$, θ, z), with origin situated at the point (x, y, 0) is introduced (Fig. 1.6). In this coordinate system, $\mathcal{R}$ is the radial distance from (x, y, 0) to a point on the element, θ is the polar angle measured clockwise from any convenient reference axis, and z is taken to be parallel to the ζ-axis. In terms of these new variables Eq. (1.18) can be written as

$$r = \sqrt{(x - \xi_e)^2 + (y - \eta_e)^2 + z^2} = \sqrt{\mathcal{R}^2 + z^2} . \qquad (1.21)$$

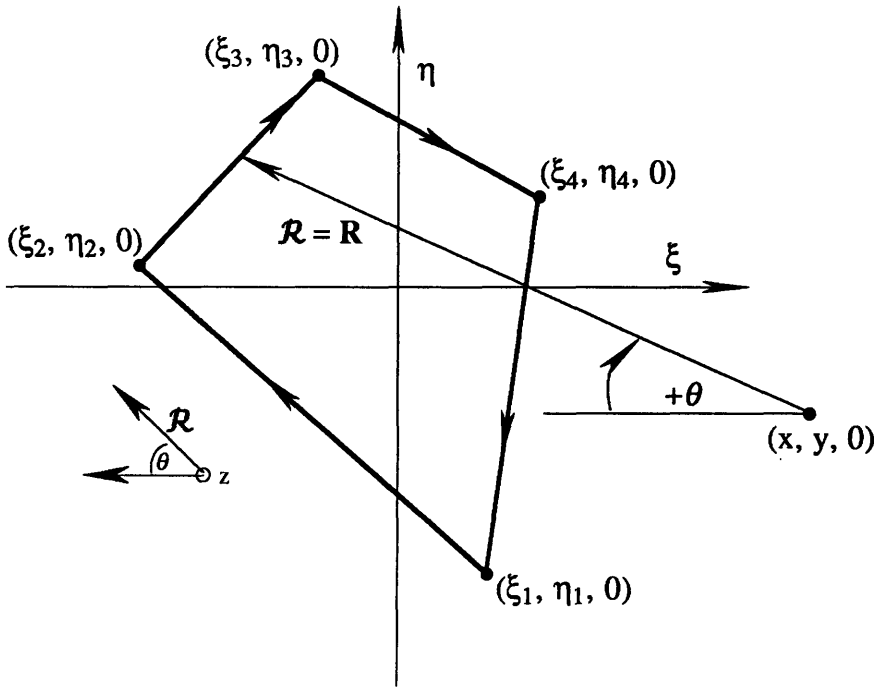

Figure 1.6 Local cylindrical coordinate system (looking down from the positive ζ axis).

Substituting Eq. (1.21) into Eq. (1.20) the potential at (x, y, z) induced by the element becomes

$$\varphi(x, y, z) = \int_s \frac{1}{r}\, dA = \int_s \left[\frac{1}{\sqrt{\mathcal{R}^2 + z^2}}\right] dA$$

$$= \int_s \frac{\mathcal{R}}{\sqrt{\mathcal{R}^2 + z^2}}\, dR\, d\theta \qquad (1.22)$$

or

$$\varphi(x, y, z) = \int_0^{2\pi} \int_0^{R} \frac{\mathcal{R}}{\sqrt{\mathcal{R}^2 + z^2}}\, d\mathcal{R}\, d\theta. \qquad (1.23)$$

In Eq. (1.23) the integration limits of the $\mathcal{R}$ variable is from $\mathcal{R} = 0$ to a point on the perimeter of the element $\mathcal{R} = \mathbf{R}$, and the integration limits of the θ variable is around the perimeter of the element from 0 to 2π in a clockwise sense (Fig. 1.6). The contribution of each side of the element to Eq. (1.23) represents the potential of the plane triangle defined by the point (x, y, 0) and the two end points of the line segment (Fig. 1.7). From Fig. 1.7a it is seen that as the perimeter of the element is being traversed in a clockwise sense, $d\theta$ is positive if the point (x, y, 0) is to the right of the line segment (segments 2 and 3) and is negative when the point is to the left of the element (segments 1 and 4). Therefore, when the potential of the four triangles corresponding to all four sides of the element are summed, the contributions of the portions of the triangles outside the element summed to zero (the shaded portion in Fig. 1.7b), and the result would be the contribution of the element itself. From Eq. (1.21) the distance from a point on the element to the point (x, y, z) is

$$\mathbf{r} = \sqrt{\mathcal{R}^2 + z^2} \,. \tag{1.24}$$

Differentiating the above equation yields

$$d\mathbf{r} = \frac{\mathcal{R}\, d\mathcal{R}}{\sqrt{\mathcal{R}^2 + z^2}} \,. \tag{1.25}$$

Substituting Eq. (1.25) into Eq. (1.23) and changing the integration limits of the $\mathcal{R}$ variable the potential at (x, y, z) becomes

$$\varphi(x, y, z) = \int_0^{2\pi} \left[\int_{|z|}^{\mathbf{r}} d\mathbf{r} \right] d\theta$$

$$= \int_0^{2\pi} [\mathbf{r}]\, d\theta - \delta_{ij}\, |z| \int_0^{2\pi} d\theta \,, \tag{1.26}$$

or

$$\varphi(x, y, z) = \int_0^{2\pi} [\mathbf{r}]\, d\theta - \delta_{ij}\, |z|\, \Delta\theta \tag{1.27}$$

where

$$\Delta\theta = \int_0^{2\pi} d\theta. \tag{1.28}$$

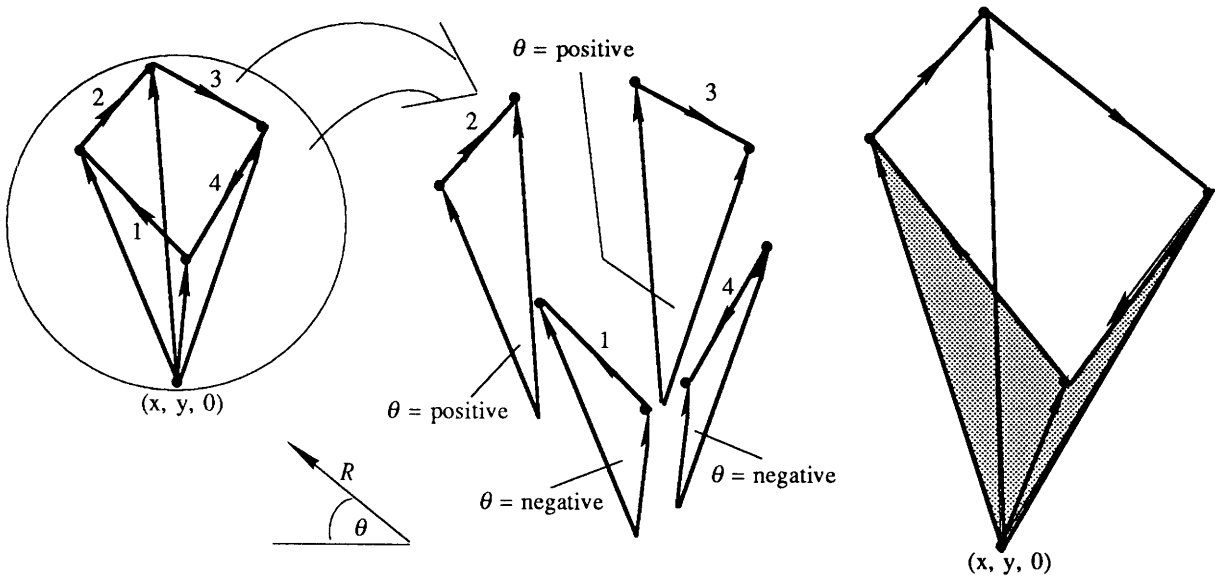

7 a

7 b

Figure 1.7 Contribution of each side of the element to the potential.

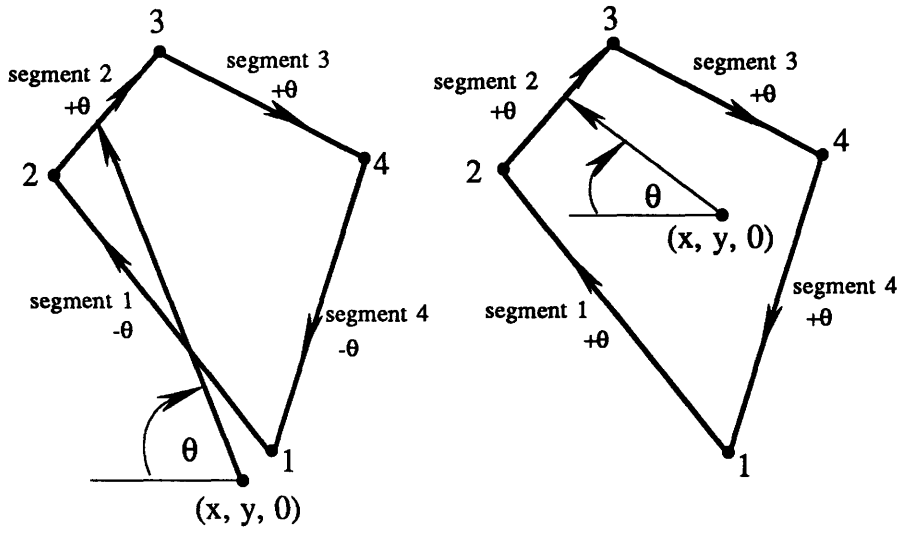

Figure 1.8 a) The point (x, y, 0) lies outside of the element. b) The point (x, y, 0) lies inside of the element.

From Fig. 1.8 it is seen that when the point (x, y, 0) is outside the element $\Delta\theta = 0$ ($\Delta\theta$'s of segments 2 and 3 cancel out $\Delta\theta$'s of segments 1 and 4), and $\Delta\theta = 2\pi$ if the point (x, y, 0) lies inside the element. (Note that when (x, y, 0) is inside the element the perimeter is always on the right-hand side of (x, y, 0) as it is being traversed, therefore, $d\theta$ is always positive.) Hence,

$$\varphi(x, y, z) = \int_0^{2\pi} [\mathbf{r}]\, d\theta \qquad (1.29)$$

if (x, y, z) lies outside of the element and

$$\varphi(x, y, z) = \int_0^{2\pi} [\mathbf{r}]\, d\theta - 2\pi\, |z| \qquad (1.30)$$

if (x, y, z) lies inside of the element. Thus, the second term of Eq. (1.27) is discontinuous as the point (x, y, 0) crosses a side of the element. However, the first term of the equation has an equal but opposite discontinuity (due to the change of sign of $d\theta$ along the side that is crossed) and thus the potential is continuous across the surface as expected. The integral of Eq. (1.27) is evaluated by calculating the contribution of a single side to the integral and summing the results for all four sides. (Note that the results can be generalized to polygons having any number of sides.) For the purpose of deriving the equations, the contribution of the side between the points $(\xi_1, \eta_1, 0)$ and $(\xi_2, \eta_2, 0)$ is used to illustrate the procedure. The contributions of the other sides can be found by advancing all the subscripts and superscripts in the equations.

Consider the line segment between $(\xi_1, \eta_1, 0)$ and $(\xi_2, \eta_2, 0)$ as shown in Fig. 1.9 and defining the following geometric quantities. The length of the side between $(\xi_1, \eta_1, 0)$ and $(\xi_2, \eta_2, 0)$ is

$$d_{12} = \sqrt{(\xi_2 - \xi_1)^2 + (\eta_2 - \eta_1)^2} \tag{1.31}$$

The cosine and sine of the angle θ_{12} are, respectively,

$$\cos\theta_{12} = \frac{\Delta x}{d_{12}} = \frac{(\xi_2 - \xi_1)}{d_{12}} \equiv C_{12} \tag{1.32}$$

$$\sin\theta_{12} = \frac{\Delta y}{d_{12}} = \frac{(\eta_2 - \eta_1)}{d_{12}} \equiv S_{12} . \tag{1.33}$$

A line perpendicular to segment 1-2 is drawn from the point (x, y, 0), and the (signed) distance from the point (x, y, 0) to the extension of segment 1-2 is

$$R_{12} = (x - \xi_1)\, S_{12} - (y - \eta_1)\, C_{12} . \tag{1.34}$$

Note that the distance is positive if (x, y, 0) lies to the right of the side with respect to the direction from $(\xi_1, \eta_1, 0)$ to $(\xi_2, \eta_2, 0)$ and is negative if (x, y, 0) lies to the left. Let L_{12} be the distance along the line segment from point o, measure positive from $(\xi_1, \eta_1, 0)$ to

$(\xi_2, \eta_2, 0)$, as shown in Fig. 1.9. The arc length associated with a general point (ξ, η) on the side is

$$L_{12} = (\xi - x)\, C_{12} + (\eta - y)\, S_{12} . \qquad (1.35)$$

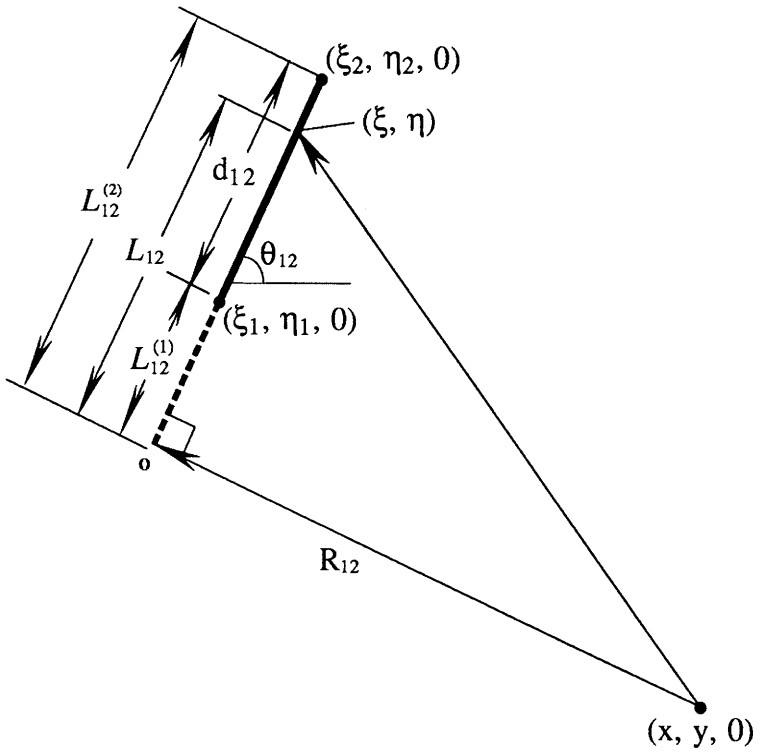

Figure 1.9 Integration over a side of the element.

In particular, the arc lengths associated with the corner points $(\xi_1, \eta_1, 0)$ and $(\xi_2, \eta_2, 0)$ are, respectively,

$$L_{12}^{(1)} = (\xi_1 - x)\, C_{12} + (\eta_1 - y)\, S_{12} \qquad (1.36)$$

and

$$L_{12}^{(2)} = (\xi_2 - x)\, C_{12} + (\eta_2 - y)\, S_{12} . \qquad (1.37)$$

The distances from the point (x, y, z) to the corner points $(\xi_1, \eta_1, 0)$ and $(\xi_2, \eta_2, 0)$ are, respectively,

$$r_1 = \sqrt{(x - \xi_1)^2 + (y - \eta_1)^2 + z^2} \qquad (1.38)$$

and

$$r_2 = \sqrt{(x - \xi_2)^2 + (y - \eta_2)^2 + z^2} \; . \qquad (1.39)$$

With the above geometric variables the following two quantities can be defined:

$$Q_{12} \equiv \ln \left[\frac{r_2 + L_{12}^{(2)}}{r_1 + L_{12}^{(1)}} \right] = \ln \left[\frac{r_1 + r_2 + d_{12}}{r_1 + r_2 - d_{12}} \right] \qquad (1.40)$$

$$J_{12} \equiv \tan^{-1} \left[\frac{R_{12} \, |z| \, (r_1 \, L_{12}^{(2)} - r_2 \, L_{12}^{(1)})}{r_1 \, r_2 \, (R_{12})^2 + z^2 \, L_{12}^{(2)} \, L_{12}^{(1)}} \right] \qquad (1.41)$$

where the range of the inverse tangent in Eq. (1.41) is from $-\pi$ to π by considering the individual signs of the numerator and denominator of its argument. With the defined quantities, the contribution of the line segment between $(\xi_1, \eta_1, 0)$ and $(\xi_2, \eta_2, 0)$ to the integral in Eq. (1.27) is then

$$\varphi_{12} = R_{12} \, Q_{12} + |z| \, J_{12} \; . \qquad (1.42)$$

The contributions of other segments of the element are found by advancing the subscripts and superscripts in the above equations. The potential at the point (x, y, z), and also the entries of the $\underset{\sim}{\mathbf{B}}$ matrix b_{ij}, induced by the element is then

$$b_{ij} = \varphi \, (x, y, z) = [\varphi_{12} + \varphi_{23} + \varphi_{34} + \varphi_{41}] - |z| \, \Delta\theta \qquad (1.43)$$

where φ_{12}, φ_{23}, φ_{34}, and φ_{41} are the contributions of the four segments to the integral in Eq. (1.27). The velocity components in

local element coordinates can be found by differentiating the velocity potential:

$$V_x = \frac{-\partial \varphi}{\partial x} = -\{S_{12} Q_{12} + S_{23} Q_{23} + S_{34} Q_{34} + S_{41} Q_{41}\}, \quad (1.44)$$

$$V_y = \frac{-\partial \varphi}{\partial y} = \{C_{12} Q_{12} + C_{23} Q_{23} + C_{34} Q_{34} + C_{41} Q_{41}\}, \quad (1.45)$$

and

$$V_z = \frac{-\partial \varphi}{\partial z} = \text{sgn}(z) \{\Delta\theta - J_{12} - J_{23} - J_{34} - J_{41}\} \quad (1.46)$$

where "sgn" is the FORTRAN sign function. The normal velocity at (x, y, z), and also the entries of the $\underset{\sim}{C}$ matrix c_{ij}, can be found by taking the dot product of the velocity vector, $\underline{V} = V_x \underline{i} + V_y \underline{j} + V_z \underline{k}$, and the unit normal vector at the point (x, y, z). Thus,

$$c_{ij} = \underline{n}_i \cdot \underline{V}_{ij} = (n_{i_1} \underline{i} + n_{i_2} \underline{j} \, n_{i_3} \underline{k}) \cdot (V_x \underline{i} + V_y \underline{j} + V_z \underline{k})$$

or

$$c_{ij} = n_{i_1} V_x + n_{i_2} V_y + n_{i_3} V_z \, . \quad (1.47)$$

It can be verified that the above equations encounter no difficulty in calculating the effects of an element at its own control point. All the Q's are singular only on the sides of the element. For z = 0, all the J's vanish. Thus φ, V_x, and V_y are regular functions, and for z = 0

$$V_z = \text{sgn}(z) \, \Delta\theta, \quad (1.48)$$

Which is 2π sgn(z) for a point on the element and zero for a point outside the element. From the discussion in Section 1.1 the control point was defined to have $z = 0_+$. Therefore, $\Delta\theta$ can be evaluated easily; it is 2π if R_{12}, R_{23}, R_{34}, and R_{41} are all positive, and it is zero otherwise.

Eqs. (1.40-1.47) are the required equations for calculating the potential and velocity matrices $\underline{\underline{B}}$ and $\underline{\underline{C}}$, respectively. The entries of matrices $\underline{\underline{B}}$ and $\underline{\underline{C}}$ can be calculated using these equations without any further approximation. However, evaluation of Eq. (1.43) requires at least four logarithms, four inverse tangents, and four square roots for each element. For three-dimensional arbitrary bodies the computational time required for calculating the velocity and potential matrices can be prohibitively large. The complication comes from the fact that the above formulas take into account of all the details of the shape of the element. Incidentally, if the receiver point (x, y, z) is located sufficiently far away from the source element, the shape of the source element becomes less significant. Thus if a point (x, y, z) is located at a distance r_o from the source element, where r_o is the distance between the centroid of the source element and the point (x, y, z) (Fig. 1.10), and if the ratio $r_o / d_{max} > 2.45$ (d_{max} is the maximum dimension of the element as defined in Fig. 1.5), Eq. (1.20) can be approximate by expanding the integrand about r_o in terms of Taylor series expansion (Ref. 12). Since r was defined as $[(x - \xi)^2 + (y - \eta)^2 + z^2]^{1/2}$, Eq. (1.20) can be rewritten as

$$\varphi(x, y, z) = \int_S [(x - \xi)^2 + (y - \eta)^2 + z^2]^{-1/2} \, dA \, . \qquad (1.49)$$

From any standard calculus text book the formula of Taylor series expansion for two variables is

$$\begin{aligned} f(x_o + \Delta x, y_o + \Delta y) = {} & f(x_o, y_o) + (\Delta x \frac{\partial}{\partial x} + \Delta y \frac{\partial}{\partial y}) f(x_o, y_o) + \\ & \frac{1}{2!} (\Delta x \frac{\partial}{\partial x} + \Delta y \frac{\partial}{\partial y})^2 f(x_o, y_o) + \ldots + \\ & \frac{1}{n!} (\Delta x \frac{\partial}{\partial x} + \Delta y \frac{\partial}{\partial y})^n f(x_o + m \Delta x, y_o + m \Delta y) \end{aligned}$$

$$0 \le m \le 1. \qquad (1.50)$$

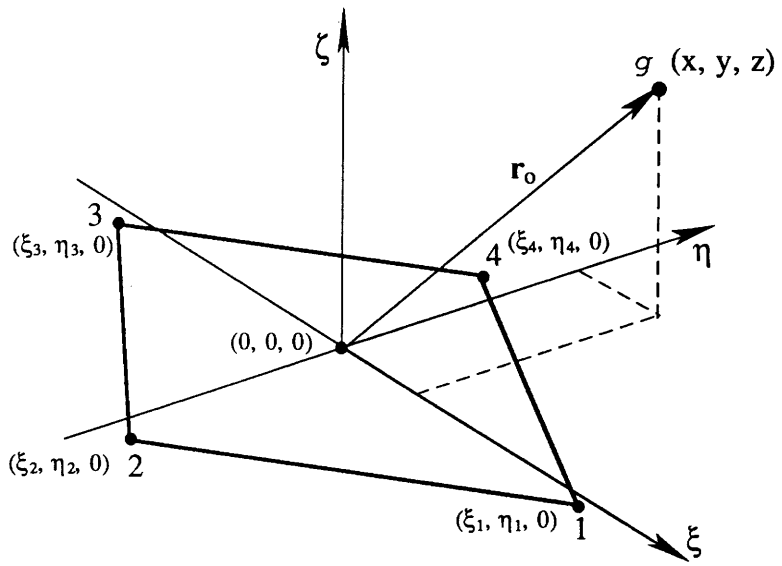

Figure 1.10 Location of the point (x, y, z) from the origin.

Applying Eq. (1.50) to the integrand of Eq. (1.49):

$$\varphi = \int_S \{\frac{1}{r_o} + [\xi \frac{\partial}{\partial x}(\frac{1}{r_o}) + \eta \frac{\partial}{\partial y}(\frac{1}{r_o})] + \frac{1}{2!}[\xi^2 \frac{\partial^2}{\partial x^2}(\frac{1}{r_o}) +$$

$$2\,\xi\,\eta \frac{\partial^2}{\partial x \partial y}(\frac{1}{r_o}) + \eta^2 \frac{\partial^2}{\partial y^2}(\frac{1}{r_o})] + \ldots\} \, dA \qquad (1.51)$$

$$= \int_S (\frac{1}{r_o}) \, dA + \int_S [\xi \frac{\partial}{\partial x}(\frac{1}{r_o}) + \eta \frac{\partial}{\partial y}(\frac{1}{r_o})] \, dA +$$

$$\frac{1}{2!}\int_S [\xi^2 \frac{\partial^2}{\partial x^2}(\frac{1}{r_o}) + 2\,\xi\,\eta \frac{\partial^2}{\partial x\,\partial y}(\frac{1}{r_o}) + \eta^2 \frac{\partial^2}{\partial y^2}(\frac{1}{r_o})] \, dA + \ldots, \qquad (1.52)$$

or

$$\varphi \approx I_{00}\, w - (I_{10}\, w_x + I_{01}\, w_y) + \frac{1}{2}(I_{20}\, w_{xx} +$$

$$2 I_{11} w_{xy} + I_{02} w_{yy}) + \ldots, \tag{1.53}$$

where

$$I_{mn} = \int_s \xi^m \eta^n \, dA, \tag{1.54}$$

$$w = \frac{1}{r_o} = \frac{1}{\sqrt{(x^2 + y^2 + z^2)}}, \tag{1.55}$$

and the subscripts x and y in Eq. (1.53) denote partial derivatives with respect to x and y, respectively. The integral terms I_{mn} are the moments of various orders of the area of the element about the origin. In particular, I_{00} is the area of the element, I_{10} and I_{01} are the first moments, and I_{20}, I_{11}, and I_{02} are the second moments etc. The various terms in Eq. (1.53) may be interpreted as the potentials of point singularities of various orders located at the origin. Thus the first term in Eq. (1.53) is the potential of a point source; the second group of terms is the potentials of two dipoles, whose axes lie along the x-axis and the y-axis, respectively; and the third group of terms is the potentials of the three independent point quadrupoles with axes in the xy-plane. The strengths of the singularities are the various moments of the area of the element. In actual calculation the series is truncated after the quadrupole terms in Eq. (1.53). Since the origin of the coordinate system is located at the centroid of the element, the first moments I_{10} and I_{01} are identically zero. Therefore, for centroidal control points there are no dipole terms in Eq. (1.53), only a source term plus the quadrupole terms. Thus, the approximation of Eq. (1.20) may be written as

$$\varphi = I_{00} w + \frac{1}{2} (I_{20} w_{xx} + 2 I_{11} w_{xy} + I_{02} w_{yy}), \tag{1.56}$$

$$V_x = \frac{-\partial \varphi}{\partial x} = -I_{00} w_x - \frac{1}{2} (I_{20} w_{xxx} + 2 I_{11} w_{xxy} + I_{02} w_{xyy}), \tag{1.57a}$$

$$V_y = \frac{-\partial \varphi}{\partial y} = -I_{00}\, w_y - \frac{1}{2}(I_{20}\, w_{xxy} + 2\, I_{11}\, w_{xyy} + I_{02}\, w_{yyy}), \qquad (1.57b)$$

$$V_z = \frac{-\partial \varphi}{\partial z} = -I_{00}\, w_z - \frac{1}{2}(I_{20}\, w_{xxz} + 2\, I_{11}\, w_{xyz} + I_{02}\, w_{yyz}), \qquad (1.57c)$$

where w and its derivatives are

$$\begin{aligned}
w &= r_o^{-1} & w_{xxx} &= 3\, x\, (3\, f + 10\, x^2)\, r_o^{-7} \\
w_x &= -x\, r_o^{-3} & w_{xxy} &= 3\, y\, f\, r_o^{-7} \\
w_y &= -y\, r_o^{-3} & w_{xyy} &= 3\, x\, h\, r_o^{-7} \\
w_z &= -z\, r_o^{-3} & w_{yyy} &= 3\, y\, (3\, h + 10\, y^2)\, r_o^{-7} \\
w_{xx} &= -(f + 2\, x^2)\, r_o^{-5} & w_{xxz} &= 3\, z\, f\, r_o^{-7} \\
w_{xy} &= -(3\, x\, y)\, r_o^{-5} & w_{yyz} &= -15\, x\, y\, z\, r_o^{-7} \\
w_{yy} &= -(f + 2\, y^2)\, r_o^{-5} & w_{yyz} &= 3\, z\, h\, r_o^{-7} \qquad (1.58)
\end{aligned}$$

and

$$f = y^2 + z^2 - 4\, x^2, \qquad h = x^2 + z^2 - 4\, y^2.$$

The moments I_{mn} may be expressed in terms of the coordinates of the corner points of the element [remember that the ξ-axis was taken to be parallel to the vector from $(\xi_1, \eta_1, 0)$ to $(\xi_3, \eta_3, 0)$] as follows:

$$I_{00} = \frac{1}{2}(\xi_3 - \xi_1)(\eta_2 - \eta_4),$$

$$I_{20} = \frac{1}{12}(\xi_2 - \xi_1)[\eta_1 (\xi_4 - \xi_2)(\xi_1 + \xi_2 + \xi_3 + \xi_4) + (\eta_2 - \eta_4)$$

$$(\xi_1^2 + \xi_1 \xi_3 + \xi_3^2) + \xi_2 \eta_2 (\xi_1 + \xi_2 + \xi_3) - \xi_4 \eta_4 (\xi_1 + \xi_3 + \xi_4)],$$

$$I_{11} = \frac{1}{24} (\xi_3 - \xi_1) [2 \xi_4 (\eta_1^2 - \eta_4^2) - 2 \xi_2 (\eta_1^2 - \eta_2^2) + (\xi_1 + \xi_3)$$
$$(\eta_2 - \eta_4) (2 \eta_1 + \eta_2 + \eta_4)],$$

and

$$I_{02} = \frac{1}{12} (\xi_3 - \xi_1) (\eta_2 - \eta_4) [(\eta_1 + \eta_2 + \eta_4)^2 -$$
$$\eta_1 (\eta_2 + \eta_4) - \eta_2 \eta_4]. \qquad (1.59)$$

Further approximation to Eq. (1.53) can be made if the ratio r_o / d_{max} is greater than 4. For $r_o / d_{max} > 4$ the quadrupole terms [all the terms multiplied by the 1/2 in Eq. (1.53)] are insignificant. Therefore, those terms can be ignored without compromising the accuracy. The quadrilateral element may further be approximated by a point source located at its centroid. For this calculation there is no need to transform to the element coordinate system. The calculation may be performed directly in the global coordinate system. Let x_o, y_o, z_o be the global coordinates of the centroid of the element, and let x_r, y_r, z_r be the global coordinates of the receiver point. The potential and velocity components are then

$$\varphi = \frac{1}{r_o} I_{00}, \qquad (1.60)$$

$$V_x = \frac{x_r - x_o}{r_o^3} I_{00}, \qquad (1.61a)$$

$$V_y = \frac{y_r - y_o}{r_o^3} I_{00}, \qquad (1.61b)$$

$$V_z = \frac{z_r - z_o}{r_o^3} I_{00}, \qquad (1.61c)$$

where

$$r_o = \sqrt{[(x_r - x_o)^2 + (y_r - y_o)^2 + (z_r - z_o)^2]} \ . \qquad (1.61d)$$

Note that the above equations are equivalent in accuracy to a source plus a dipole (since the dipole terms = 0 for centroidal control points).

From the above analysis, it is seen that three set of formulas for calculating the potential and velocity induced by a surface element at a point in space can be used. The choice of which set of equations to used is determined solely by the value of the ratio r_o / d_{max}. If r_o / d_{max} is less than 2.45 (an arbitrary choice) then the (numerical) exact formulas Eqs. (1.40-1.48) are used; if r_o / d_{max} is greater than 2.45 but is less than 4, the multipole-expansion formulas, Eqs. (1.56-1.59), are used; and if r_o / d_{max} is greater than 4 the potential and velocity can be calculated directly in the global coordinate system with Eqs. (1.60-1.61).

1.3 Numerical Examples

Analytical added mass solutions of three-dimensional bodies are scarce owing to the lack of three-dimensional theories. Most of the existing theoretical solutions in the literature are for simple geometries such as rectangular plates, circular plates, and triangular plates etc. In order to be able to compare the numerical solutions with the analytical solutions, a square plate whose physical and material parameters as given in Table 1.1 will be used for the two examples followed.

Young's modulus	E	$= 6.895(10^{10})$ N/m^2
Poisson's ratio	ν	$= 3.000(10^{-1})$
Density	ρ	$= 7794.6$ Kg/m^3
Length	L	$= 3.048(10^{-1})$ m
Width	W	$= 3.048(10^{-1})$ m
Thickness	h	$= 3.048(10^{-3})$ m

Table 1.1 Material properties for the plate.

The computational scheme presented in Section 1.2 was programmed in FORTRAN for the solution of the added mass matrix with a minimum of six finite element grids for each case. Outputs from the program were then compared to the exact solutions. All the analytical solutions given in this section were obtained from Ref. 3. The equation for the exact natural frequencies of rectangular plates is given by

$$f_{ij} = \frac{\lambda_{ij}^2}{2\pi L^2}\sqrt{\left[\frac{E h^3}{12\,\gamma(1-\nu^2)}\right]} \quad ; \; \begin{matrix} i = 1, 2, 3,... \\ j = 1, 2, 3, ... \end{matrix} \qquad (1.62)$$

where γ = mass per unit area of the plate, i = number of half-waves in mode shape along horizontal axis, j = number of half-waves in mode shape along vertical axis, and λ_{ij} is the dimensionless frequency parameter. The dimensionless frequency parameter λ_{ij} is generally a function of the boundary conditions applied to the edges of the plate, the aspect ratio of the plate (L/W), and in certain cases Poisson's ratio (ν):

$$\lambda_{ij} = \lambda_{ij}(\text{boundary conditions, L/W, } \nu).^{5} \qquad (1.63)$$

The natural frequencies of the first six modes of rectangular plates for all 21 possible combinations of the three elementary boundary conditions on the four edges of the plates (clamped, free, simply supported) are given in Ref. 3. The following two cases with two different types of boundary conditions were chosen to demonstrate the solution procedure and the results generated by the program. [Note that number of elements in the following examples denotes the total number of elements for the full plate (without symmetry boundary conditions).]

---

[5] It is shown in Ref. 3 that λ_{ij} is independent of Poisson's ratio ν unless one or more edges of the plate are free.

CASE 1 Square Plate with Free-Free Boundary Conditions

All edges of the plate are free to vibrate for this case. The analytical solutions for the first four modes for a plate to vibrate freely in vacuum are f_{22} = 5.283 Hz, f_{13} = 7.750 Hz, f_{31} = 9.568 Hz, and f_{32} = 13.715 Hz.[6] Fig. 1.11 shows the computed first mode (f_{22}) natural frequency of the plate plotted as function of the number of elements. The numerical solution is seemed to exhibit rapid monotonic convergence from below. Note that when only one element was used to model the plate, the error is well over 60%. The reason for this large error is due to the fact that lumped mass formulation was used to calculate the structural mass matrix. For a single quadrilateral element the lumped mass approximation resulted in all the mass of the plate being concentrated in the four corner nodes; hence, the program was not able to capture the first modal vibration in this case. As the number of elements was increased, more elements (and nodes) were being distributed inside the plate and the solution converged rapidly toward the exact solution. Note that for a model of only 36 elements (6 x 6) the numerical solution is already within 2% of the exact solution. Fig. 1.12 presents the absolute error in the computed natural frequency for free vibration of the first mode. The absolute error of the numerical solution starts from 3.429 for a one-element model and decreases to less than 0.09 for a model of 10 x 10 elements.

---

[6] The subscripts are the vibration mode indices. f_{22} is the first nonrigid-body mode for a completely free plate.

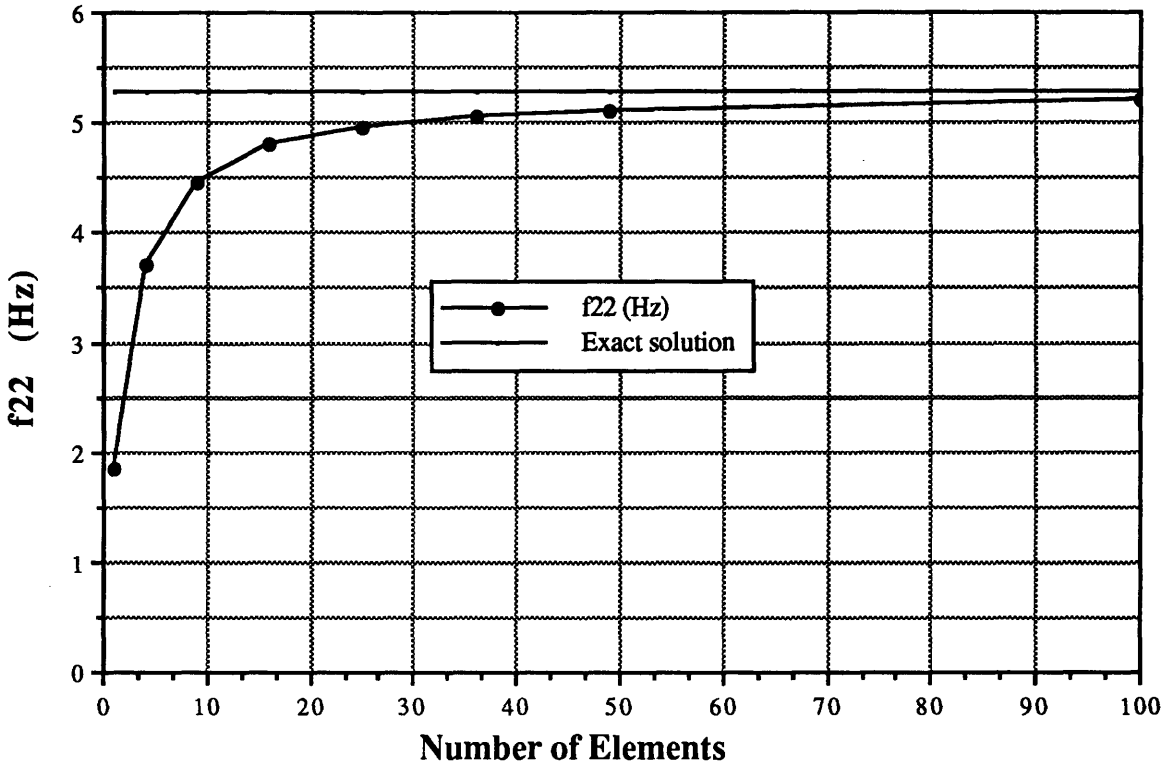

Figure 1.11 FFFF boundary conditions-first mode frequency convergence history (no added mass).

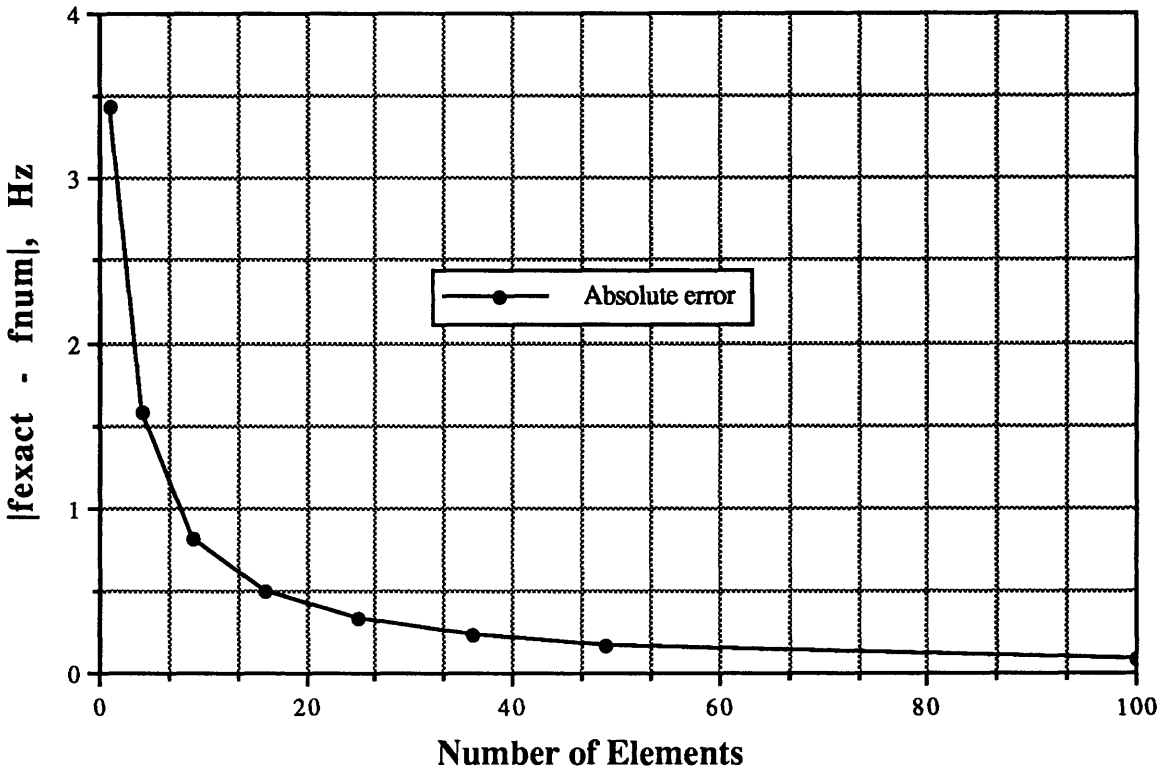

Figure 1.12 FFFF boundary conditions-first mode frequency absolute error.

The previous example was valid only for a plate vibrating freely in vacuum. As discussed in the introduction section, the surrounding fluid can alter the natural frequencies of vibration of a structure significantly if the fluid density is of the same order of magnitude as the average density of the structure. If the plate were to vibrate freely in a body of water of infinite extent, the analytical solutions for the first four modes of the natural frequencies of the plate are f_{22} = 1.485 Hz, f_{13} = 2.179 Hz, f_{31} = 2.690 Hz, and f_{32} = 3.856 Hz. Comparing these frequencies with the (in vacuum) frequencies given above, one sees that the presence of the water is indeed to have a profound effect on the natural frequencies of the plate. Fig. 1.13 shows the numerical solution of the first mode natural frequency (f_{22}) for the plate vibrating in water. The program based on the scheme presented in Section 1.2 was used to generate the added mass matrix $\underset{\sim}{M}_f$. After the added mass matrix was generated, it was combined with the structural mass matrix as shown in Eq. (1.64) to form the dynamic equilibrium equations for the structure

$$(\underset{\sim}{M}_s + \underset{\sim}{M}_f)\,\ddot{\underline{X}} + \underset{\sim}{K}_s\,\underline{X} = \underline{F} \,. \qquad (1.64)$$

In Eq. (1.64) $\underset{\sim}{M}_s$ is the structural mass matrix, $\underset{\sim}{K}_s$ is the structural stiffness matrix, and $\underline{F}$ is the force vector which may include structural damping forces as well as prescribed external forces. From Fig. 1.13, it is seen that the added mass matrix did not seem to affect the convergence rate of the finite element program at all. Note that even with the added mass matrix, the solution still exhibit monotonic convergence. For this case, the computed first mode natural frequency converged to within 1.6% of the analytical solution for a mess of 10 x 10 elements. The absolute error for this case is presented in Fig. 1.14. Comparing Figs. 1.12 and 1.14, although both plots have the same shape, the absolute error for the case with added mass decreased more rapidly and the absolute magnitude of the error decreased to less than 0.03 for a mesh of 10 x 10 elements.

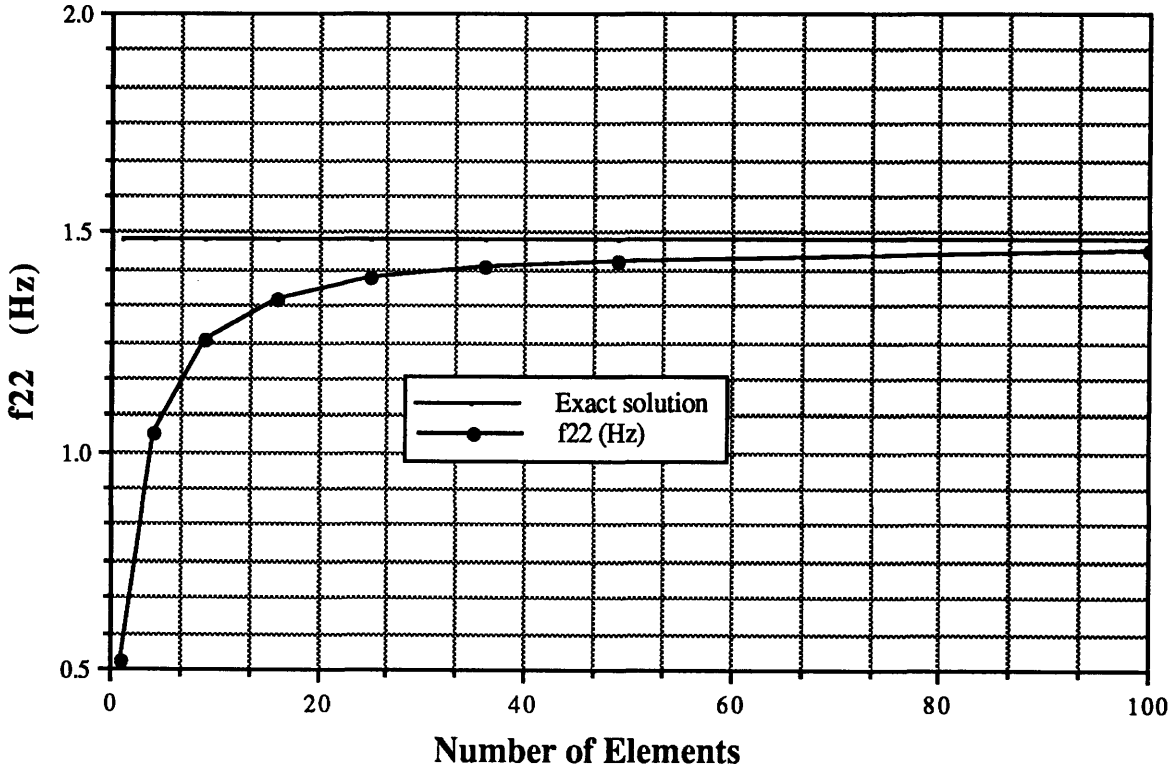

Figure 1.13 FFFF boundary conditions-first mode frequency convergence history (with added mass).

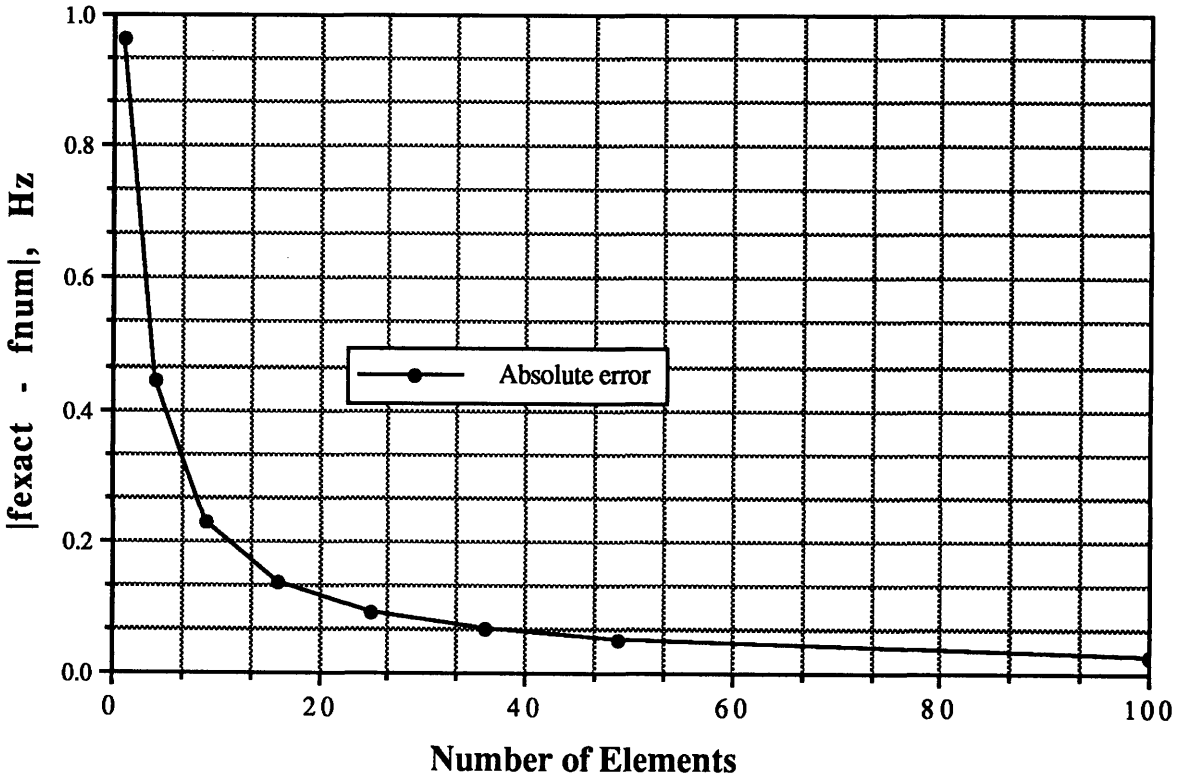

Figure 1.14 FFFF boundary conditions-first mode frequency absolute error (with added mass).

The ratios of numerical to the exact solutions (f_{num}/f_{exact}) for the first four modes are presented in Fig. 1.15. Note that only the first mode exhibits complete monotonic convergence. The other three higher modes started from above at the beginning and dropped down rapidly before converging to the exact solutions. For a model of 10 x 10 elements, the first mode converged to within 2% of the exact solution and the other three modes are only within 5%. This information can be seen more clearly in Fig. 1.16. The analytical and the converged numerical solutions (with added mass) for the first four modes of the plate are shown in Fig. 1.17. (The numerical solutions were obtained using a mesh of 10 x 10 elements.) Note that the converged numerical solutions fall almost right on top of the analytical solutions.

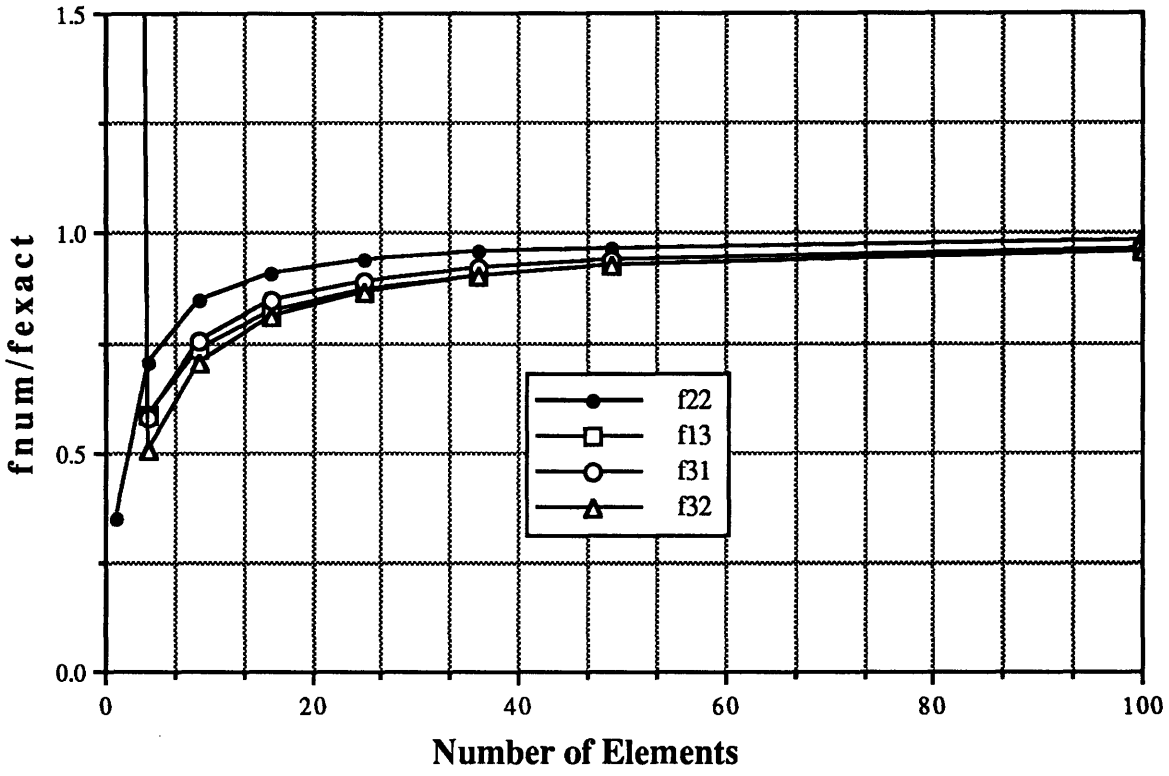

Figure 1.15 FFFF boundary conditions-modes 1-4 f_{num}/f_{exact} (with added mass).

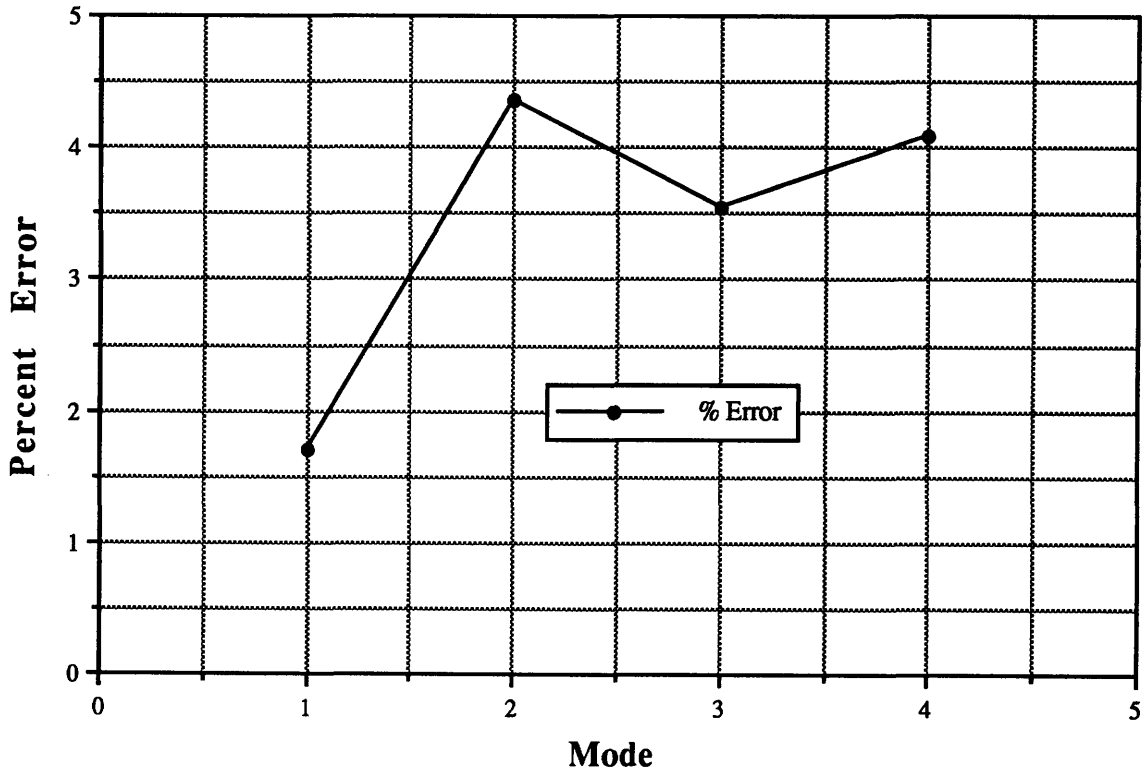

Figure 1.16 FFFF boundary conditions-modes 1-4 natural frequency percent error (with added mass).

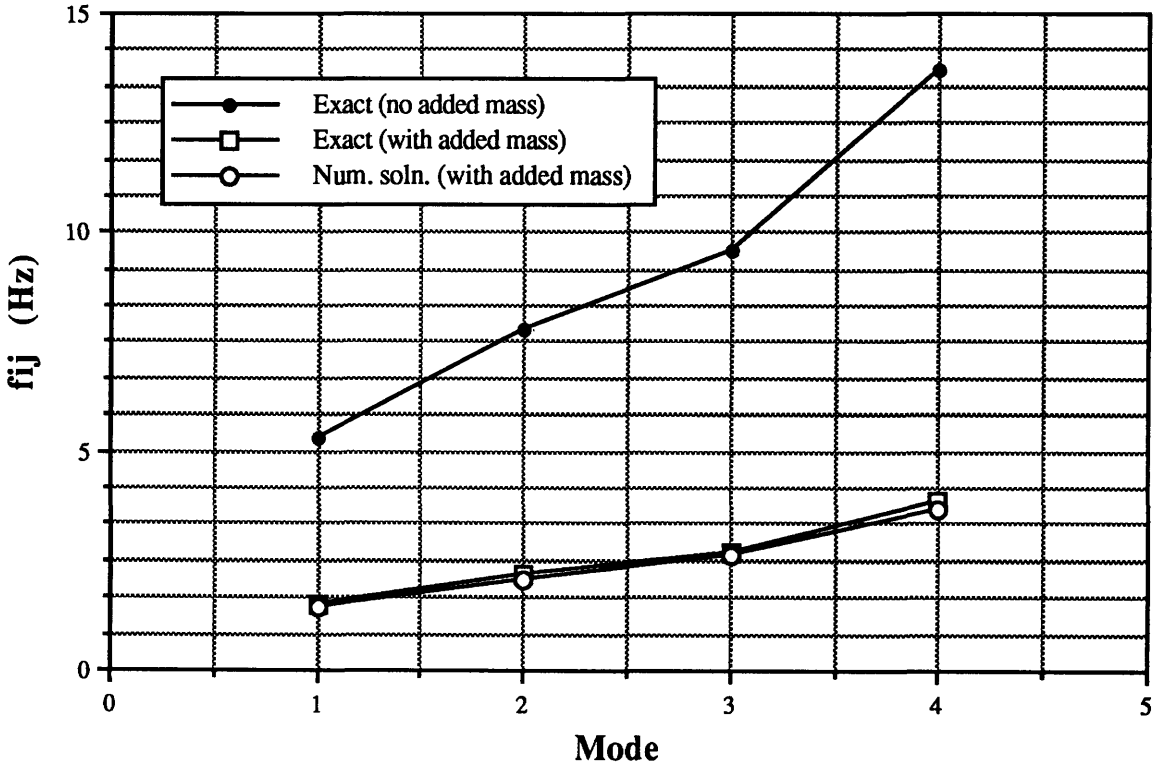

Figure 1.17 FFFF boundary conditions-modes 1-4 natural frequencies.

Fig. 1.18 compares the first mode natural frequency (f_{22}) for the cases with and without added mass. This figure shows clearly that the inertia of the water cannot be neglected for this case since the water density if of the same order of magnitude as the average structural density. A very large error will result if the inertia effect of the water is neglected when calculating the natural frequencies. Finally, Figs. 1.19 and 1.20 show the first four mode natural frequencies for a freely vibrating plate in vacuum and in water, respectively.

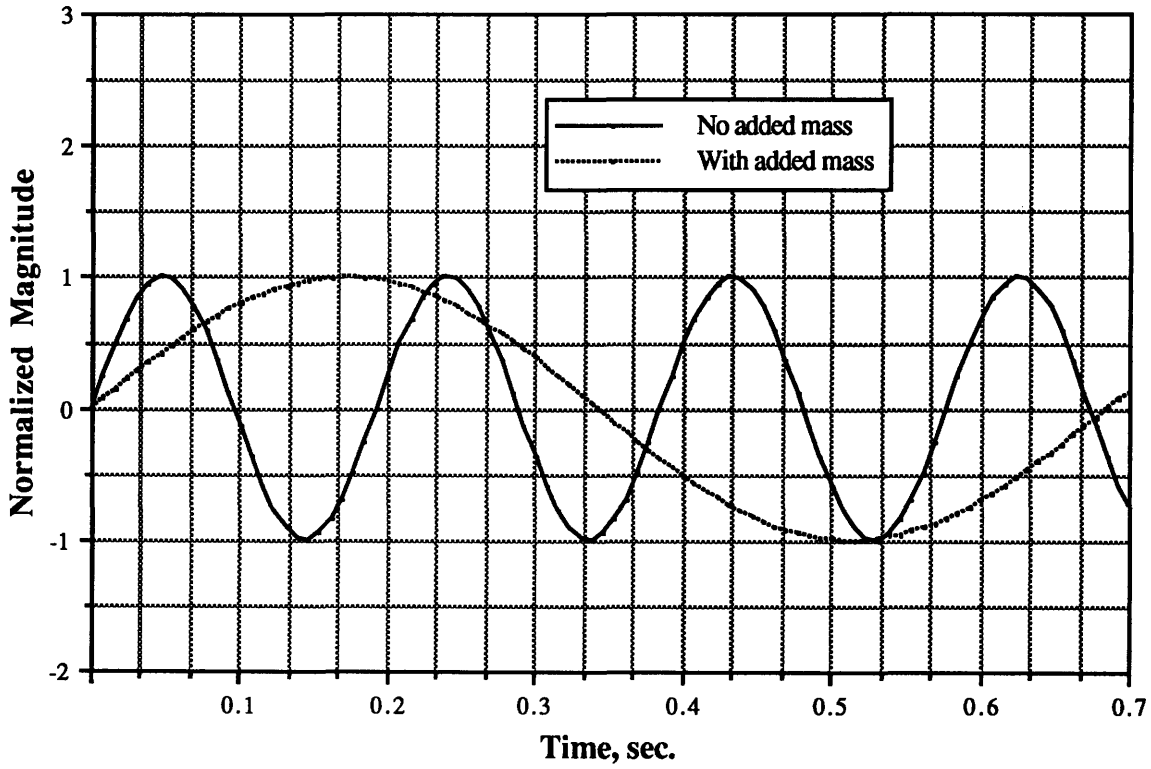

Figure 1.18 FFFF boundary conditions-first mode natural frequency with and without added mass.

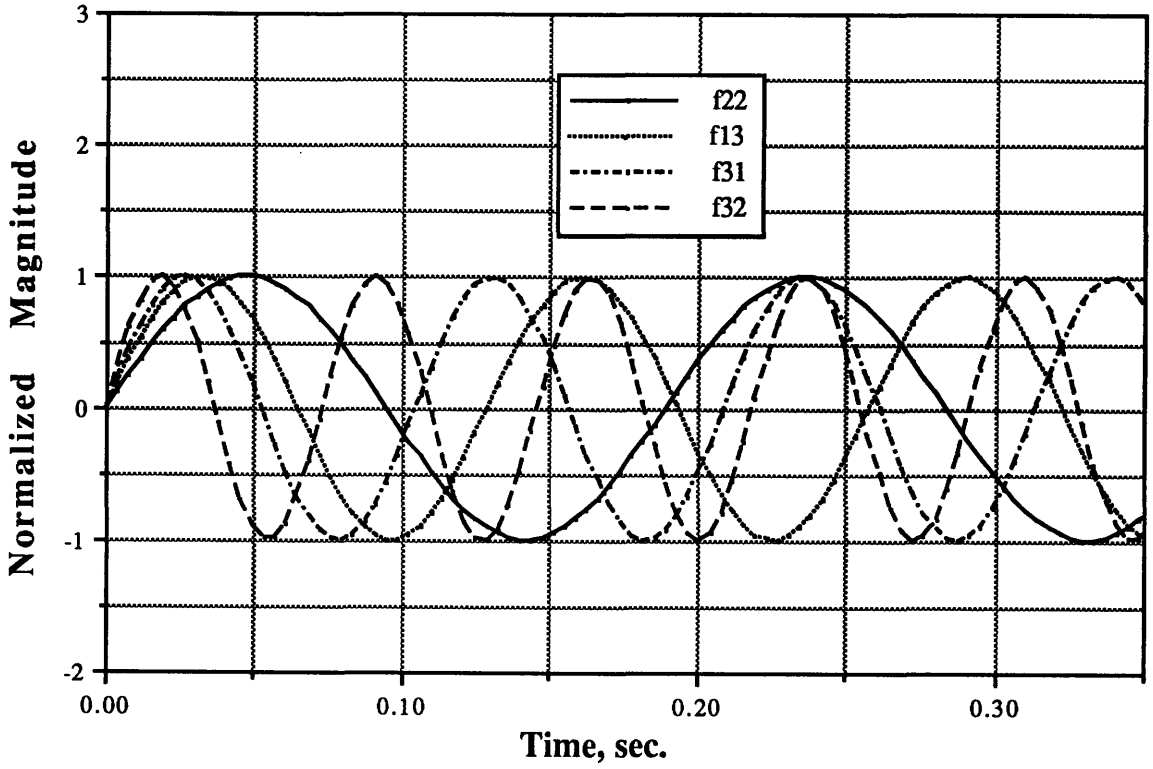

Figure 1.19 FFFF boundary conditions-modes 1-4 natural frequencies (without added mass).

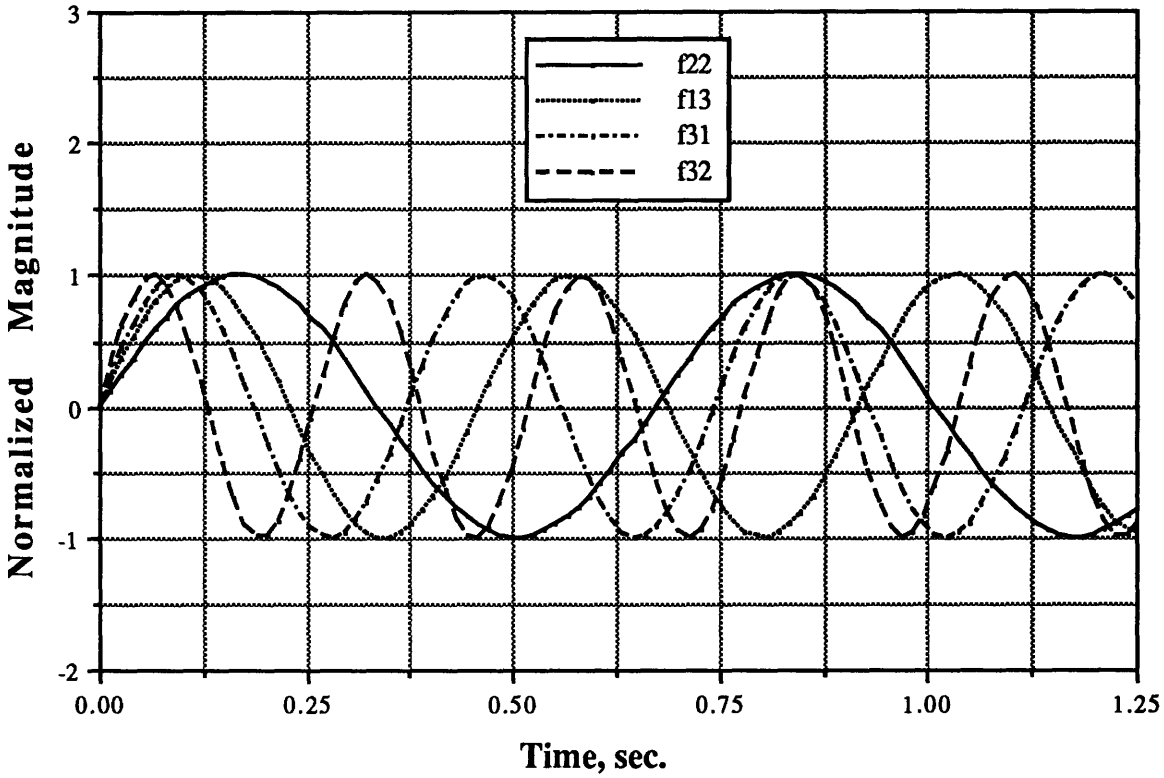

Figure 1.20 FFFF boundary conditions-modes 1-4 natural frequencies (with added mass).

CASE 2 Square Plate with Simply-Supported Boundary Conditions

For this case, all four edges are restrained from moving in all directions but are free to rotate. The (in vacuum) analytical solutions for the first four mode natural frequencies are f_{11} = 7.731 Hz, f_{21} = 19.327 Hz, f_{12} = 19.327 Hz, and f_{22} = 30.923 Hz. Note that the second and third natural frequencies are exactly identical for this set of boundary conditions. The computed first four mode natural frequencies of the plate plotted as function of the number of elements are shown in Fig. 1.21. From the figure, it is seen that all the frequencies started from above at the beginning and dropped below the exact solutions before converging. The convergence histories for the different frequencies are shown in Fig. 1.22. Unlike the previous case, the three higher modes for this set of boundary conditions have much slower convergence rates than the first mode. For a mesh of 10 x 10 elements the first mode has converged to within 5% of the exact solution whereas the other three modes are only within 20% of the exact solutions (see Fig. 1.23). Again, this could be due to the lumped mass formulation of the structural mass matrix and the more complicate boundary conditions. For lumped mass formulation, particle "lumps" have no rotary inertia.[7] The importance of rotary inertia generally increases with increasing mode number; however, these effects are generally insignificant for plates whose thickness is less than 1/10 of the plate length for vibrations in the fundamental mode. Looking at the trend of the converging history plots, one would expect those three higher modes to converge to their exact solutions as more elements are to be used in the model. For this set of boundary conditions, if the plate were to vibrate in water the natural frequencies of the plate are f_{11} = 1.657 Hz, f_{21} = 4.141 Hz, f_{12} = 4.141 Hz, and f_{22} = 6.626 Hz. Fig. 1.24 shows the convergence histories for the case with added mass. Unlike Case 1, with the added mass matrix the convergence histories for the various modes changed slightly for this case. The first mode exhibits monotonic convergence with added mass, but the added mass did not seem to have any effect on the second and third modes. Fig. 1.25 shows the ratios of the

---

[7] Rotary inertia is the inertia associated with local rotation of the plate as it flexes.

computed frequencies to the exact solutions. For some reason, the added mass matrix seems to improve the overall rates of convergence of all the modes for this case. Fig. 1.26 compares the numerical solutions to the exact solutions for the first four modes (with and without added mass). As pointed out in the above discussion, for a mesh of 10 x 10 elements the higher mode natural frequencies did not converge as completely as the first mode for the case without added mass. For the case with the added mass, the convergence rates for the higher modes are much better but they are still slower than the convergence rate of the first mode.

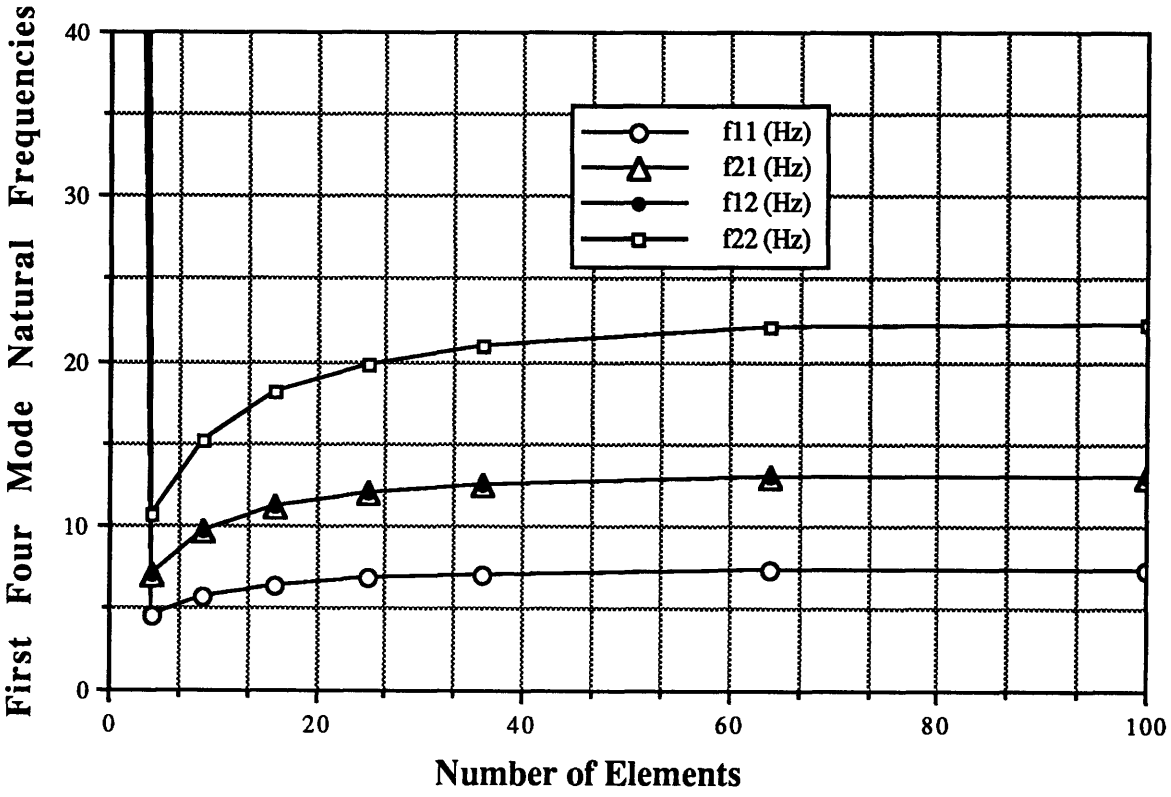

Figure 1.21 SSSS boundary conditions-modes 1-4 natural frequencies (no added mass).

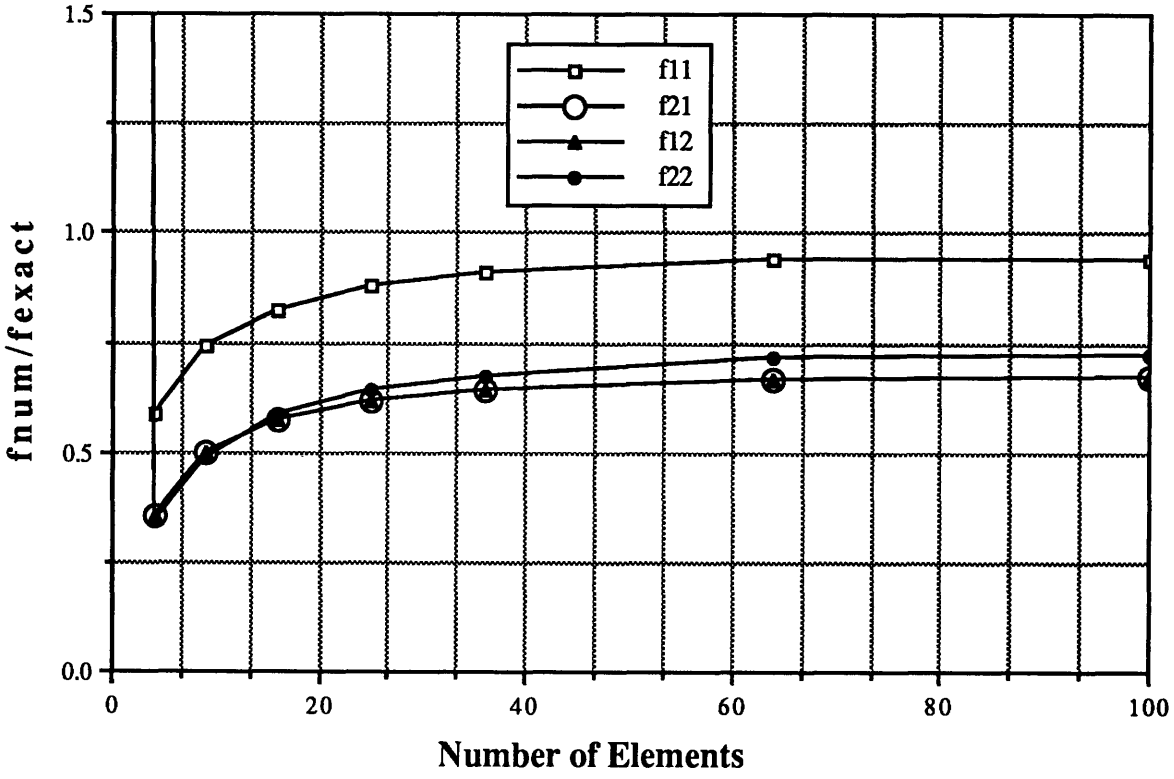

Figure 1.22 SSSS boundary conditions-modes 1-4 f_{num}/f_{exact} (no added mass).

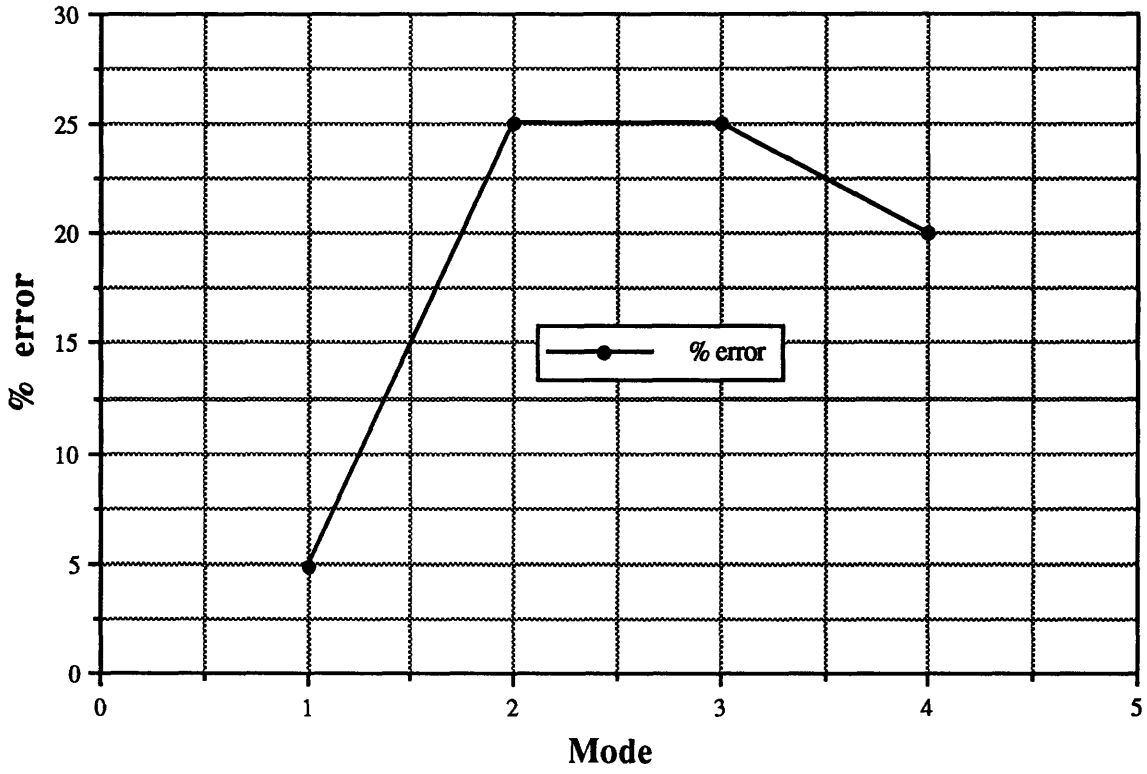

Figure 1.23 SSSS boundary conditions-modes 1-4 percent error (no added mass).

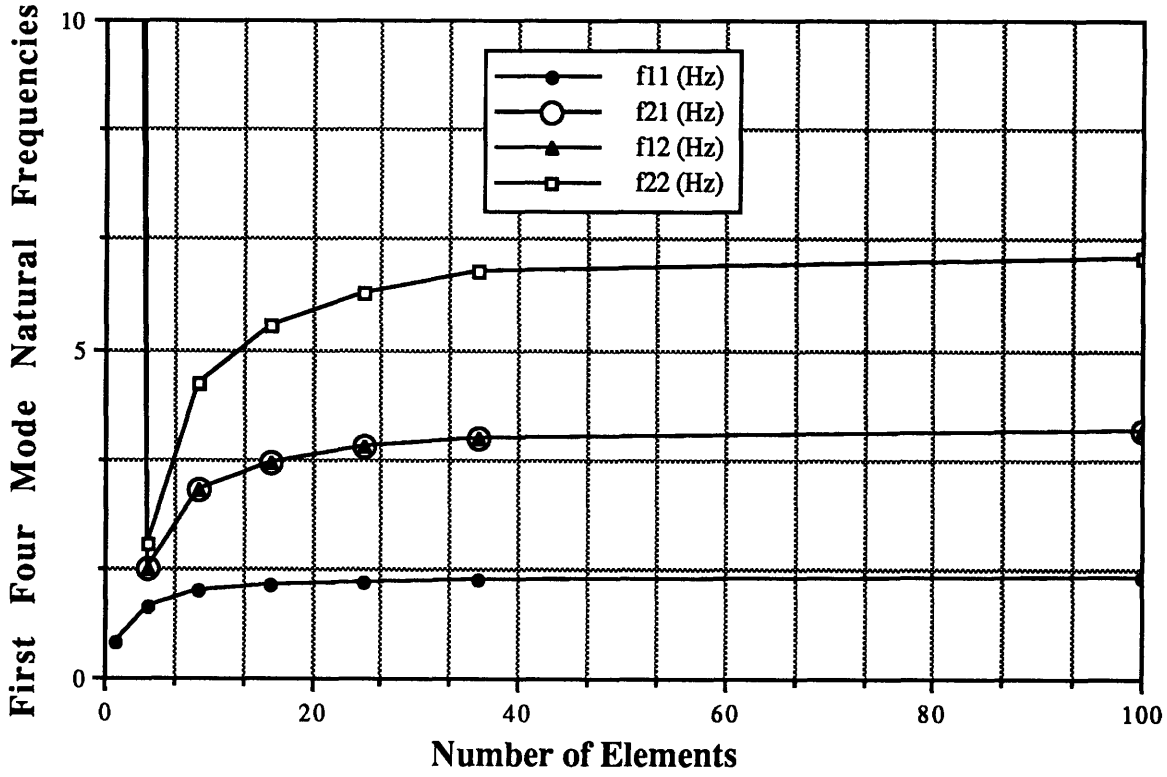

Figure 1.24 SSSS boundary conditions-modes 1-4 natural frequency convergence histories (with added mass).

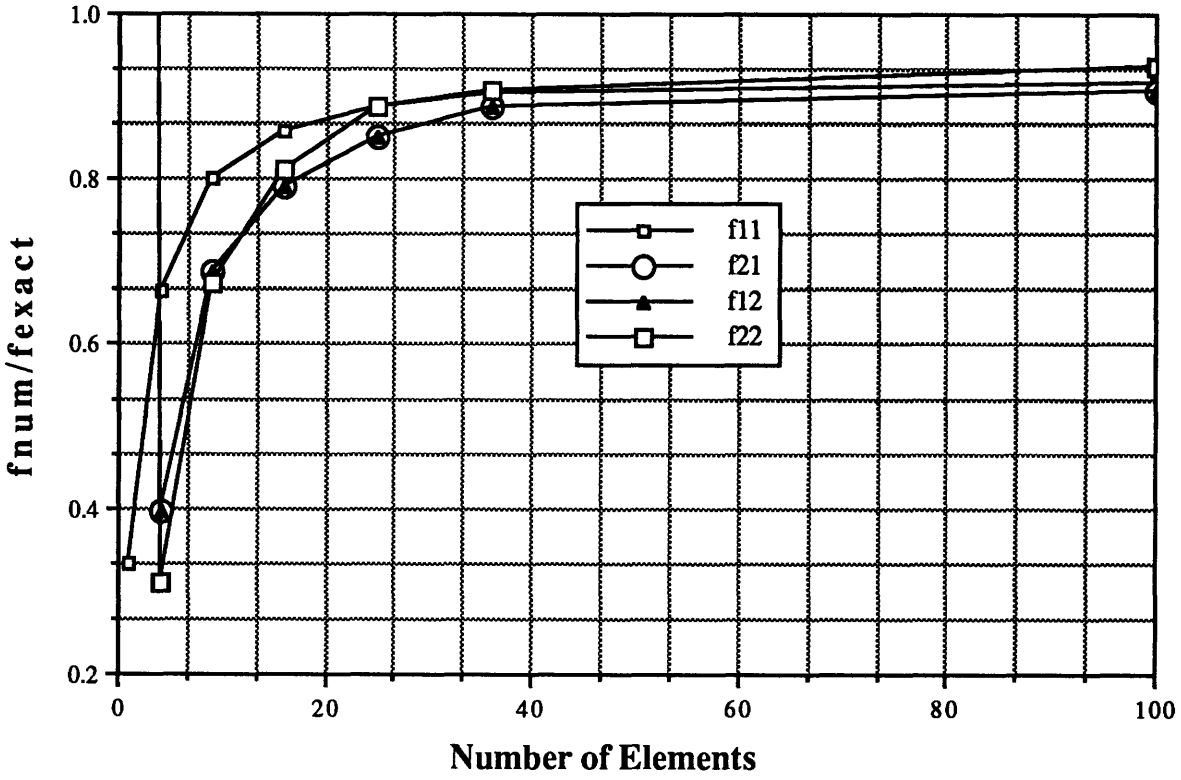

Figure 1.25 SSSS boundary conditions-modes 1-4 f_{num}/f_{exact} (with added mass).

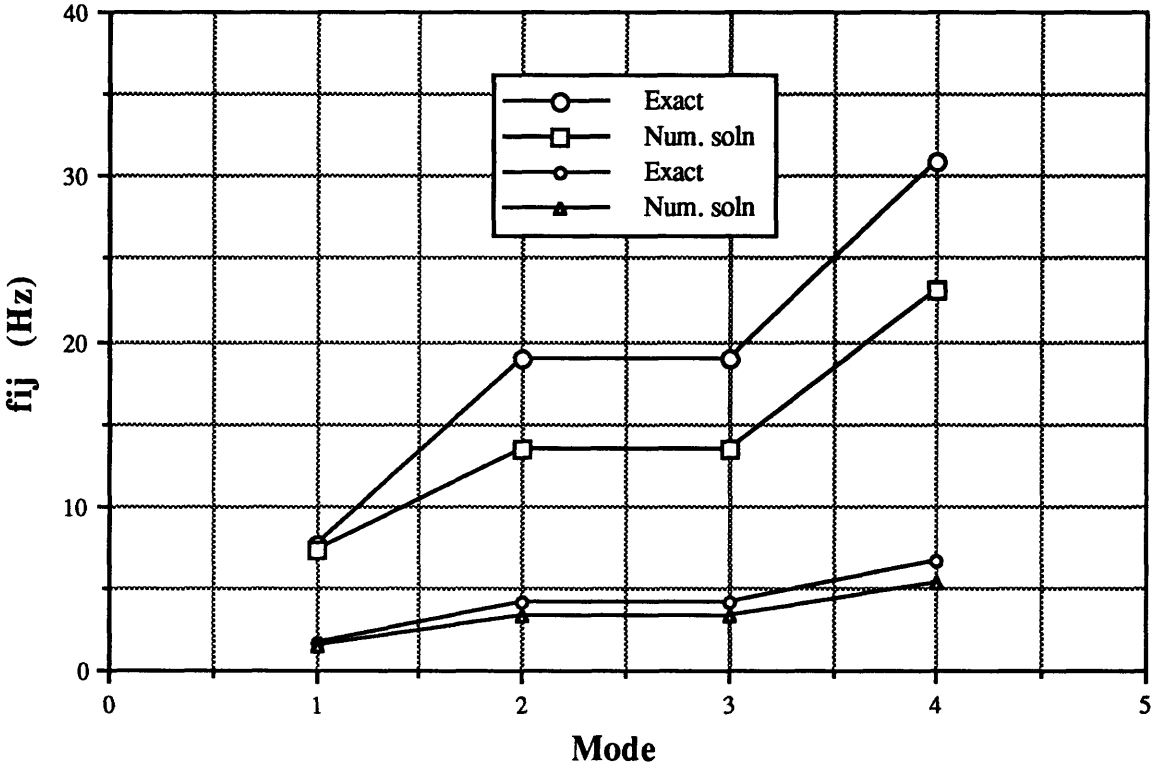

Figure 1.26 SSSS boundary conditions-modes 1-4 natural frequencies.

2. Coupling Fluid-Structure Interaction

As mentioned in the Introduction, if the frequency of excitation applied to the structure is less than roughly one-third of the structure's lowest natural frequency of vibration, then the effect of the fluid on the structure can be treated as added mass and the equation of motion for the submerged structure is

$$(\underset{\sim}{M}_s + \underset{\sim}{M}_f)\,\ddot{\underline{X}} + \underset{\sim}{K}_s\,\underline{X} = \underline{F} \qquad (2.1)$$

where $\underset{\sim}{M}_s$ is the structure mass matrix, $\underset{\sim}{M}_f$ is the fluid added mass matrix, $\underset{\sim}{K}_s$ is the structure stiffness matrix, and $\underline{F}$ is the force vector. However, the fluid can no longer be treated merely as added mass to the structure if the applied frequencies are higher than noted above. The system representing by the fluid and structure must be coupled together as at any time the behavior of one influences the other and vice versa.

In many coupled problems the system can usually be associated with a physical region of the problem. The governing equation(s) for each region can separately be written in matrix form using finite element, boundary element, or finite difference method. This separation of domain gives rise to the possibility of using different methods in treating the governing equation(s) in each domain and the resulting equations combined at the onset of solving the system of equations. For this fluid-structure interaction problem, the structure is modeled using finite elements. However, boundary elements are used to modeled the external fluid due to the ease of treating the far-field radiation boundary condition with Green's theorem. All the theories and numerical procedure for carrying out the solution procedure for this coupled problem are presented in Sections 2.1-2.3.

2.1 Dynamic Equations for the Structure

The structural dynamic equations can be derived using the variational principle. The equations are obtained by requiring the work of external forces to be equal to the work of internal, inertial, and viscous forces for any small kinematically admissible motion; that is, any small motion that satisfies both compatibility and essential boundary conditions (Refs. 6, 7). For a single element, the work balance becomes

$$\int_{V_e} \left[\underline{\delta u}^T \underline{F}\right] dV + \int_{S_e} \left[\underline{\delta u}^T \underline{\Phi}\right] dS + \sum_{i=1}^{n} \left[\underline{\delta u_i}^T \underline{P_i}\right]$$

$$= \int_{V_e} \left[\underline{\delta \varepsilon}^T \underline{\sigma} + \underline{\delta u}^T \rho \, \underline{\ddot{u}} + \underline{\delta u}^T \kappa_d \, \underline{\dot{u}}\right] dV \qquad (2.2)$$

where $\underline{\delta u}$ and $\underline{\delta \varepsilon}$ are small arbitrary admissible displacements and their corresponding strains, respectively; $\underline{F}$ are the body forces; $\underline{\Phi}$ are prescribed surface tractions (which are typically nonzero over only a portion of the surface S_e); $\underline{P_i}$ are concentrated loads that act at a total of n locations on the element; $\underline{\delta u_i}^T$ is the displacement of the point at which load $\underline{P_i}$ is applied; ρ is the mass density of the material; κ_d is the material damping coefficient; and the volume integral is carried out over the element volume V_e. Using standard finite element method, the displacement field $\underline{u}$ (which is a function of both space and time) and its first and second time derivatives can be written as

$$\underline{u} = \underset{\sim}{N}\,\underline{d}, \quad \underline{\dot{u}} = \underset{\sim}{N}\,\underline{\dot{d}}, \quad \underline{\ddot{u}} = \underset{\sim}{N}\,\underline{\ddot{d}}. \qquad (2.3)$$

In the above equations the shape function $\underset{\sim}{N}$ are function of space only and the nodal degrees of freedom $\underline{d}$ are function of time only. Thus, representing the displacement field and its derivatives with Eq. (2.3) has the effect of separating the variables locally. Combining Eqs. (2.2) and (2.3) yields

$$\int_{V_e} \left[\underline{\delta d}^T \underset{\sim}{N}^T \underline{F}\right] dV + \int_{S_e} \left[\underline{\delta d}^T \underset{\sim}{N}^T \underline{\Phi}\right] dS + \sum_{i=1}^{n} \left[\underline{\delta d}^T \underline{P_i}\right]$$

$$= \int_{V_e} \left[\underline{\delta d}^T \underline{B}^T \underline{\sigma}\right] dV + \left[\int_{V_e} \left(\underline{\delta d}^T \rho \underline{N}^T \underline{N}\right) dV\right] \underline{\ddot{d}}$$

$$+ \left[\int_{V_e} \left(\kappa_d \underline{\delta d}^T \underline{N}^T \underline{N}\right) dV\right] \underline{\dot{d}}, \tag{2.4}$$

or

$$\underline{\delta d}^T \left\{\left[\int_{V_e} \left[\underline{B}^T \underline{\sigma}\right] dV\right] + \left[\int_{V_e} \left(\rho \underline{N}^T \underline{N}\right) dV\right] \underline{\ddot{d}}\right.$$

$$+ \left[\int_{V_e} \left(\kappa_d \underline{N}^T \underline{N}\right) dV\right] \underline{\dot{d}} - \int_{V_e} \left(\underline{N}^T \underline{F}\right) dV$$

$$\left. - \int_{S_e} \left(\underline{N}^T \underline{\Phi}\right) dS - \sum_{i=1}^{n} \underline{P}_i \right\} = 0 \tag{2.5}$$

where $\underline{B}$ is the strain-displacement matrix (the derivative of the shape function $\underline{N}$). In Eqs. (2.4-2.5), it has been assumed that the locations of concentrated loads $\underline{P}_i$ are coincided with nodal locations. Since $\underline{\delta d}$ is an arbitrary variation vector, Eq. (2.5) is true for any $\underline{\delta d}$ only if

$$\left[\int_{V_e} \left[\underline{B}^T \underline{\sigma}\right] dV\right] + \left[\int_{V_e} \left(\rho \underline{N}^T \underline{N}\right) dV\right] \underline{\ddot{d}}$$

$$+ \left[\int_{V_e} \left(\kappa_d \underline{N}^T \underline{N}\right) dV\right] \underline{\dot{d}} - \int_{V_e} \left(\underline{N}^T \underline{F}\right) dV$$

$$- \int_{S_e} \left(\underline{N}^T \underline{\Phi}\right) dS - \sum_{i=1}^{n} \underline{P}_i = 0. \tag{2.6}$$

or

$$\underline{m}\, \underline{\ddot{d}} + \underline{c}\, \underline{\dot{d}} + \underline{r}^{int} = \underline{r}^{ext} \tag{2.7}$$

where the element mass and damping matrices are defined as

$$\underline{\underline{m}} \equiv \int_{V_e} \left(\rho\, \underline{\underline{N}}^T \underline{\underline{N}}\right) dV \tag{2.8}$$

$$\underline{\underline{c}} \equiv \int_{V_e} \left(\kappa_d\, \underline{\underline{N}}^T \underline{\underline{N}}\right) dV\,, \tag{2.9}$$

and the elemental generalized internal force and external load vectors are defined as

$$\underline{r}^{int} \equiv \int_{V_e} \left(\underline{\underline{B}}^T \underline{\sigma}\right) dV \tag{2.10}$$

$$\underline{r}^{ext} \equiv \int_{V_e} \left(\underline{\underline{N}}^T \underline{F}\right) dV + \int_{S_e} \left(\underline{\underline{N}}^T \underline{\Phi}\right) dS + \sum_{i=1}^{n} \underline{P}_i\,. \tag{2.11}$$

The generalized internal force vector represents loads at nodal locations caused by the straining of the material. Eqs. (2.7) and (2.10) are valid for both linear and nonlinear material behavior; that is, $\underline{\sigma}$ in Eq. (2.10) could be a nonlinear function of strain (or strain rate). For linear elastic material behavior, $\underline{\sigma} = \underline{\underline{E}}\, \underline{\underline{B}}\, \underline{d}$ and Eq. (2.10) becomes

$$\underline{r}^{int} = \underline{\underline{k}}\, \underline{d} \tag{2.12}$$

where

$$\underline{\underline{k}} = \int_{V_e} \left(\underline{\underline{B}}^T \underline{\underline{E}}\, \underline{\underline{B}}\right) dV \tag{2.13}$$

is the stiffness matrix of the structure, and $\underline{\underline{E}}$ is the material property matrix. Therefore, with linear material behavior assumption Eq. (2.7) becomes

$$\underline{\underline{m}}\, \ddot{\underline{d}} + \underline{\underline{c}}\, \dot{\underline{d}} + \underline{\underline{k}}\, \underline{d} = \underline{r}^{ext}\,. \tag{2.14}$$

Global structural equations can be constructed by expansion of element matrices $\underset{\sim}{m}$, $\underset{\sim}{c}$, $\underset{\sim}{k}$, and $\underline{r}^{ext}$ to structure size as described in Ref. 6. The resulting global structure matrix equation is

$$\underset{\sim}{M}\,\ddot{\underline{D}} + \underset{\sim}{C}\,\dot{\underline{D}} + \underset{\sim}{K}\,\underline{D} = \underline{R}^{ext} \tag{2.15}$$

where $\underset{\sim}{M}$ is the global mass matrix, $\underset{\sim}{C}$ is the global (viscous) damping matrix, $\underset{\sim}{K}$ is the global stiffness matrix, and $\underline{R}^{ext}$ corresponds to loads $\underline{R}$ of a static problem but is in general a function of time.

An important special case of Eq. (2.15) is that the input forces and the responses of the system vary harmonically with time. Assume the nodal displacement vector of the structure and the input force vector have the following form:

$$\underline{D} = \underline{u}\, e^{i\omega t} \tag{2.16}$$

$$\underline{R}^{ext} = \underline{F}\, e^{i\omega t} \tag{2.17}$$

where i is the imaginary number $\sqrt{-1}$, ω is the circular excitation frequency, $\underline{F}$ are the magnitudes of the applied forces, and $\underline{u}$ are the magnitudes of the structure displacements. Substituting Eqs. (2.16) and (2.17) and the derivatives of $\underline{D}$ into Eq. (2.15), the global structure equation becomes

$$\left[\left(-\omega^2 \underset{\sim}{M} + \underset{\sim}{K}\right) + i\,\omega\,\underset{\sim}{C}\right] \underline{u}\, e^{i\omega t} = \underline{F}\, e^{i\omega t}. \tag{2.18}$$

Canceling out $e^{i\omega t}$ on both sides of Eq. (2.18), the equation of motion of the structure in the frequency domain is

$$\left[\left(-\omega^2 \underset{\sim}{M} + \underset{\sim}{K}\right) + i\,\omega\,\underset{\sim}{C}\right] \underline{u} = \underline{F}. \tag{2.19}$$

If a structure impedance is defined to be the ratio of the applied force to velocity,

$$Z_s \equiv \frac{F}{\dot{D}} = \frac{\left[\left(-\omega^2 m + K\right) + i\,\omega\,C\right] u\, e^{i\omega t}}{i\,\omega\, u\, e^{i\omega t}}, \tag{2.20}$$

then the structural impedance matrix can be written as

$$\underset{\sim}{Z}_s = \underset{\sim}{C} + (\omega \underset{\sim}{M} - \frac{\underset{\approx}{K}}{\omega}) i \qquad (2.21)$$

where $\underset{\sim}{C}$ is the resistance and $(\omega \underset{\sim}{M} - \frac{\underset{\approx}{K}}{\omega})$ can be interpreted as the structural reactance.

2.2 Governing Equations for the External Fluid

Consider the body as shown in Fig. 2.1, an arbitrary finite object whose total surface area is S is immersed in an infinite ideal homogeneous fluid. The fluid fills the region D exterior to S. The region interior to S is designated E. Thus, the total space of the problem is $D \cup S \cup E$. If the surface of the body is made to oscillate about its mean position, a force will be exerted on the fluid in contact with the surface. The fluid is hence disturbed from its equilibrium position. As a result, disturbances (acoustic waves) are produced and propagated away from the body in all directions. The propagation of the acoustic waves through the fluid is described by the homogeneous wave equation (Ref. 2)

$$\frac{1}{c^2}\frac{\partial^2 \Psi}{\partial t^2} - \nabla^2 \Psi = 0 \qquad \text{in } D, \tag{2.22}$$

where ∇^2 is the Laplacian operator. The function Ψ is the excess acoustic pressure[8] or the wave potential function at an arbitrary point $\underline{r}$ at time t in the fluid domain, and c is the speed of sound in the fluid. For a simple harmonic excitation of the form[9] $\Psi(\underline{r}, t) = P(\underline{r})\, e^{i\omega t}$, Eq. (2.22) reduces to the Helmholtz wave equation [also known as the reduced wave equation (**A-1**)]

$$\nabla^2 P(\underline{r}) + K^2 P(\underline{r}) = 0 \tag{2.23}$$

where $K = \omega/c$ is the acoustic wave number. The main problem of interest in this case is the determination of unique solutions to the excess pressure field generated by vibrating surface(s), and the problem of scattering of acoustic waves from the submerged body. In general, the excess acoustic pressure at a given point in the fluid domain can be represented as a sum of the incident pressure

---

8 Excess acoustic pressure is the change of pressure at any given point from its undisturbed hydrostatic pressure.

9 Ψ is taken as the excess pressure in this case.

and the scattered pressure (from the surfaces).[10] Thus, the total excess pressure at any given point in the fluid domain is

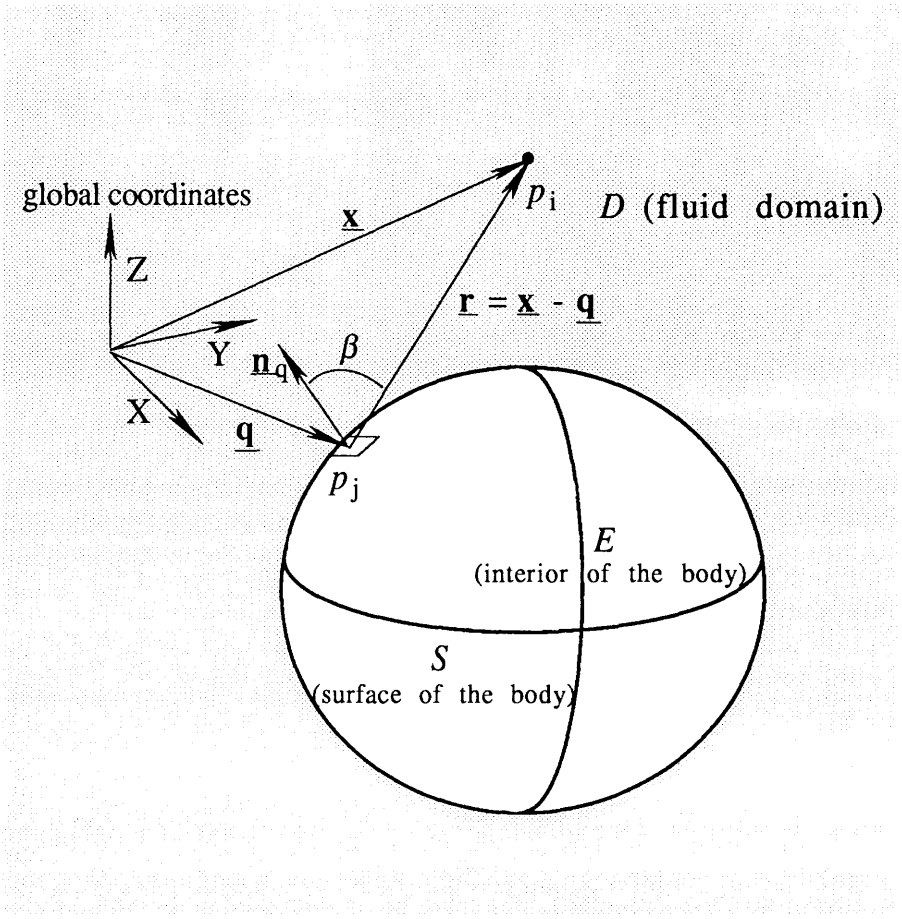

Figure 2.1 An elastic body immersed in an infinite, inviscid, incompressible fluid.

$$P(\underline{r}) = P_I(\underline{r}) + P_S(\underline{r}) \qquad (2.24)$$

where the subscripts I and S denote incident and scatter, respectively. The scatter pressure also needs to satisfy the Sommerfeld far-field radiation condition (Ref. 22)

---

10 This is true only for linear waves. For linear waves, the sum of solutions is also a solution of the problem.

$$\lim_{R\to\infty}\int_{S_R}\left|\frac{\partial P_S(\underline{r})}{\partial r}+ i\,KP_S(\underline{r})\right|^2_{r=R} dS = 0, \qquad (2.25)$$

where r is the radial distance from the origin of coordinates and S_R represents the surface of a large sphere of radius R centered at the origin and surrounded the object. The pressure field must also satisfy the Neumann boundary condition on the surface of the object

$$\frac{\partial P}{\partial n_q} \equiv \underline{n}_q \cdot \left[\nabla P(\underline{r})\right] = -i\omega\rho\,|\underline{v}(\underline{q})| \qquad \underline{q} \in S\,. \qquad (2.26)$$

For this problem, the attention is centered on finding the surface pressure since if the surface pressure is found, other useful quantities such as far-field patterns, $P(\underline{r})$, radiation efficiency of the body, and many other desired quantities can always be computed. Although Eq. (2.23) [with boundary conditions Eqs. (2.25) and (2.26)] is valid for any point in the fluid domain, it is not in a convenient form for numerical analysis of this infinite domain problem. With the help of the Green's identities, Eq. (2.23) can be recast into the form of a boundary integral equation known as the *Helmholtz integral equation for the exterior problem* (**A-2**):

$$\int_S\left[P(\underline{q})\frac{\partial G(\underline{x},\underline{q})}{\partial \underline{n}_q} - G(\underline{x},\underline{q})\frac{\partial P(\underline{q})}{\partial \underline{n}_q}\right] dS = \begin{cases} P(\underline{x})/2 - P_I & \underline{x}\in S \\ P(\underline{x}) - P_I & \underline{x}\in D \\ 0 & \underline{x}\in E \end{cases} \qquad (2.27)$$

where $G(\underline{x},\underline{q})$ is the free space Green's function[11]

$$G(\underline{x},\underline{q}) = \frac{e^{-iKr}}{4\pi r}, \qquad r = |\underline{x} - \underline{q}|, \qquad (2.28)$$

---

11 The free-space Green's function satisfies the inhomogeneous reduced wave equation $(\nabla^2 + K^2)G = -\delta(\underline{r} - \underline{r}')$.

and

$$\frac{\partial P(\underline{q})}{\partial \underline{n}_q} = -i\omega \rho_f |\underline{v}_n| . \tag{2.29}$$

In the above equation, ρ_f is the fluid density, and $|\underline{v}_n|$ is the magnitude of the outward normal velocity on the surface S. With the above two equations, Eq. (2.27) can be rewritten as

$$\int_S \left[P(\underline{q}) \frac{\partial \left(e^{-iKr}/4\pi r\right)}{\partial \underline{n}_q} - \left(\frac{e^{-iKr}}{4\pi r}\right)\left(-i\omega\rho_f |\underline{v}_n|\right) \right] dS =$$

$$\begin{cases} P(\underline{x})/2 - P_I & \underline{x} \in S \\ P(\underline{x}) - P_I & \underline{x} \in D \\ 0 & \underline{x} \in E \end{cases} \tag{2.30}$$

As shown in Fig. 2.1, $\underline{q}$ in Eq. (2.30) is the position vector of a typical point p_j on the surface S, $\underline{x}$ is the position vector for an arbitrary point p_i which may be either on the surface or in the exterior field D, and $\underline{n}_q$ is the unit outward normal at p_j. The normal derivative of Green's function appears in Eq. (2.30) is

$$\frac{\partial \left(e^{-iKr}/4\pi r\right)}{\partial n_q} = \left(\frac{e^{-iKr}}{4\pi r}\right)\left(iK + \frac{1}{r}\right) \cos(\beta) \tag{2.31}$$

where β is the angle between the unit normal $\underline{n}_q$ and the vector $\underline{r}$. Substituting Eq. (2.31) into the surface integral equation [the first of Eq. (2.30)] yields

$$\frac{P(\underline{x})}{2} - \int_S P(\underline{q}) \left[\left(\frac{e^{-iKr}}{4\pi r}\right)\left(iK + \frac{1}{r}\right) \cos(\beta) \right] dS =$$

$$i\omega\rho_f \int_S \left[\left(\frac{e^{-iKr}}{4\pi r}\right) |\underline{v}(\underline{q})_n| \right] dS + P_I. \tag{2.32}$$

Eq. (2.32) is an integral equation relating the total surface pressure P and normal velocity $\underline{v}_n$ on S. The integral on the left-hand side of Eq. (2.32) is the pressure integral and the one on the right-hand side is the velocity integral. Eq. (2.32) is the integral equation suitable for numerical computation.

Using standard boundary element method, the discretized version of Eq. (2.32) can be written as

$$\underset{\sim}{\mathbf{E}}\,\underline{\mathbf{P}} = \underset{\sim}{\mathbf{U}}\,\underline{\mathbf{v}}_n + \underline{\mathbf{P}}_I \tag{2.33}$$

where the dimension of the coefficient matrices $\underset{\sim}{\mathbf{E}}$ and $\underset{\sim}{\mathbf{U}}$ is (f × f) [with f being the fluid nodal degrees of freedom]. In the above equation $\underline{\mathbf{P}}$ is the nodal pressure vector and $\underline{\mathbf{v}}_n$ is the nodal normal velocity vector. The off-diagonal entries in the $\underset{\sim}{\mathbf{E}}$ matrix is (Ref. 10)

$$E_{ij} = -\left(\frac{e^{-iKr_{ij}}}{4\pi r_{ij}}\right)\left(iK + \frac{1}{r_{ij}}\right)(\cos(\beta_{ij}))\,A_j \qquad i \neq j \tag{2.34}$$

where A_j is the surface area assigned to the point $\underline{\mathbf{q}}_j$ and $r_{ij} = |\underline{\mathbf{x}}_i - \underline{\mathbf{q}}_j|$. Similarly, the off-diagonal entries in the $\underset{\sim}{\mathbf{U}}$ matrix is

$$U_{ij} = i\omega\rho_f \left(\frac{e^{-iKr_{ij}}}{4\pi r_{ij}}\right) A_j \qquad i \neq j. \tag{2.35}$$

Eqs. (2.34) and (2.35) are applicable only for the off-diagonal terms ($i \neq j$) in the $\underset{\sim}{\mathbf{E}}$ and $\underset{\sim}{\mathbf{U}}$ matrices, respectively. For the diagonal entries $r_{ii} = 0$, therefore, different approaches must be used in order to obtain expressions for E_{ii} and U_{ii}. Consider first the velocity integral in Eq. (2.32), assume that the normal velocity $\underline{\mathbf{v}}_n$ is constant over a small circular area of radius b_i centered at $\underline{\mathbf{x}}$, then,

$$U_{ii} = i\omega\rho_f \int_0^{2\pi}\int_0^{b_i}\left(\frac{e^{-iKr}}{4\pi r}\right) r\, dr\, d\theta \tag{2.36}$$

where b_i is chosen such that $\pi b_i^2 = A_i$, the total area assigned to point i. Evaluating the integral in Eq. (2.36) yields

$$U_{ii} = \frac{i\omega\rho_f A_i}{2\,\pi\,b_i}, \tag{2.37}$$

where $b_i = \sqrt{\left(\frac{A_i}{\pi}\right)}$.

The evaluation of the self term of the pressure integral is similar; however, the curvature of the vibrating surface at the given point must be taken into account in this case since the singularity in the pressure integral is one order higher than that of the velocity integral (Ref. 10). Assuming that the pressure P is constant over a small spherical cap locating at $\underline{x}_i$ and having mean curvature c_i and area A_i; then,

$$E_{ii} = \frac{1}{2} - \int_0^{2\pi} \int_0^{b_i} \left(\frac{e^{-iKr}}{4\,\pi\,r}\right)\left(iK + \frac{1}{r}\right)\left(\frac{-r c_i}{2}\right) r\; dr\; d\theta. \tag{2.38}$$

In Eq. (2.38) $\cos(\beta)$ has been approximated by $\frac{-\,r\,c_i}{2}$. Evaluating the integral of Eq. (2.38) yields

$$E_{ii} = \frac{1}{2} + (1 + iKb_i)\left(\frac{c_i\,A_i}{4\,\pi\,b_i}\right). \tag{2.39}$$

With Eqs. (2.34-2.39), all the entries in the fluid matrices $\underset{\sim}{E}$ and $\underset{\sim}{U}$ can be computed. In general, the above discretization procedure yields two (f × f) fluid matrices $\underset{\sim}{E}$ and $\underset{\sim}{U}$ which are fully populated, nonsymmetric, complex, and frequency dependent.

2.3 The Coupled Fluid-Structure Equations

The excess pressure on the surface of the submerged body is related to the surface normal velocity by Eq. (2.33). Assuming for now that the incident pressure is identically zero, then Eq. (2.33) becomes

$$\underset{\sim}{\mathbf{E}}\,\underline{\mathbf{P}} = \underset{\sim}{\mathbf{U}}\,\underline{\mathbf{v}}_n \,. \tag{2.40}$$

Since force is equal to pressure times the surface area, F = PA, and if a fluid impedance Z_f is defined to be the ratio of the surface force to the surface normal velocity

$$Z_f \equiv \frac{F}{v_n} \tag{2.41}$$

then the fluid impedance matrix can be written as

$$\underset{\sim}{\mathbf{Z}}_f = \underset{\sim}{\mathbf{A}}\,\underset{\sim}{\mathbf{E}}^{-1}\,\underset{\sim}{\mathbf{U}} \tag{2.42}$$

where $\underset{\sim}{\mathbf{A}}$ is a diagonal area matrix for the wet surface. The structural and fluid impedance matrices as given by Eqs. (2.21) and (2.42) cannot simply be added together to yield the impedance matrix for the submerged structure since the two matrices have different dimensions. The structure impedance matrix $\underset{\sim}{\mathbf{Z}}_s$ has dimension (S x S) where S is the total number of structural degrees of freedom and the fluid impedance matrix $\underset{\sim}{\mathbf{Z}}_f$ has dimension (f x f) where f is the total fluid number degrees of freedom[12]. Several matrix operations must be done to the impedance matrices before they can be combined. For the

---

[12] A three-dimensional finite element structure model usually has three translational and three rotational degrees of freedom per node. The total number of structural degrees of freedom S = 6 N_s where N_s = total number of nodes in the model. For non-shell structures there may be internal nodes as well as surface nodes and only the surface nodes are in contact with the fluid. Therefore, the number of fluid nodes N_f is always less than or equal to N_s with the equality holds for shell structures (without internal nodes). For the fluid, there is only one degree of freedom per node (the excess pressure at that node) and the total fluid degrees of freedom f = N_f. Hence, even for a shell structure with $N_s = N_f$, the total structural degrees of freedom S is still larger than the fluid degrees of freedom f by a factor of 6.

following analysis, the structure is assumed to be a shell (without internal nodes); hence, total number of structure nodes N_s is exactly equal to the total number of fluid nodes N_f[13]. Let $N = N_f$ (= N_s) to be defined as the total number of surface nodes of the structure, then f = N. In terms of the wet degrees of freedom of the problem, the applied force and the resulting surface normal velocities are related by

$$(\underset{\sim}{Z}_s + \underset{\sim}{Z}_f)\,\underline{v}_n = \underline{F}^{(n)} \tag{2.43}$$

where $\underset{\sim}{Z}_f$ is the fluid impedance matrix $\underset{\sim}{z}_s$ is the impedance matrix of the structure in terms of the wet degrees of freedom, $\underline{v}_n$ is the surface normal velocity vector, and $\underline{F}^{(n)}$ is the nodal normal force vector. The global structural impedance matrix $\underset{\sim}{Z}_s$ and the global force vector $\underline{F}$ (expressed in terms of all the structural degrees of freedom) are related to the reduced structural impedance matrix $\underset{\sim}{z}_s$ and the reduced normal force vector $\underline{F}^{(n)}$ by the rectangular transformation matrix $\underset{\sim}{T}$ defined by

$$\underline{F} = \underset{\sim}{T}\,\underline{F}^{(n)} \quad \text{and} \quad \underline{V} = \underset{\sim}{T}\,\underline{v}_n \tag{2.44}$$

where the dimensions of $\underline{F}$ and $\underline{F}^{(n)}$ are (S x 1) and (f x 1), respectively. $\underset{\sim}{T}$ is an (S x f) rectangular matrix of directional cosines which transforms $\underline{F}^{(n)}$ to $\underline{F}$. In terms of the total structure degrees of freedom

$$\underset{(S \times S)}{\underset{\sim}{Z}_s}\ \underset{(S \times 1)}{\underline{V}} = \underset{(S \times 1)}{\underline{F}}\,. \tag{2.45}$$

Solving for the velocity vector $\underline{V}$ in Eq. (2.45):

$$\underline{V} = \underset{\sim}{Z}_s^{-1}\,\underline{F}\,. \tag{2.46}$$

Substituting Eq. (2.44) into Eq. (2.46), the following Eq. is obtained

---

13 For a general structure, there are internal nodes as well as surface nodes. In this case, the surface nodes of the structure impedance matrix must be condensed out first by using the method of static condensation (Ref. 6) before performing the matrix operations presented in this section.

$$\underline{V} = \underset{\sim}{Z}_s^{-1}\, \underset{\sim}{T}\, \underline{F}^{(n)}. \tag{2.47}$$

Since $\underline{V} = \underset{\sim}{T}\, \underline{v}_n$, then

$$\underset{\sim}{T}\, \underline{v}_n = \underset{\sim}{Z}_s^{-1}\, \underset{\sim}{T}\, \underline{F}^{(n)} \tag{2.48}$$

or[14]

$$\underline{v}_n = \underset{\sim}{T}^T \underset{\sim}{Z}_s^{-1}\, \underset{\sim}{T}\, \underline{F}^{(n)}. \tag{2.49}$$

For the reduced structure matrix $\underset{\sim}{z}_s$,

$$\underset{\sim}{z}_s\, \underline{v}_n = \underline{F}^{(n)} \tag{2.50}$$

or

$$\underline{v}_n = \underset{\sim}{z}_s^{-1}\, \underline{F}^{(n)}. \tag{2.51}$$

Therefore,

$$\underset{\sim}{T}\, \underline{v}_n = \underset{\sim}{T}\, \underset{\sim}{z}_s^{-1}\, \underline{F}^{(n)}. \tag{2.52}$$

Combining Eqs. (2.48) and (2.52) yields

$$\underset{\sim}{Z}_s^{-1}\, \underset{\sim}{T}\, \underline{F}^{(n)} = \underset{\sim}{T}\, \underset{\sim}{z}_s^{-1}\, \underline{F}^{(n)}. \tag{2.53}$$

Premultiplying both sides of Eq. (2.53) by $\underset{\sim}{T}^T$, Eq. (2.53) becomes

$$\underset{\sim}{T}^T \underset{\sim}{Z}_s^{-1}\, \underset{\sim}{T}\, \underline{F}^{(n)} = \underset{\sim}{T}^T \underset{\sim}{T}\, \underset{\sim}{z}_s^{-1}\, \underline{F}^{(n)} \tag{2.54}$$

or

$$\underset{\sim}{T}^T \underset{\sim}{Z}_s^{-1}\, \underset{\sim}{T} = \underset{\sim}{z}_s^{-1}. \tag{2.55}$$

---

[14] Note that the inverse of the transformation matrix is equal to its transpose (see Ref. 6).

Solving for the normal velocity vector of Eq. (2.40) and substituting the result into Eq. (2.43) yields

$$(\underset{\sim}{Z}_s + \underset{\sim}{Z}_f)(\underset{\sim}{U}^{-1}\,\underset{\sim}{E}\,\underline{P}) = \underline{F}^{(n)} \tag{2.56}$$

or

$$(\underset{\sim}{Z}_s\,\underset{\sim}{U}^{-1}\,\underset{\sim}{E}\,\underline{P} + \underset{\sim}{Z}_f\,\underset{\sim}{U}^{-1}\,\underset{\sim}{E}\,\underline{P}) = \underline{F}^{(n)}. \tag{2.57}$$

Substituting Eq. (2.42) for $\underset{\sim}{Z}_f$ in the above equation yields

$$(\underset{\sim}{Z}_s\,\underset{\sim}{U}^{-1}\,\underset{\sim}{E}\,\underline{P} + (\underset{\sim}{A}\,\underset{\sim}{E}^{-1}\,\underset{\sim}{U})\,\underset{\sim}{U}^{-1}\,\underset{\sim}{E}\,\underline{P}) = \underline{F}^{(n)}. \tag{2.58}$$

Simplifying Eq. (2.58)

$$(\underset{\sim}{Z}_s\,\underset{\sim}{U}^{-1}\,\underset{\sim}{E}\,\underline{P} + \underset{\sim}{A}\,\underline{P}) = \underline{F}^{(n)}$$

$$(\underset{\sim}{U}^{-1}\,\underset{\sim}{E}\,\underline{P} + \underset{\sim}{Z}_s^{-1}\,\underset{\sim}{A}\,\underline{P}) = \underset{\sim}{Z}_s^{-1}\,\underline{F}^{(n)}$$

$$(\underset{\sim}{U}^{-1}\,\underset{\sim}{E}\,\underline{P} + \underset{\sim}{Z}_s^{-1}\,\underset{\sim}{A}\,\underline{P}) = (\underset{\sim}{T}^T\,\underset{\sim}{Z}_s^{-1}\,\underset{\sim}{T})\,\underline{F}^{(n)}$$

$$(\underset{\sim}{U}^{-1}\,\underset{\sim}{E}\,\underline{P} + \underset{\sim}{Z}_s^{-1}\,\underset{\sim}{A}\,\underline{P}) = \underset{\sim}{T}^T\,\underset{\sim}{Z}_s^{-1}\,\underline{F}$$

$$(\underset{\sim}{E}\,\underline{P} + \underset{\sim}{U}\,\underset{\sim}{T}^T\,\underset{\sim}{Z}_s^{-1}\,\underset{\sim}{T}\,\underset{\sim}{A}\,\underline{P}) = \underset{\sim}{U}\,\underset{\sim}{T}^T\,\underset{\sim}{Z}_s^{-1}\,\underline{F}.$$

Grouping the terms and rearranging the equation:

$$(\underset{\sim}{E} + \underset{\sim}{U}\,\underset{\sim}{T}^T\,\underset{\sim}{Z}_s^{-1}\,\underset{\sim}{T}\,\underset{\sim}{A})\,\underline{P} = \underset{\sim}{U}\,\underset{\sim}{T}^T\,\underset{\sim}{Z}_s^{-1}\,\underline{F}, \tag{2.59}$$

or

$$\underset{\sim}{H}\,\underline{P} = \underline{Q} \tag{2.60}$$

where

$$\underset{\sim}{H} \equiv (\underset{\sim}{E} + \underset{\sim}{U}\,\underset{\sim}{T}^T\,\underset{\sim}{Z}_s^{-1}\,\underset{\sim}{T}\,\underset{\sim}{A}) \tag{2.61}$$

and

$$\underline{Q} \equiv (\underset{\sim}{U}\,\underset{\sim}{T}^T\,\underset{\sim}{Z}_s^{-1}\,\underline{F}) \tag{2.62}$$

where matrices $\underline{\underline{E}}$, $\underline{\underline{U}}$, and $\underline{\underline{A}}$ have dimension (f × f), $\underline{\underline{Z}}_s$ has dimension (S × S), $\underline{\underline{T}}$ has dimension (S × f), and $\underline{F}$ has dimension (S × 1). If scattering problems are to be considered, an incident pressure vector needed to be added to the right-hand side of Eq. (2.62), that is,[15]

$$\underline{\underline{H}}\,\underline{P} = \underline{Q} + \underline{P}_I \,. \tag{2.63}$$

Since the matrix $\underline{\underline{H}}$ and vector $\underline{Q}$ depend only on geometry, material properties, and frequencies, Eq. (2.60) [or (2.63)] may be solved to yield the surface excess pressure $\underline{P}$. After the surface pressure $\underline{P}$ is obtained, surface normal velocity may then be calculated using the following equation:

$$\underline{v}_n = \underline{\underline{T}}^T \underline{\underline{Z}}_s^{-1} \underline{F} - \underline{\underline{T}}^T \underline{\underline{Z}}_s^{-1} \underline{\underline{T}}\,\underline{\underline{A}}\underline{P} \,. \tag{2.64}$$

After the surface excess pressure vector $\underline{P}$ and the surface normal velocity vector $\underline{v}_n$ are obtained, the process of obtaining the surface solution is completed. All the far-field properties can be obtained by integrating the surface quantities using the second integral of Eq. (2.30).

---

15 Again, this is possible because only linear waves are considered.

2.4 Frequency Limitations

With the present boundary integral formulations, it is well known that the surface Helmholtz integral equation has nonunique or nonexistence solutions if the excitation frequencies correspond to the eigenvalues of the interior Dirichlet problem of the same structure. This nonuniqueness or nonexistence of solutions does not have any physical significance. It simply implies that the integral equation formulation is not valid at frequencies that are characteristic of the associated interior Dirichlet problem. The fluid matrices $\underset{\sim}{\mathbf{E}}$ and $\underset{\sim}{\mathbf{U}}$ in Eqs. (2.61) and (2.62) are either singular or poorly conditioned at these critical frequencies. Hence, poor results should be expected when the excitation frequency approaches one of these critical frequencies of the structure. For spheres, the lowest critical frequency occurs at $Ka = \pi$, while for long cylinders with flat ends the lowest critical frequency occurs at $Ka \approx 2.4$, where $K = \omega/c$ is the acoustic wave number and a is the radius of the sphere or cylinder. Many methods have been developed to circumvent the problem of nonuniqueness at characteristic frequencies. Some of these well-known methods are the *combined Helmholtz integral formulation* (CHIEF) first proposed by Schenck (Ref. 19) and the *composite outward normal derivative overlap relation* (CONDOR) developed by Burton and Miller (Ref. 4).

2.5 Numerical Example----Far-field Acoustic Radiation From a Uniformly Driven Spherical Shell

In this section a classical radiation problem in acoustic is solved numerically on a computer using the equations presented in Sections 2.1-2.3. Numerical outputs generated by the program are compared to the closed-form analytic solution.

The problem to be solved is an elastic spherical shell immersed in an inviscid fluid of infinite extent. The shell is subjected to an internal spherically-symmetric, harmonically oscillating pressure load. For this classical problem, there exists an analytic solution (Ref. 10).

Analytic Solution

For a given shell, the stiffness of the shell is given by

$$K_s = \frac{(8 \pi E h)}{1 - \nu} \tag{2.65}$$

where E and ν are the Young's modulus and Poisson's ratio, respectively; and h is the shell thickness. The mass of the shell is

$$m_s = 4 \pi a^2 h \rho_s \tag{2.66}$$

where a is the mean radius of the shell and ρ_s is the material density. With a uniform internal pressure load the structure impedance is

$$Z_s = \frac{(\omega^2 m_s - K_s) i}{\omega} \tag{2.67}$$

where ω is the angular frequency of excitation (in Rad/s). For the fluid in contact with the surface of the shell, the ratio of surface pressure to surface normal velocity is

$$\frac{P}{v_n} = \frac{(\omega \rho_f a) i}{1 + i (Ka)} \tag{2.68}$$

where ρ_f is the density of the fluid, and $K = \omega/c$ is the wave number. Therefore, the fluid impedance is given by

$$Z_f = \frac{(4 \pi \omega \rho_f a^3) i}{1 + i (Ka)}, \tag{2.69}$$

and the surface normal velocity is

$$v_n = \frac{(4 \pi a^2 P_o)}{(Z_s + Z_f)} \tag{2.70}$$

where P_o is the amplitude of the internal pressure. Hence, for a given shell and a given internal drive pressure P_o, the surface normal velocity can be computed using Eq. (2.70). After the surface normal velocity is obtained, surface pressure can be calculated using Eq. (2.68). The excess pressure at any point in the fluid domain is then

$$P_r = P \left(\frac{a}{r}\right) e^{-iK(r-a)} \tag{2.71}$$

where P_r is the excess pressure at a given point a distance **r** from the origin and P is the pressure on the surface of the sphere.

Numerical Solution

The spherical shell used for this example problem has the following geometric and material properties:

shell radius	a	= 1.000 m
shell thickness	h	= $5.000(10^{-3})$ m
Young's modulus	E	= $2.070(10^{11})$ N/m^2
Poisson's ratio	ν	= $3.000(10^{-1})$
fluid density	ρ_f	= $1.000(10^3)$ kg/m^3
structure density	ρ_s	= $7.669(10^3)$ kg/m^3
internal pressure	P_o	= $1.000(10^5)$ N/m^2.

Table 2.1 Material properties for the shell.

An octant of the shell was modeled using four-noded quadrilateral elements (three planes of symmetry were imposed). A total of six meshes were run in order to obtain the convergence history plots. The octant model with the finest mesh has 243 surface elements, 271 grid points, and a total of 1626 structural degrees of freedom. Figs. (2.2-2.5) present the convergence histories of the surface pressures as function of the nondimensional wave number Ka (K = ω/c is the acoustic wave number and a is the radius of the sphere). From these figures, it is seen that the surface pressures converge monotonically from below except for Ka = 1.0. Despite the nonmonotonic convergence rate, the surface pressure for Ka = 1.0 still converges much quicker than the other three higher frequency modes as the mesh is refined. The frequency with the slowest convergence rate is Ka = 3.0. As discussed in Section 2.4, this is to be expected since the first critical frequency for a spherical shell occurs at Ka = π (3.1416). For excitation frequencies which are close to the critical frequencies, the fluid matrices $\underset{\sim}{E}$ and $\underset{\sim}{U}$ in Eqs. (2.61) and (2.62) become poorly conditioned (these two matrices become singular at the critical frequencies). Hence, the convergence rates for drive frequencies which are close to the critical frequencies should not be expected as good as the other drive frequencies which are far away from the critical frequencies. Also note from the plots that the convergence rate goes down with increasing frequencies. Figs. (2.6-2.9) present the absolute errors ($|P_{exact} - P_{num.}|$) for the different frequencies for each mesh. The maximum percent errors for the above four frequencies are shown together in Fig. 2.10 for comparison. From the figure, it is seen that the error for Ka = 1.0 is much less than the other three higher frequencies even for the coarse mesh and that it decreases to less than 2% for the finest mesh model. The error for Ka = 4.0 is over 70% for the coarse mesh, which is much higher than that for Ka = 3.0. However, while the error for Ka = 3.0 remains to be more than 13% for the finest mesh, the error for Ka = 4.0 has dropped to about 9%. This information can be seen more clearly in Fig. 2.11. The surface pressure as function of Ka is presented in Fig. 2.12. In this figure, the numerical data were obtained using the model with the finest mesh. A total of 18 drive frequencies ranging from Ka = 0.1 to Ka = 4.0 were run. Note that the numerical solutions fall almost right on top of the analytic solution for Ka $\leq$ 1.0. However, as the frequencies increase, the numerical solutions start to deviate from the analytic solution. This increasing error in higher frequency

finer mesh must be used in order to obtain better solution when the drive frequencies are high. The predicted surface pressures are 13% and 9% too low as compared to the analytic solution for Ka = 3.0 and Ka = 4.0, respectively. Figs. 2.13 and 2.14 present the far-field pressures at 2.0 m for the excitation frequencies of Ka = 1.0 and Ka = 3.0, respectively. Note that the numerical solution agrees quite well with the analytic solution for Ka = 1.0 but deviates considerably from the analytic solution for Ka = 3.0. In summary, the present boundary integral formulation is capable of predicting the excess pressure induced in a fluid by a totally submerged vibrating body. However, a very fine mesh[16] is required for high excitation frequencies and the scheme will not work if the given drive frequency coincides with one of the critical frequencies of the structure.

16 This means large array sizes in the FORTRAN program and long run times.

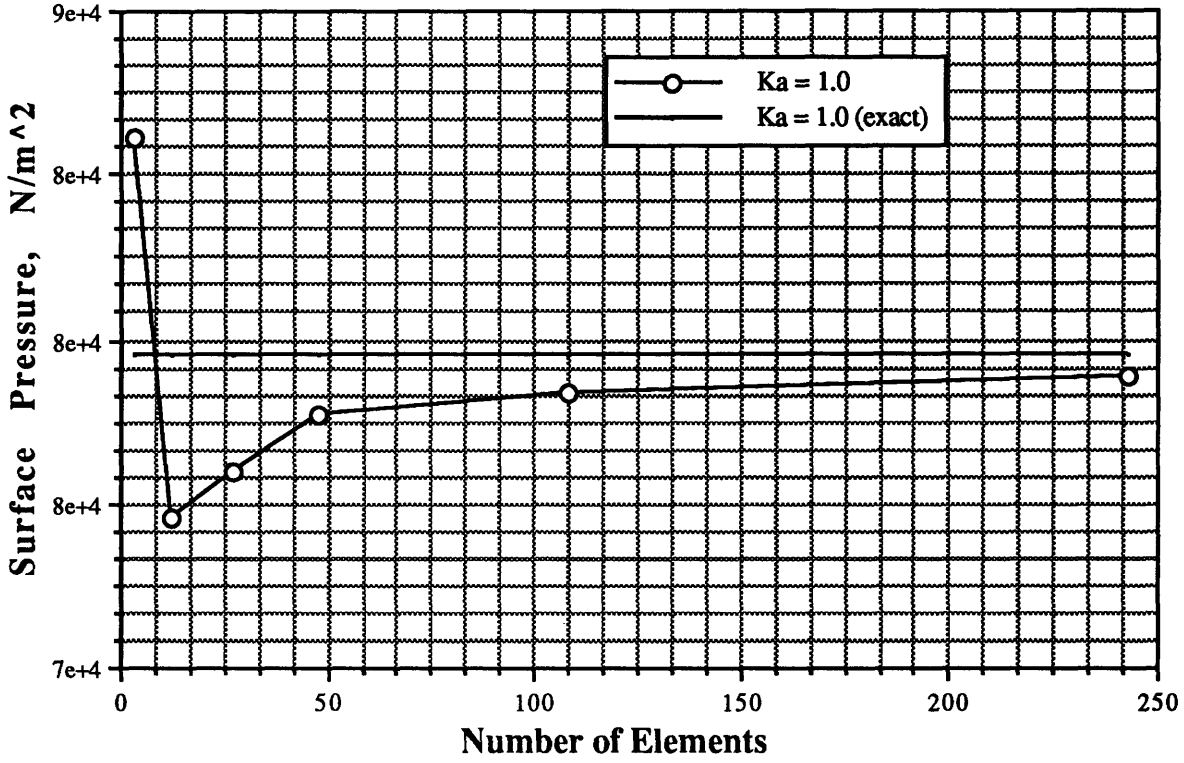

Figure 2.2 Surface pressure convergence history, Ka = 1.0.

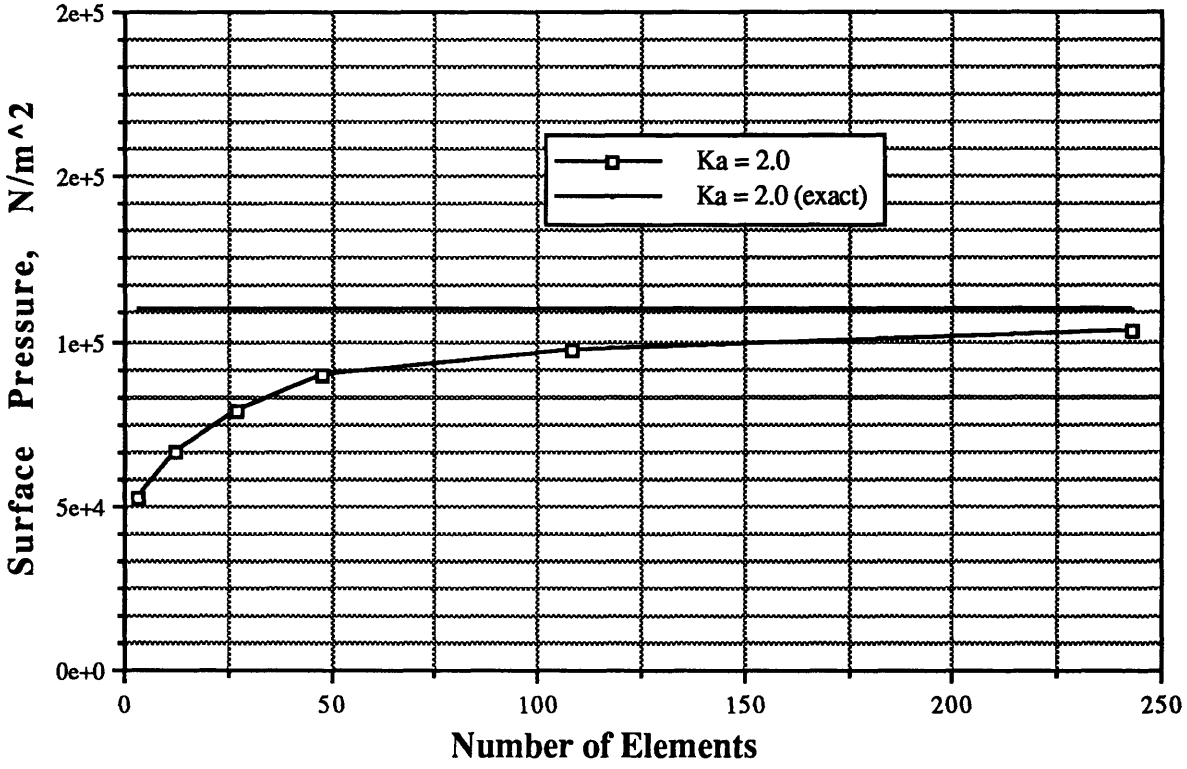

Figure 2.3 Surface pressure convergence history, Ka = 2.0.

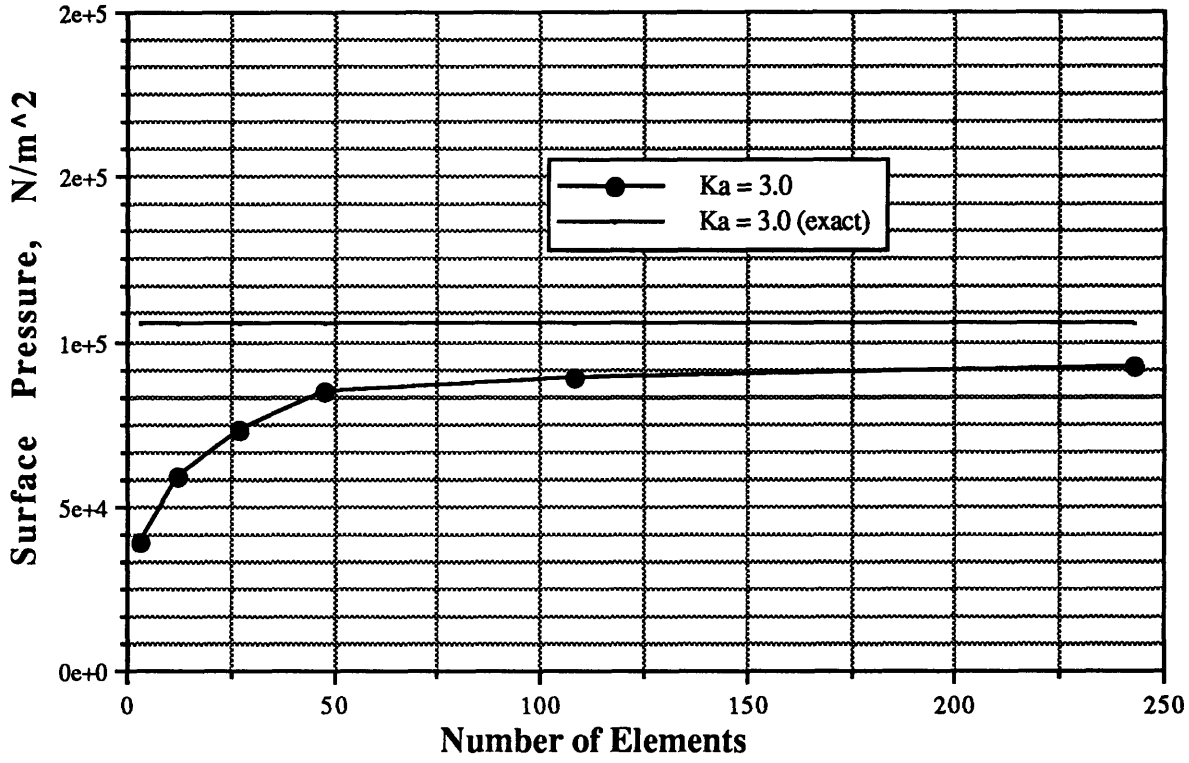

Figure 2.4 Surface pressure convergence history, Ka = 3.0.

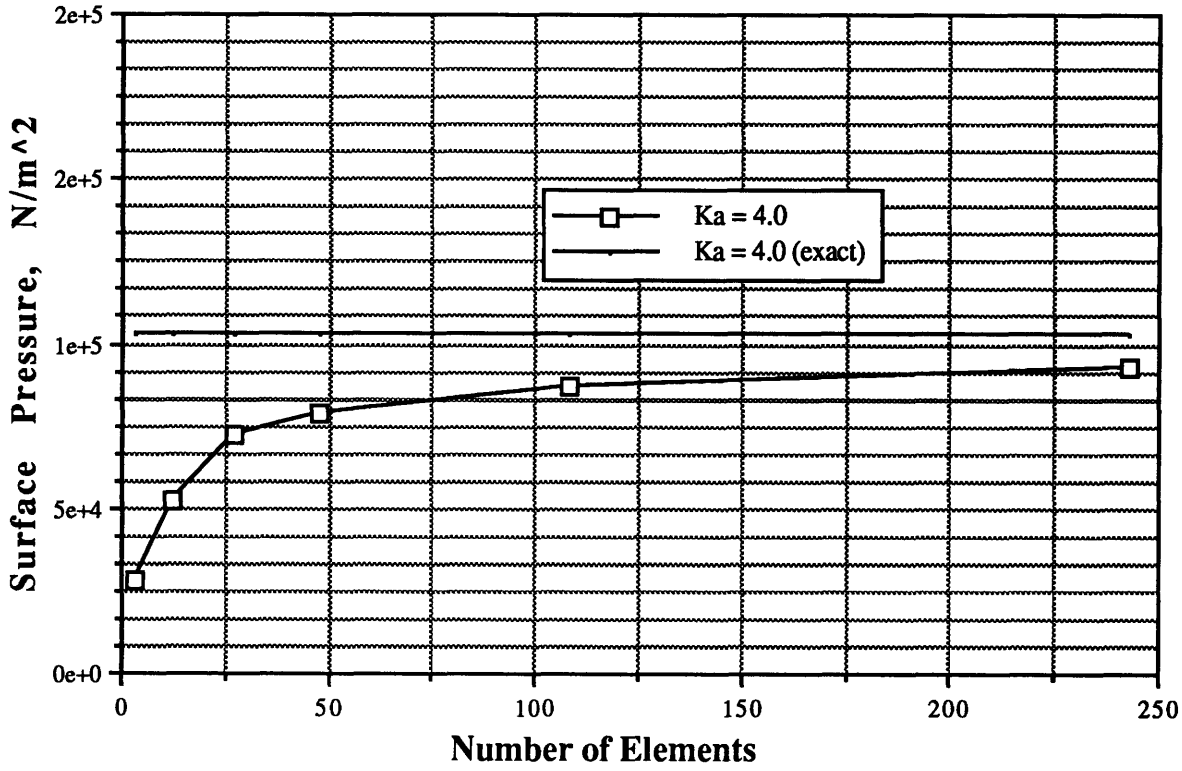

Figure 2.5 Surface pressure convergence history, Ka = 4.0.

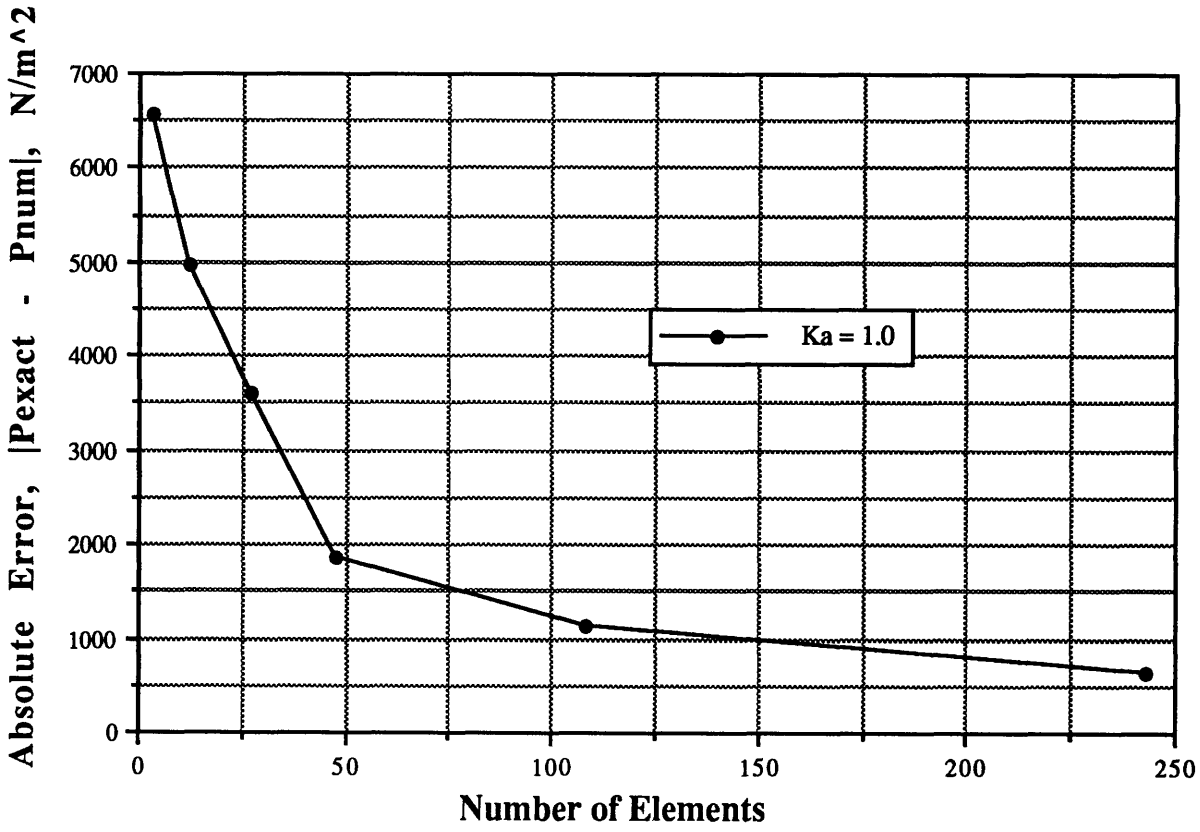

Figure 2.6 Surface pressure absolute error, Ka = 1.0.

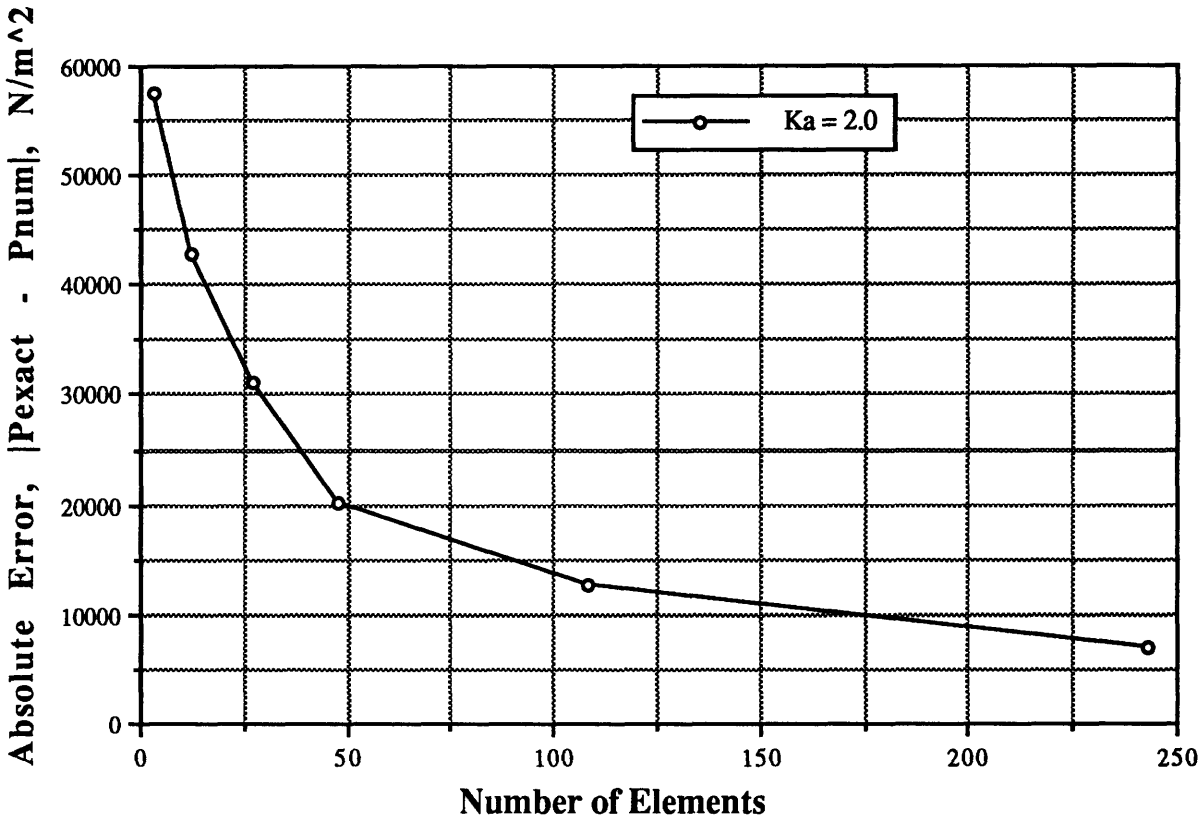

Figure 2.7 Surface pressure absolute error, Ka = 2.0.

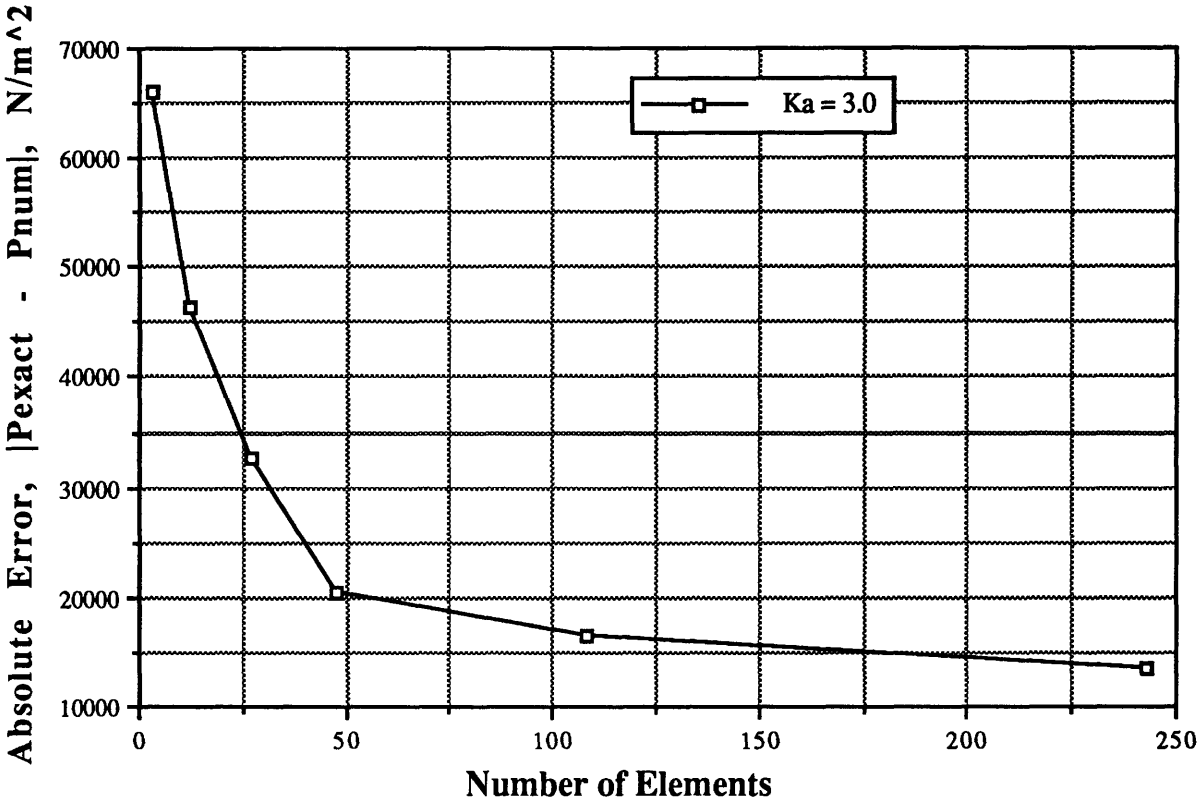

Figure 2.8 Surface pressure absolute error, Ka = 3.0.

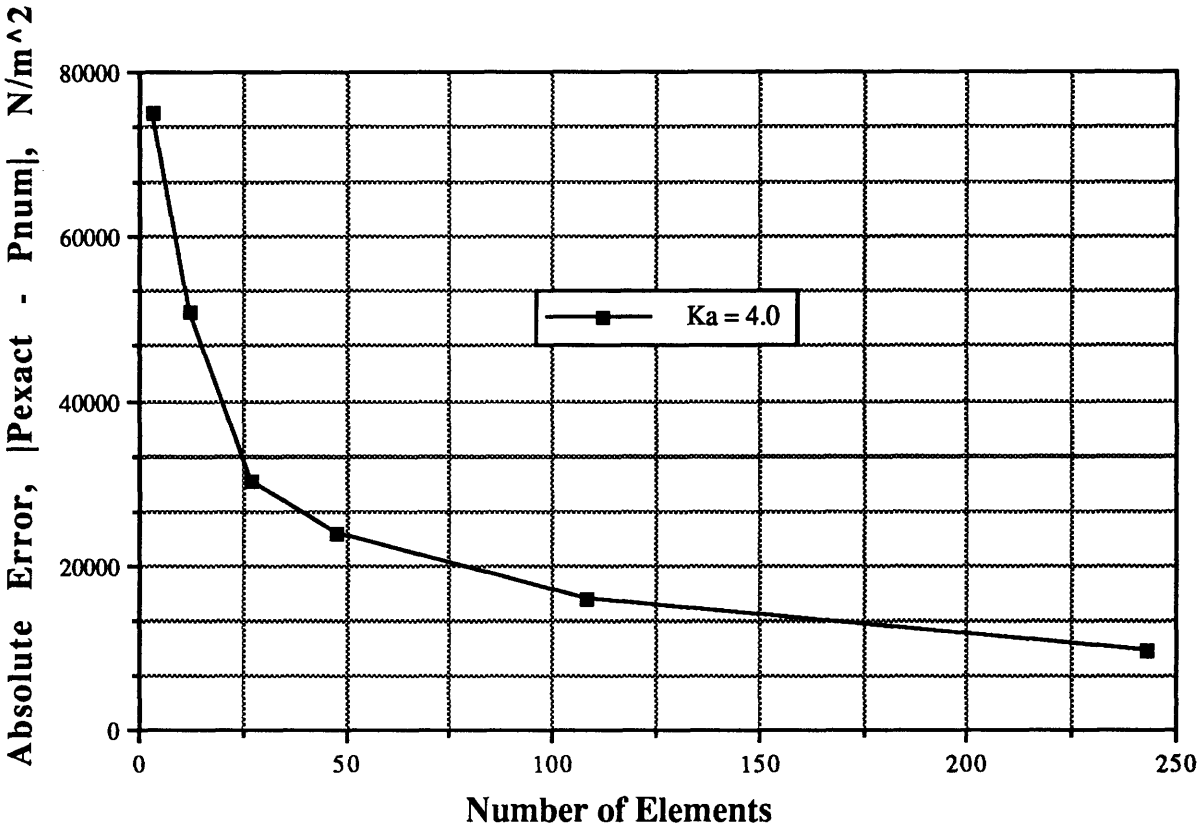

Figure 2.9 Surface pressure absolute error, Ka = 4.0.

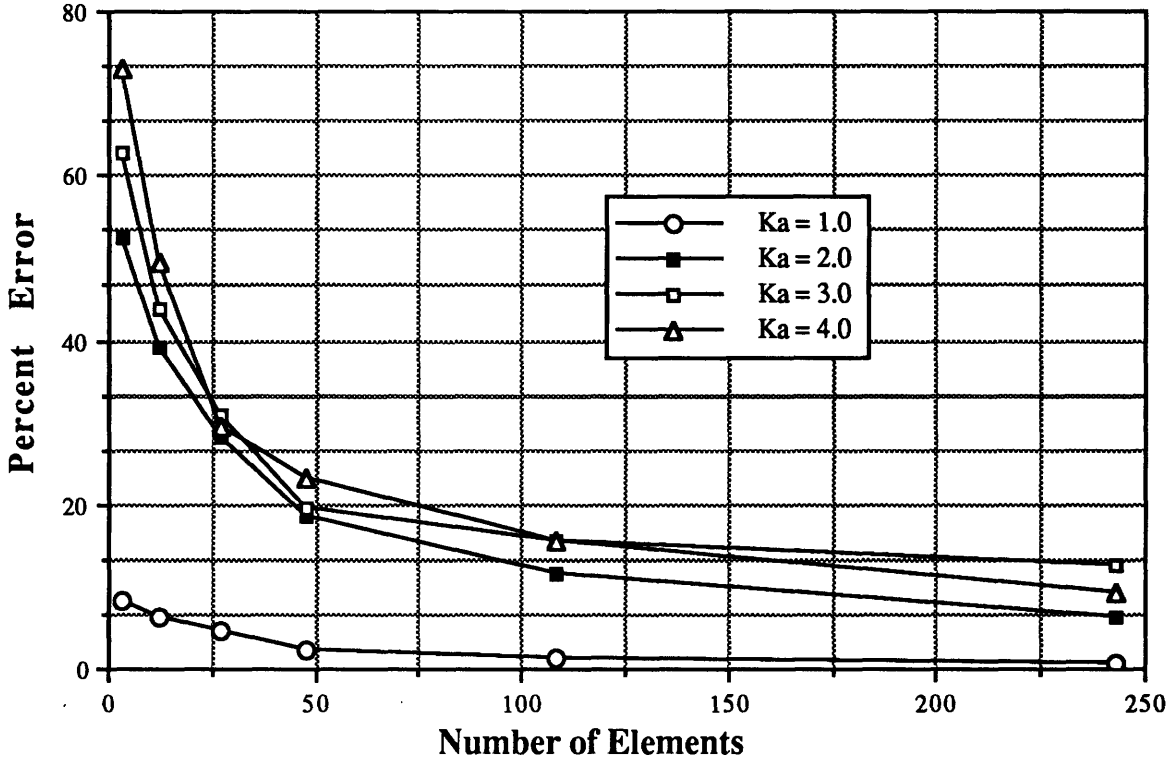

Figure 2.10 Percent error, Ka = 1-4.

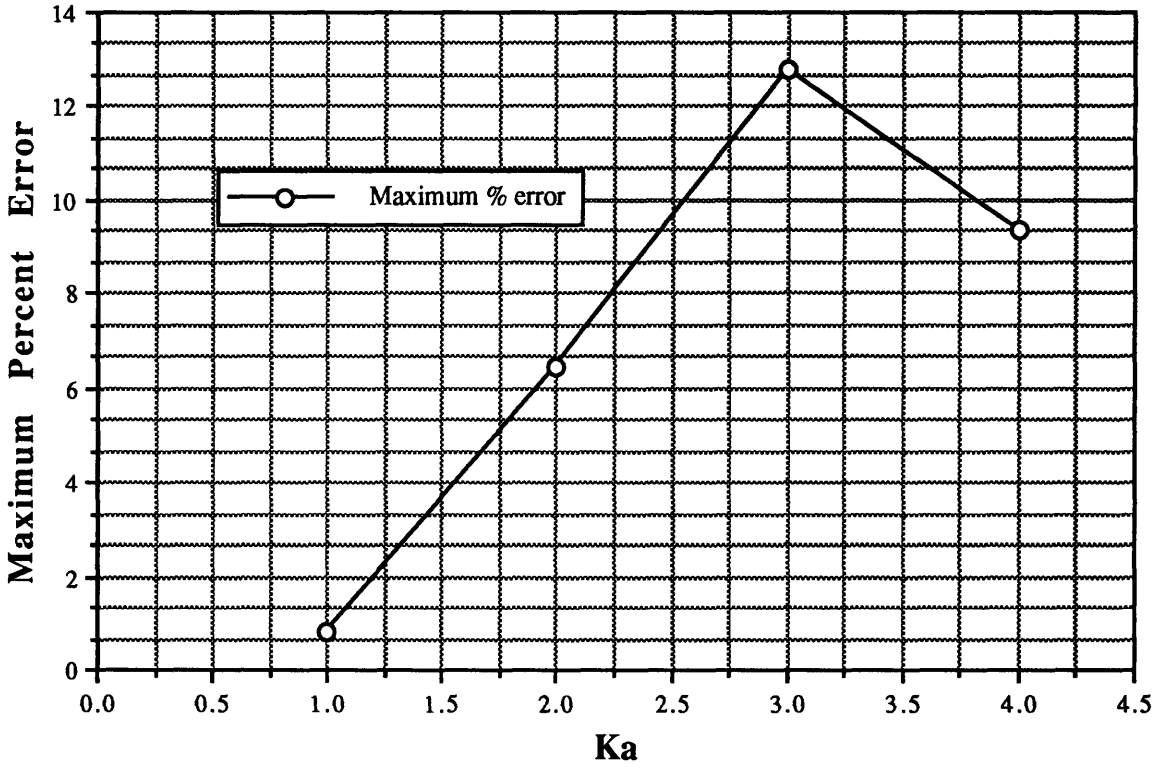

Figure 2.11 Maximum percent error, Ka = 1-4 (243 surface elements)

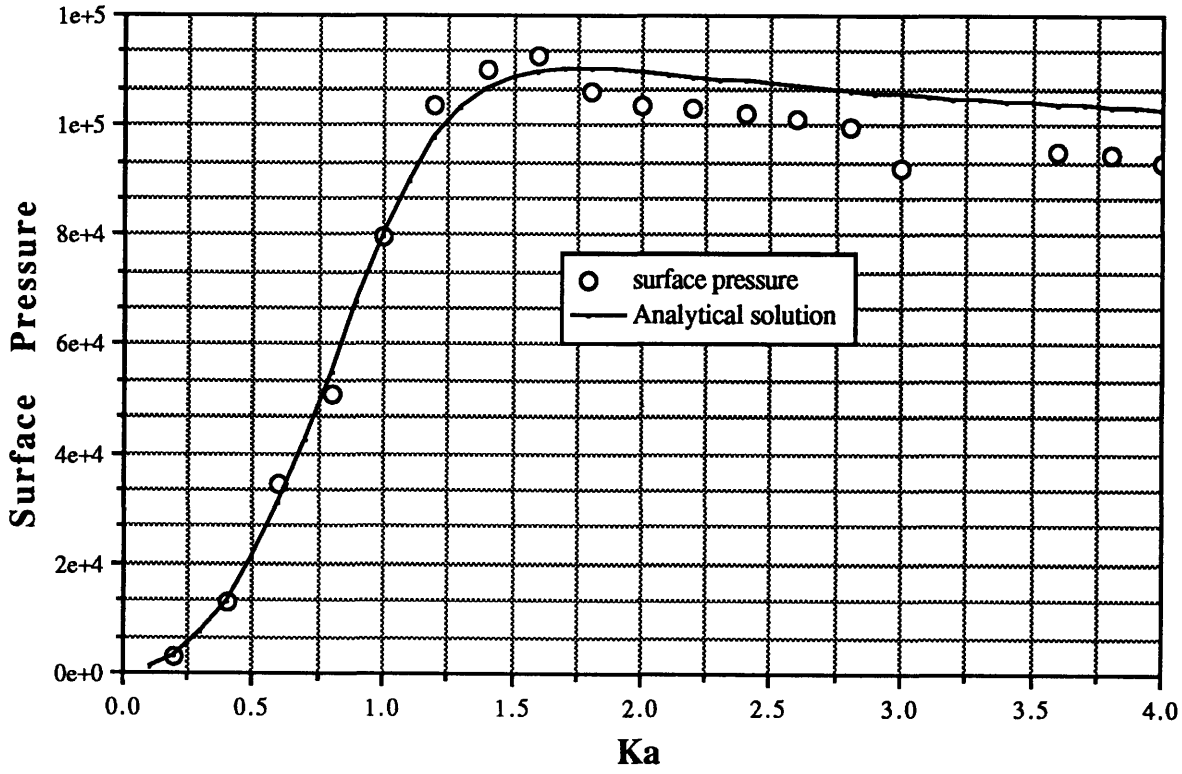

Figure 2.12 Surface pressure as function of Ka.

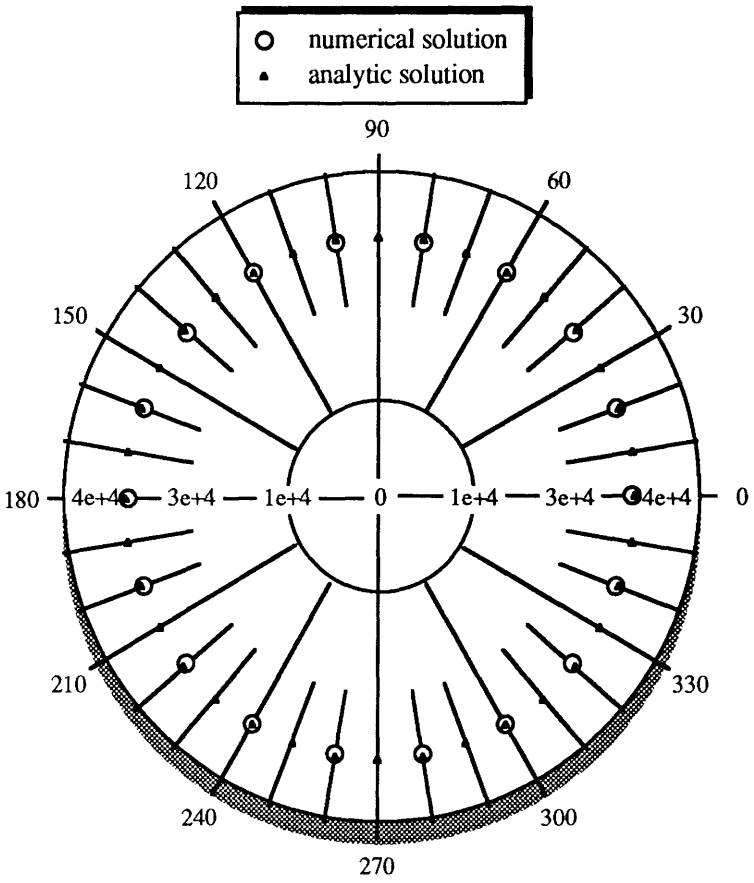

Figure 2.13 Far-field pressure, **r** = 2.0 m, Ka = 1.0.

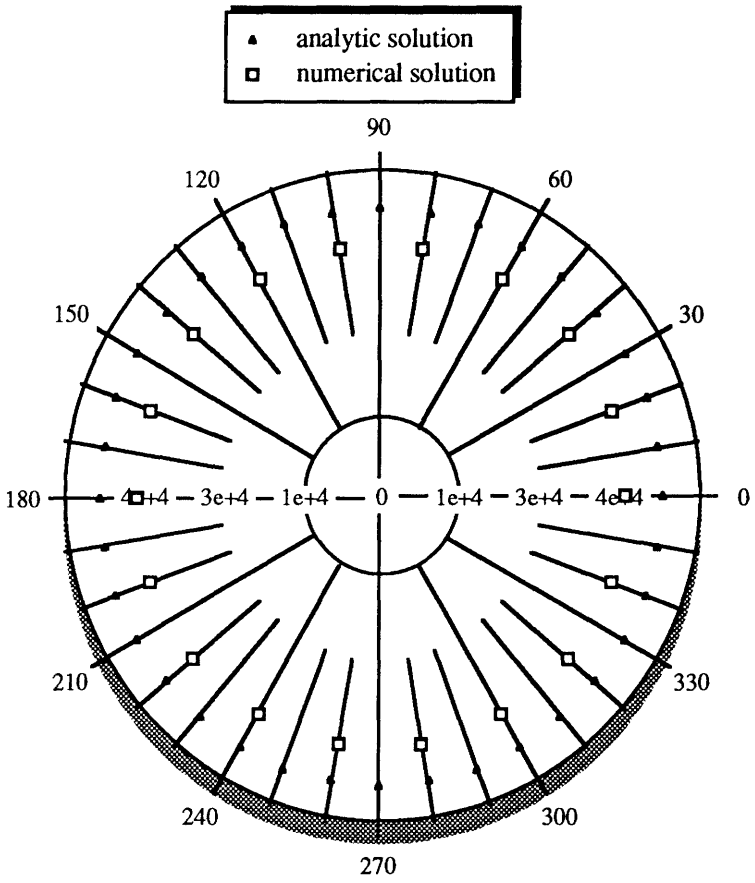

Figure 2.14 Far-field pressure, **r** = 2.0 m, Ka = 3.0.

3. Discussion

As mentioned in Section 2.4 and demonstrated in Section 2.5, the solution of the surface Helmholtz integral equation becomes nonunique or nonexistence when the excitation frequency coincides with a critical frequency. However, this nonuniqueness or nonexistence of the solution to the exterior problem does not have any physical significance. It simply implies that the assumptions used in deriving the exterior Helmholtz equation become invalid as the excitation frequency approaches the characteristic frequencies of the interior problem. Many methods have been proposed in order to circumvent the problem. Some of the better known methods are the *combined Helmholtz integral formulation* (CHIEF) method proposed by Schenck (Ref. 19) and the *composite outward normal derivative overlap relation* (CONDOR) method developed by Burton and Miller (Ref. 4).

The basic principle of the original CHIEF method is to augment the (N x N) system of equations that resulted from the surface Helmholtz integral formulation by additional compatible equations based on the interior Helmholtz integral for selected interior points. The nonsquare, or overdetermined complex system of equations are then solved by a least-squares orthonormalizing procedure. By using this procedure, the approximate surface pressure vector $\underline{\mathbf{P}}^*$ minimizes the magnitude of the error vector. Once the least-squares approximation $\underline{\mathbf{P}}^*$ of the surface pressure $\underline{\mathbf{P}}$ is found, the far-field excess pressure can be computed as discussed in Sec. 2.3.

The method developed by Burton and Miller combines a multiple of the differentiated Helmholtz equation with the surface Helmholtz equation (Eq. 2.30). By doing so they had proved that although the surface Helmholtz integral equation, and the integral equation for the normal derivative, failed to yield unique solutions at the characteristic frequencies of the interior Dirichlet and Neumann problems, respectively, the combination of the two integral equations has a unique solution for the exterior problem for all wave numbers. However, the successful numerical implementation of this formulation hinges on the successful numerical representation of the highly singular integral (known as the hypersigular integral) resulted from differentiating the

Helmholtz equation. Many procedure have been proposed for regularizing the hypersingularities (Refs. 4, 5), however, most methods required extensive computation.

From the discussion above, it is clear that the present basic formulation provides a basis for more robust methods. Most techniques for circumventing the problem of nonuniqueness or nonexistence solution based on augmenting the basic surface Helmholtz equation by one or more constraining equation. Therefore, the frequency limitations inherent in the present formulation can be removed without requiring much modification of the main structure of the basic FORTRAN code.

As mentioned in the introduction section, BIE method is currently the most popular method in the acoustic field for solving fluid-structure interaction problems. In view of the recent development in the field of computational fluid dynamics (CFD), a better approach in solving this fluid-structure interaction problem would be to solve the reduced wave equation (or the integral form of the full wave equation) in the fluid domain using finite element method without resorting to Green's theorems. This idea is not new and has been criticized by many researchers in the acoustic field as inconvenient and impractical due to the difficulties in treating the infinite far-field radiation boundary condition. However, problems with infinite far-field boundary conditions have been solved routinely by researchers in the field of CFD using finite different, finite volume, and more recently, finite element methods. Using finite element method to solve the reduced wave equation in the fluid domain would completely eliminate the problem of nonuniqueness and nonexistence of the solution as in the BIE method. It also eliminate the need of using complex arithmetic on the computer (which is quite expensive in terms of storage and operational counts). Two major criticisms about using finite elements in the fluid domain are that the artificial outer boundary must be very far away and that finite element method will only yield solutions at some finite number of grid points. Both of these criticisms are not quite true any more. Researchers in CFD have solved airfoil problems and have obtained good results with outer artificial boundary no more than two or three chord lengths from the airfoil. As for the second point, one can use finite element method to obtain the surface pressure of the structure and then use the exterior Helmholtz integral [the second of Eq. (2.27)] in order to obtain far-field

pressure at any point in the fluid domain. Doing so will not only eliminate the problems of the surface Helmholtz formulation, at the same time, it will also allow the flexibility (which enjoys by the BIE method) of obtaining solution at any point in the far-field.

Finite element method would also opening up the possibility of solving the full wave equation rather than the reduced wave equation. Solving the full wave equation will eliminate the requirements that the inputs and the responses of the structure are simple-harmonic, and the transient response of the structure can also be obtained if desired (this is not possible when BIE method is used). In summary, due to the recent development in other field, many methods and ideas once deemed to be impractical are becoming more attractive for this fluid-structure interaction problem. It is recommended that all these other possibilities be explored in future research in addition to the more traditional BIE method.

4. Conclusions

Numerical techniques for the determination of the added mass matrix and the excess pressure induced in a fluid of infinite extent by a totally submerged vibrating elastic structure have been presented. For low vibrational frequencies, the surface excess pressure P and the surface normal velocity $\underline{v}_n$ have nearly orthogonal phase; hence, the fluid behaves like an added mass. Theoretical and numerical aspects of calculating the added mass matrix using boundary integral equation method were discussed in Sections 1.1-1.2. Numerical examples for a uniform, rectangular plate with different boundary conditions vibrating in water were presented in Section 1.3.

The results presented in Section 1.3 clearly shown that the presence of the fluid cannot be ignored for calculating the natural vibrational frequencies and mode shapes of a submerged structure if the fluid density is comparable to the average density of the structure. On the other hand, the results also pointed out that a computationally more expensive coupled fluid-structure interaction problem needed not to be solved if the vibrational frequencies are low. In this case, the effect of the fluid can be lumped into an added mass merely superimposed on the structural mass.

For higher vibrational frequencies, the lumped-mass approximation is no longer valid and a coupled fluid-structure problem must be solved. Sections 2.0-2.3 discussed the problem of fluid-structure interaction for an elastic structure submerged in an inviscid fluid of infinite extent.

The example presented in Section 2.5 showed that the present boundary integral formulation is capable of predicting the behavior of the vibrating structure in the fluid provided that the excitation frequency is far away from the critical frequencies of the associated interior Dirchlet problem of the same structure. As mentioned in Section 2.4 and demonstrated in Section 2.5, the solution becomes nonunique or nonexistence when the excitation frequency coincides with a critical frequency. However, this nonuniqueness or nonexistence of the solution to the exterior problem does not have any physical significance. It simply implies that the assumptions used in deriving the exterior Helmholtz

equation become invalid as the excitation frequency approaches the characteristic frequencies of the interior problem.

References

1) Anderson, J. D. Jr., *Fundamentals of Aerodynamics*, McGraw-Hill Book Company, New York, 1984.

2) Barton, G., *Element of Green's Functions and Propagation Potentials, Diffusion, and Waves*, Clarendon Press, Oxford, 1989.

3) Blevins, R. D., *Formulas for Natural Frequency and Mode Shape*, Robert E. Krieger Publishing Company, Malabar, Florida, 1984.

4) Burton, A. J., and Miller, G. F., "The Application of Integral Equation Methods to the Numerical Solution of Some Exterior Boundary-Value Problems," **Proc. Roy. Soc. Lond. A. 323**, 201-210, 1971.

5) Chien, C. C., Rajiyah, H., and Atluri, S. N., "An Effective Method for Solving the Hypersingular Integral Equations in 3-D Acoustics," **The Journal of the Acoustical Society of America**, Vol. 88, No. 2, August 1990.

6) Cook, R. D., Malkus, D. S., and Plesha, M. E., *Concepts and Applications of Finite Element Analysis*, 3rd ed., John Wiley & Sons, Inc., NY, 1989.

7) Crandall, S. H., Karnopp, D. C., Kurtz, E. F. Jr., and Pridmore-Brown, D. C., *Dynamics of Mechanical and Electromechanical Systems*, Robert E. Krieger Publishing Company, Malabar, Florida, 1982.

8) Cruse, T. A. and Rizzo, F. J., Ed., *Boundary-Integral Equation Method: Computational Applications in Applied Mechanics*, AMD-Vol. 11, **ASME**, New York, 1975.

9) Deruntz, J. A. and Geers, T. L., "Added Mass Computation by the Boundary Integral Method," Lockheed Palo Alto Research Laboratory, Palo Alto, CA.

10) Everstine, G. C., Henderson, E. A., Schroeder, E. A. , and Lipman, R. R., "A general Low Frequency Acoustic Radiation Capability for NASTRAN," Fourteenth NASTRAN Users'

Colloquium, NASA CP-2419, National Aeronautics and Space Administration, Washington, D C, May 1986, pp. 293-310.

11) Gordon, E. C. and Francis, H. M., "Coupled Finite Element/Boundary Element Approach for Fluid-Structure Interaction," **J. Acoust. Soc. Am.** 87 (5) 1938-1947, May 1990.

12) Hess, J. L. and Smith, A. M. O., "Calculation of Potential Flow About Arbitrary Bodies," in *Progress in Aeronautical Sciences*, Vol. 8, Pergamon Press, London, 1967.

13) Kang, D. S., Program MULE (MULtibody Environment), The Charles Stark Draper Laboratory, Inc., 555 Technology Square, Cambridge, MA 02139.

14) Karamcheti, K., *Principles of Ideal-Fluid Aerodynamics*, Robert Krieger Publishing Company, Malabar, Florida, 1980.

15) Kellogg, O. D., *Foundations of Potential Theory*, Dover Publications, Inc., New York, 1954.

16) Lamb, H., *Hydrodynamics*, Dover Publications, Inc., New York, 1945.

17) Milne-Thomson, L. M., *Theoretical Hydrodynamics*, Macmillan, New York, 1960.

18) Newman, J. N., *Marine Hydrodynamics*, The MIT Press, 1977.

19) Schenck, H. A., "Improved Integral Formulation for Acoustic Radiation Problems," **The Journal of the Acoustical Society of America**, VOL. 44, Number 1, 44-58 (1967).

20) Shirron, J., Program AXSAR, Theoretical Acoustics Code 5131, Naval Research Laboratory, Washington, D.C. 20375.

21) Sobolev, S. L., *Partial Differential Equations of Mathematical Physics*, Pergamon Press, London, 1964.

22) Sommerfeld, A, *Partial Differential Equations in Physics*, Academic Press Inc., Publishers, New York, N.Y., 1949.

23) Wilton, D. T., "Acoustic Radiation and Scattering from Elastic Structures," **International Journal for Numerical Methods in Engineering**, VOL. 13, 123-138 (1978).

Appendix

A - 1 The Helmholtz Equation (Reduced Wave Equation)

The Helmholtz equation governs the space-dependence of those solutions of the wave equation that are simple-harmonic in time. Consider the nonhomogeneous wave equation

$$\frac{1}{c^2}\frac{\partial^2\Psi}{\partial t^2} - \nabla^2\Psi = \rho(\underline{r}, t) \qquad \text{(A1-1)}$$

where Ψ could be the excess pressure or velocity of the fluid [$\Psi = \Psi(\underline{r}, t)$], and $\rho(\underline{r}, t)$ is the nonhomogeneous source term. If all the prescribed inputs are simple-harmonic, for instance

$$\rho(\underline{r}, t) = \rho_o(\underline{r})\, e^{-i\omega t}, \qquad \text{(A1-2)}$$

and similar expressions for any prescribed boundary values one can look for oscillatory solutions to the wave equation of the form

$$\Psi(\underline{r}, t) = \Psi_o(\underline{r})\, e^{-i\omega t}. \qquad \text{(A1-3)}$$

Differentiating Eq. (A1-3) with respect to the space and time variables the following equations are obtained

$$\Psi_{xx} = \Psi_{o_{xx}}\, e^{-i\omega t} \qquad \text{(A1-4a)}$$

$$\Psi_{yy} = \Psi_{o_{yy}}\, e^{-i\omega t} \qquad \text{(A1-4b)}$$

$$\Psi_{zz} = \Psi_{o_{zz}}\, e^{-i\omega t} \qquad \text{(A1-4c)}$$

$$\Psi_{tt} = -\omega^2 \Psi_o\, e^{-i\omega t}. \qquad \text{(A1-4d)}$$

On substituting the above equations into the wave equation, the factor $e^{-i\omega t}$ cancels out and one obtains the inhomogeneous Helmholtz equation:

$$\left(\Psi_{xx} + \Psi_{yy} + \Psi_{zz} + \frac{\omega^2}{c^2}\Psi\right) e^{-i\omega t} = -\rho(\underline{r}, t)\, e^{-i\omega t} \qquad \text{(A1-5)}$$

or

$$(\nabla^2 \Psi + k^2 \Psi) = -\rho(\underline{r}, t) \qquad \text{(A1-6)}$$

where $k = \omega/c$ is the wave number. If the source term $\rho(\underline{r}, t)$ on the right-hand side of Eq. (A1-6) is set equal to zero, the resulting equation is the well-known homogeneous Helmholtz equation

$$(\nabla^2 \Psi + k^2 \Psi) = 0. \qquad \text{(A1-7)}$$

A - 2 Green's Identities

Green's First, Second, and Third Identities can be derived by applying the divergence theorem to an arbitrary control volume. Consider a control volume as shown in Fig. (A2.1), the surface and volume integrals are related through the divergence theorem

$$\int_V [\nabla \cdot \underline{\mathbf{v}}]\, dV = \int_S [\underline{\mathbf{v}} \cdot \underline{\mathbf{n}}]\, dS \qquad \text{(A2-1)}$$

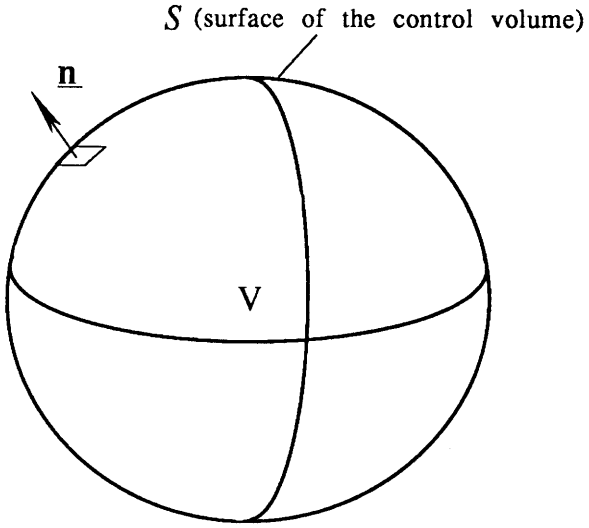

Figure A2.1 Control volume for deriving Green's identities

where $\underline{\mathbf{v}}$ is an arbitrary vector. Let $\Psi(\underline{\mathbf{r}})$ and $\phi(\underline{\mathbf{r}})$ be two scalar functions of position, a vector field can be formed by multiplying one of the functions by the gradient of the other

$$\Psi \nabla \phi = \Psi \ (\text{grad}\phi)\,. \qquad \text{(A2-2)}$$

Substituting Eq. (A2-2) for the vector field $\underline{\mathbf{v}}$ in Eq. (A2-1):

$$\int_V [\nabla \cdot (\Psi \nabla \phi)]\, dV = \int_S [(\Psi \nabla \phi) \cdot \underline{\mathbf{n}}]\, dS \qquad \text{(A2-3)}$$

or

$$\int_V \left[\nabla\Psi \cdot \nabla\phi + \Psi\nabla^2\phi\right] dV = \int_S \left[(\Psi\nabla\phi) \cdot \underline{\mathbf{n}}\right] dS . \qquad \text{(A2-4)}$$

Introducing $\partial\phi/\partial n$ to denote the derivative of ϕ with respect to distance in the direction of the outward normal $\underline{\mathbf{n}}$

$$\nabla\phi \cdot \underline{\mathbf{n}} \equiv \frac{\partial\phi}{\partial \mathbf{n}} . \qquad \text{(A2-5)}$$

Eq. (A2-4) , therefore, may be rewritten as

$$\int_V \left[\nabla\Psi \cdot \nabla\phi + \Psi\nabla^2\phi\right] dV = \int_S \left[\Psi \frac{\partial\phi}{\partial \mathbf{n}}\right] dS \qquad \text{(A2-6)}$$

which is commonly known as **Green's First Identity.**

Now, consider the following vector field

$$\Psi\nabla\phi - \phi\nabla\Psi, \qquad \text{(A2-7)}$$

and substituting it for the vector $\underline{\mathbf{V}}$ in Eq. (A2-1):

$$\int_V \left[\nabla \cdot (\Psi\nabla\phi - \Psi\nabla\Psi)\right] dV = \int_S \left[(\Psi\nabla\phi - \phi\nabla\Psi) \cdot \underline{\mathbf{n}}\right] dS . \qquad \text{(A2-8)}$$

Expanding Eq. (A2-8) and using Eq. (A2-5) to replace the gradient operator, **Green's Second Identity** is obtained

$$\int_V \left[\Psi\nabla^2\phi - \phi\nabla^2\Psi\right] dV = \int_S \left[\Psi\frac{\partial\phi}{\partial \mathbf{n}} - \phi\frac{\partial\Psi}{\partial \mathbf{n}}\right] dS . \qquad \text{(A2-9)}$$

Consider the vector field in Eq. (A2-7) again and let

$$\Psi \equiv \frac{1}{\mathbf{r}} = \frac{1}{\sqrt{(x-x_o)^2 + (y-y_o)^2 + (z-z_o)^2}} \qquad \text{(A2-10)}$$

Note that $1/\mathbf{r}$ satisfies Laplace's equation except at the point (x_o, y_o, z_o). Assuming first that ϕ has continuous second derivatives throughout the domain D and on its boundary S. Let's cut out a sphere of volume ω with radius ε and surface area σ and centered at the point (x_o, y_o, z_o). Applying Green's second identity to the remaining volume $(D - \omega)$ yields the following equation

$$\lim_{\varepsilon \to 0} \int_{D-w} \left[\frac{1}{\mathbf{r}} \nabla^2 \phi - \phi \nabla^2 \frac{1}{\mathbf{r}}\right] dV = \int_S \left[\frac{1}{\mathbf{r}} \frac{\partial \phi}{\partial \mathbf{n}} - f \frac{\partial}{\partial \mathbf{n}} \left(\frac{1}{\mathbf{r}}\right)\right] dS +$$

$$\lim_{\varepsilon \to 0} \int_\sigma \left[\frac{1}{\mathbf{r}} \frac{\partial \phi}{\partial \mathbf{n}} - \phi \frac{\partial}{\partial \mathbf{n}} \left(\frac{1}{\mathbf{r}}\right)\right] dS \,. \qquad \text{(A2-11)}$$

Since $\nabla^2(1/\mathbf{r}) = 0$ (the function $1/\mathbf{r}$ satisfies Laplace's equation), Eq. (A2-11) can be rewritten as

$$\int_\omega \left[\frac{1}{\mathbf{r}} \nabla^2 \phi\right] dV = \int_S \left[\frac{1}{\mathbf{r}} \frac{\partial \phi}{\partial \mathbf{n}} - \phi \frac{\partial}{\partial \mathbf{n}} \left(\frac{1}{\mathbf{r}}\right)\right] dS +$$

$$\lim_{\varepsilon \to 0} \int_\sigma \left[\frac{1}{\mathbf{r}} \frac{\partial \phi}{\partial \mathbf{n}} - \phi \frac{\partial}{\partial \mathbf{n}} \left(\frac{1}{\mathbf{r}}\right)\right] dS \,, \qquad \text{(A2-12)}$$

The second integral on the right-hand side of Eq. (A2-12) can be separated into two terms:

$$\lim_{\varepsilon \to 0} \int_\sigma \left[\frac{1}{\mathbf{r}} \frac{\partial \phi}{\partial \mathbf{n}} - \phi \frac{\partial}{\partial \mathbf{n}} \left(\frac{1}{\mathbf{r}}\right)\right] dS = \lim_{\varepsilon \to 0} \int_\sigma \left[\frac{1}{\mathbf{r}} \frac{\partial \phi}{\partial \mathbf{n}}\right] dS -$$

$$\lim_{\varepsilon \to 0} \int_s \left[\phi \frac{\partial}{\partial n} \left(\frac{1}{r}\right) \right] dS \, . \qquad \text{(A2-13)}$$

For the second integral on the left-hand side

$$\lim_{\varepsilon \to 0} \int_\sigma \left[\phi \frac{\partial}{\partial n} \left(\frac{1}{r}\right) \right] dS \, , \qquad \text{(A2-14)}$$

note that $\frac{\partial}{\partial n} = \frac{d}{dr}$ since the radius vector $\underline{r}$ is in the direction of the surface unit normal $\underline{n}$ on a sphere. Therefore, $\frac{\partial(1/r)}{\partial n} = -\frac{1}{r^2} = -\frac{1}{\varepsilon^2}$ and Eq. (A2-14) becomes

$$\lim_{\varepsilon \to 0} \int_\sigma \left[\phi \left(-\frac{1}{\varepsilon^2} \right) \right] dS = \lim_{\varepsilon \to 0} \left(-\frac{1}{\varepsilon^2} \right) \int_\sigma [\phi] \, dS =$$

$$\lim_{\varepsilon \to 0} \left(-\frac{1}{\varepsilon^2} \right) \int_\sigma \left[\phi(x_o, y_o, z_o) + \eta \right] dS \qquad \text{(A2-15)}$$

where η is some well behave function which tends uniformly to zero in ω as $\varepsilon \to 0$ so that $\phi = \phi(x_o, y_o, z_o)$ at (x_o, y_o, z_o); that is, $0 < |\eta| < \delta(\varepsilon)$ and $\delta(\varepsilon) \to 0$ as $\varepsilon \to 0$. Evaluating the integral in Eq. (A2-15):

$$\lim_{\varepsilon \to 0} \left(-\frac{1}{\varepsilon^2} \right) \int_\sigma \left[\phi(x_o, y_o, z_o) + \eta \right] dS$$

$$= \lim_{\varepsilon \to 0} \left\{ \left(-\frac{1}{\varepsilon^2} \right) \phi(x_o, y_o, z_o) \int_\sigma dS + \int_s (\eta) \, dS \right\}$$

$$= \lim_{\varepsilon \to 0} \left\{ \left(-\frac{1}{\varepsilon^2} \right) \left[-4 \pi \varepsilon^2 \phi(x_o, y_o, z_o) + \int_\sigma (\eta) \, dS \right] \right\}. \qquad \text{(A2-16)}$$

Because it was assumed that $|\eta| < \delta(\varepsilon)$, then,

$$\left| \int_\sigma (\eta)\, dS \right| \leq \left| \int_\sigma \delta(\varepsilon)\, dS \right| = \delta(\varepsilon)\, 4\, \pi\, \varepsilon^2 . \qquad \text{(A2-17)}$$

Since $\delta(\varepsilon) \to 0$ as $\varepsilon \to 0$, it is clear that $\int_\sigma (\eta)\, dS \to 0$ as $\varepsilon \to 0$. Therefore,

$$\lim_{\varepsilon \to 0} \left\{ \left(-\frac{1}{\varepsilon^2} \right) \left[-4\, \pi\, \varepsilon^2\, \phi(x_o, y_o, z_o) + \int_\sigma (\eta)\, dS \right] \right\} =$$

$$4\, \pi\, \phi(x_o, y_o, z_o). \qquad \text{(A2-18)}$$

Now, for the first integral on the right-hand side of Eq. (A2-13),

$$\lim_{\varepsilon \to 0} \int_\sigma \left[\frac{1}{\mathbf{r}} \frac{\partial \phi}{\partial \mathbf{n}} \right] dS \ , \qquad \text{(A2-19)}$$

because $\dfrac{\partial \phi}{\partial \mathbf{n}}$ is bounded, therefore, the normal derivative has an upper bound, that is, $\left| \dfrac{\partial \phi}{\partial \mathbf{n}} \right| < K$ where K is a constant. Since

$$\int_\sigma (K)\, dS = K\, (4\, \pi\, \varepsilon^2) \qquad \text{(A2-20)}$$

and

$$\frac{1}{\varepsilon} \int_\sigma (K)\, dS = K\, (4\, \pi\, \varepsilon) \qquad \text{(A2-21)}$$

thus

$$\left| \int_{\sigma} \left[\frac{1}{\mathbf{r}} \frac{\partial \phi}{\partial \mathbf{n}} \right] dS \right| \leq \int_{\sigma} \left(\frac{1}{\varepsilon} K \right) dS \leq K (4 \pi \varepsilon) . \qquad \text{(A2-22)}$$

As $\varepsilon \rightarrow 0$, $(4 \pi K \varepsilon \rightarrow 0)$; hence,

$$\lim_{\varepsilon \rightarrow 0} \int_{\sigma} \left[\frac{1}{\mathbf{r}} \frac{\partial \phi}{\partial \mathbf{n}} \right] dS \rightarrow 0. \qquad \text{(A2-23)}$$

Combining Eqs. (A2-13), (A2-18), and (A2-23) yields

$$\lim_{\varepsilon \rightarrow 0} \int_{\sigma} \left[\frac{1}{\mathbf{r}} \frac{\partial \phi}{\partial \mathbf{n}} - \phi \frac{\partial}{\partial \mathbf{n}} \left(\frac{1}{\mathbf{r}} \right) \right] dS = - 4 \pi \phi(x_o, y_o, z_o). \qquad \text{(A2-24)}$$

Therefore Eq. (A2-12),

$$\int_{\omega} \left[\frac{1}{\mathbf{r}} \nabla^2 \phi \right] dV = \int_{S} \left[\frac{1}{\mathbf{r}} \frac{\partial \phi}{\partial \mathbf{n}} - \phi \frac{\partial}{\partial \mathbf{n}} \left(\frac{1}{\mathbf{r}} \right) \right] dS + \lim_{\varepsilon \rightarrow 0} \int_{\sigma} \left[\frac{1}{\mathbf{r}} \frac{\partial \phi}{\partial \mathbf{n}} - \phi \frac{\partial}{\partial \mathbf{n}} \left(\frac{1}{\mathbf{r}} \right) \right] dS ,$$

becomes

$$\int_{\omega} \left[\frac{1}{\mathbf{r}} \nabla^2 \phi \right] dV = \int_{S} \left[\frac{1}{\mathbf{r}} \frac{\partial \phi}{\partial \mathbf{n}} - \phi \frac{\partial}{\partial \mathbf{n}} \left(\frac{1}{\mathbf{r}} \right) \right] dS - 4 \pi \phi(x_o, y_o, z_o) \qquad \text{(A2-25)}$$

which is commonly known as **Green's Third Identity**. Note that if the point (x_o, y_o, z_o) is outside of the domain D, then Green's Third Identity becomes

$$\int_{\omega} \left[\frac{1}{\mathbf{r}} \nabla^2 \phi \right] dV = \int_{S} \left[\frac{1}{\mathbf{r}} \frac{\partial \phi}{\partial \mathbf{n}} - \phi \frac{\partial}{\partial \mathbf{n}} \left(\frac{1}{\mathbf{r}} \right) \right] dS , \quad \phi(x_o, y_o, z_o) = 0. \qquad \text{(A2-26)}$$

A - 3 Free-space Green's Function for Laplace's Equation

Laplace's equation written in three-dimensional spherical coordinate system is

$$\nabla^2 \Psi = \frac{1}{r^2 \sin(\theta)} \left\{ \frac{\partial}{\partial r}\left(r^2 \frac{\partial \Psi}{\partial r} \right) + \frac{\partial}{\partial \theta}\left(\sin(\theta) \frac{\partial \Psi}{\partial \theta} \right) + \frac{\partial}{\partial \phi}\left(\frac{1}{\sin(\theta)} \frac{\partial \Psi}{\partial \phi} \right) \right\} = 0. \qquad \text{(A3-1)}$$

If $\Psi = 1/r$ and since $r \neq r(\theta, \phi)$, then

$$\nabla^2\left(\frac{1}{r}\right) = \left(\frac{1}{r^2 \sin(\theta)}\right)\left[\frac{\partial}{\partial r}\left(r^2 \sin(\theta) \frac{\partial (1/r)}{\partial r} \right)\right] =$$

$$\left(\frac{1}{r^2 \sin(\theta)}\right)\left\{\frac{\partial}{\partial r}\left[r^2 \sin(\theta) \left(\frac{-1}{r^2}\right)\right]\right\} =$$

$$\left(\frac{1}{r^2 \sin(\theta)}\right)\left\{\frac{\partial}{\partial r}\left[-\sin(\theta)\right]\right\} = 0. \qquad \text{(A3-2)}$$

A-4 Free-space Green's Function for the Helmholtz Equation

The typical solution of the homogeneous Helmholtz equation [Eq. (A1-7)], from which all other solutions can be derived, is that which corresponds to a unit source

$$\Psi = \frac{e^{-iKr}}{4\pi r}. \tag{A4-1}$$

Proof:

The gradient operator in spherical coordinate system is

$$\nabla^2 = \frac{1}{r^2}\frac{\partial}{\partial r}\left(r^2\frac{\partial}{\partial r}\right)+\left(\frac{1}{r^2\sin(\theta)}\right)\frac{\partial}{\partial\theta}\left(\sin(\theta)\frac{\partial}{\partial\theta}\right)+$$

$$\frac{1}{r^2\sin^2(\theta)}\frac{\partial^2}{\partial^2\phi}. \tag{A4-2}$$

Since $\Psi = \Psi(r)$ only, therefore,

$$\nabla^2 = \frac{1}{r^2}\frac{\partial}{\partial r}\left(r^2\frac{\partial}{\partial r}\right) = \frac{1}{r^2}\frac{d}{dr}\left(r^2\frac{d}{dr}\right). \tag{A4-3}$$

$$r^2\frac{d\Psi}{dr} = r^2\left[\frac{-iKe^{-iKr}}{4\pi r} - \frac{-iKe^{-iKr}}{4\pi r^2}\right] = \frac{-iKe^{-iKr}}{4\pi} - \frac{-iKe^{-iKr}}{4\pi r} \tag{A4-4}$$

and

$$\frac{1}{r^2}\frac{d}{dr}\left(r^2\frac{d\Psi}{dr}\right) = \frac{1}{r^2}\left[\frac{-K^2e^{-iKr}}{4\pi}\right] = \frac{-K^2e^{-iKr}}{4\pi r}, \tag{A4-5}$$

therefore,

$$\left(\nabla^2+K^2\right)\Psi = \frac{1}{r^2}\frac{d}{dr}\left(r^2\frac{d\Psi}{dr}\right) = \left[\frac{-K^2e^{-iKr}}{4\pi r}\right] + \frac{K^2e^{-iKr}}{4\pi r} = 0. \tag{A4-6}$$

A - 5 Helmholtz Integral Equations

From Green's Second Identity

$$\int_V \left[\Psi\nabla^2\phi - \phi\nabla^2\Psi\right] dV = \int_S \left[\Psi\frac{\partial\phi}{\partial n} - \phi\frac{\partial\Psi}{\partial n}\right] dS . \qquad \text{(A5-1)}$$

If Ψ and ϕ and their first and second derivatives are continuous and single-valued and if Ψ and ϕ satisfied the homogeneous Helmholtz equation, then

$$\int_V \left[\Psi\nabla^2\phi - \phi\nabla^2\Psi\right] dV = \int_V \left[\Psi\left(-K^2\phi\right) - \phi\left(-K^2\Psi\right)\right] dV$$

$$= \int_V \left[-K^2\Psi\phi + K^2\Psi\phi\right] dV = 0. \qquad \text{(A5-2)}$$

Hence, Green's Second Identity becomes

$$\int_S \left[\Psi\frac{\partial\phi}{\partial n} - \phi\frac{\partial\Psi}{\partial n}\right] dS = 0. \qquad \text{(A5-3)}$$

Let

$$\Psi = \frac{e^{-iKr}}{4\pi r}. \qquad \text{(A5-4)}$$

then Eq. (A5-3) becomes

$$\int_S \left[\frac{e^{-iKr}}{4\pi r}\frac{\partial\phi}{\partial n} - \phi\frac{\partial}{\partial n}\left(\frac{e^{-iKr}}{4\pi r}\right)\right] dS = -\phi_p \qquad \text{(A5-5)}$$

(from Green's Third Identity), or

$$\int_S \left[\phi \frac{\partial}{\partial n}\left(\frac{e^{-iKr}}{4\pi r}\right) - \frac{e^{-iKr}}{4\pi r}\frac{\partial \phi}{\partial n} \right] dS = \phi_p \,. \qquad \text{(A5-6)}$$

Eq. (A5-6), which is the same as the second equation in (2.30) (without the incident pressure term), gives the value of ϕ at any point p of a region in terms of the value of ϕ and $\partial\phi/\partial n$ at the boundary. If r' denotes the distance from a point p' external to the domain D, then

$$\int_S \left[\phi \frac{\partial}{\partial n}\left(\frac{e^{-iKr}}{4\pi r}\right) - \frac{e^{-iKr}}{4\pi r}\frac{\partial \phi}{\partial n} \right] dS = 0 \qquad \text{(A5-7)}$$

which is the third of Eq. (2.30). Finally, if point p is on the surface of the body, then

$$\int_S \left[\phi \frac{\partial}{\partial n}\left(\frac{e^{-iKr}}{4\pi r}\right) - \frac{e^{-iKr}}{4\pi r}\frac{\partial \phi}{\partial n} \right] dS = \frac{\phi_p}{2}^{\dagger} \qquad \text{(A5-8)}$$

---

† If the point (x,y,z) is situated on the surface S, the surface S_ε is chosen to be a small hemisphere that indents the original surface S inside the source point. The contribution from this hemisphere is just half that given by Eq. (A5-6). Therefore, Eq. (A5-8) is half of Eq. (A5-6) (see Ref. 18).